interdisciplinary
toxicology

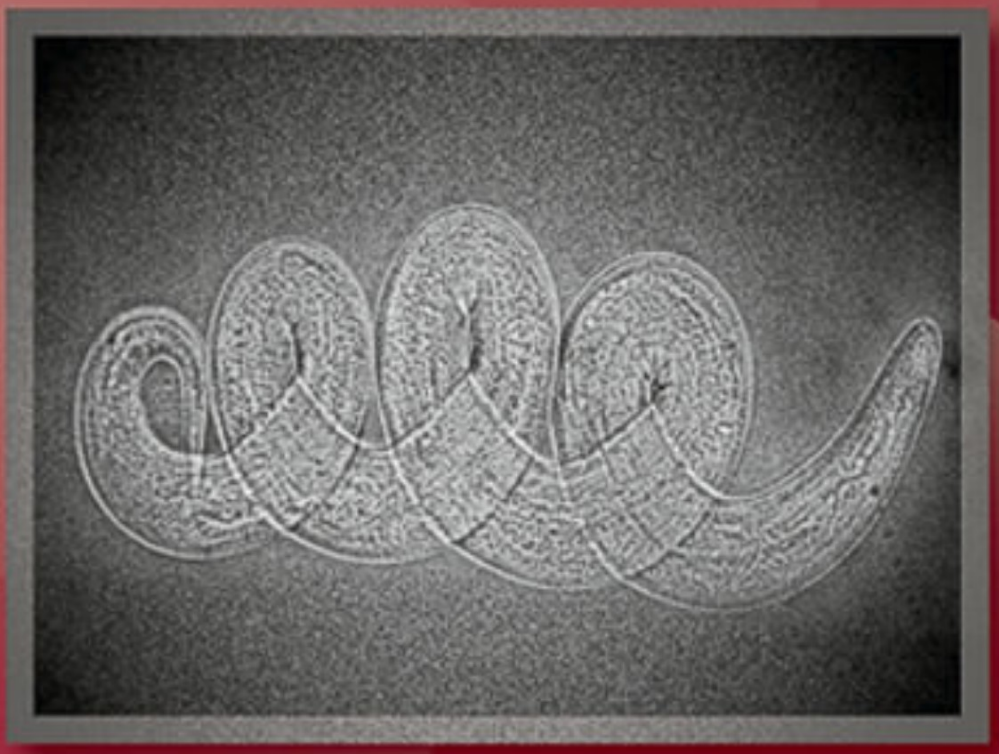

Interdiscip Toxicol. 2020; **Vol. 13**(1): 1–12.
doi: 10.2478/intox-2020-0001

sciendo

interdisciplinary toxicology

REVIEW ARTICLE

Ozone decomposition – state of the art and new approaches

Todor BATAKLIEV [1], Vladimir GEORGIEV [1], Slavcho RAKOVSKY [1], Gennadi E. ZAIKOV [2]

[1] Institute of Catalysis, Bulgarian Academy of Sciences, Sofia, Bulgaria
[2] N.M. Emanuel Institute of Biochemical Physics, Russian Academy of Sciences, Moscow, Russia

ITX130120A01 • Received: 06 October 2019 • Accepted: 26 February 2020

ABSTRACT

The effective ozone decomposition is still a scientific challenge because of its rising industrial use in global scale. Wide application of high ozone concentrations forces researchers to work on new catalytic systems for ozone removal concerning mostly the surrounding human environment (airplane cabins, copiers, laser printers, sterilizers, *etc.*). It is not an easy task considering the fact that above concentration of 0.1 mg/m^3 the ozone could seriously harm human health. Current studies estimate a huge number of untimely deceased people per year on a global scale as a direct consequence of air pollution. It is imposing to reinforce the efforts in workable ozone decomposition on ground atmospheric layer as an important part of air purification process. This review comprises general look on basic physico-chemical properties of ozone completed by recently reported literature about catalytic ozone destruction. Discussion over kinetics and mechanisms of ozone decomposition reaction will be represented in order to do an attempt to clarify these most outstanding parts of the topic.

KEY WORDS: catalysts; synthesis; kinetics; mechanism; ozone; decomposition

Introduction

In last years, the scientific researchers from all over the world are trying to solve deep environmental problems on earth such as the global warming, water and air pollution. A main factor affecting negatively these processes is the presence of ozone on ground level in many overpopulated cities that is a result of its large industrial synthesis and application (Batakliev *et al.*, 2014). The outdoor ozone break-in into buildings is a threat causing health effects such as decreased lung function and respiratory symptoms (Lai *et al.*, 2015). A number of large-scale studies have found a serious relationship between human mortality and outdoor/indoor ozone exposure (Chen *et al.*, 2012). Contrariwise, the atmospheric ozone, so precious for every living being, is situated mostly in the so-called "ozone layer" from 15 to 30 km above the earth surface wherein the ozone concentration is in the range 10–20 (Ulmann, 1991). The ozone synthesis in the stratosphere runs photochemically by means of solar radiation impact on molecular oxygen (Rakovsky *et al.*, 2007). The atmospheric ozone is really valuable to everything alive on Earth thanks to ozone property to absorb the hard UV-B and UV-C sun radiation in the wavelength range 220–310 nm. The study of kinetics and mechanism of ozone reactions in modern science is closely related to solving the ozone gap problem despite the positive trend of ozone layer recovery in recent years (Figure 1).

The catalytic ozone decomposition on the surface of diverse oxides based on transition metals as well as the use of catalysts modified with noble metals is much more green and low cost method then other techniques as thermal ozone destruction or gas rarefaction by massive air compressors.

Physico-chemical properties and synthesis of ozone

The ozone molecule consists of three oxygen atoms with length of each O-O-bond: $\rho_{o\text{-}o}$ = 1.278 Å and blunt angle between the oxygen bonds of 116.8°. Ozone can get through into each physical state but at normal conditions, the ozone is colorless gas with sharp odor. When the ozone concentration is more than 15–20% it has blue color. At atmospheric pressure and temperature of

Correspondence address:
Dr. Todor Batakliev
Institute of Catalysis,
Bulgarian Academy of Sciences, Sofia, Bulgaria
E-MAIL: todorbat@gmail.com

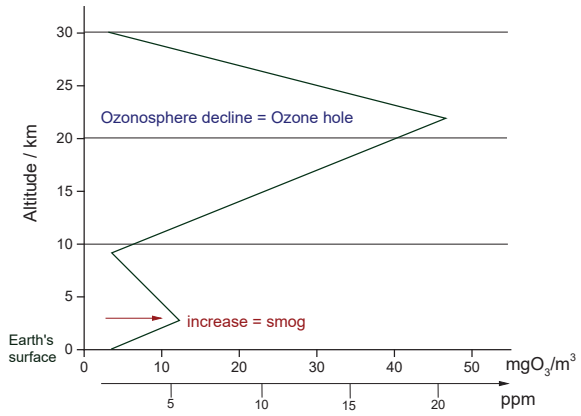

Figure 1. Atmospheric ozone concentration depending on altitude.

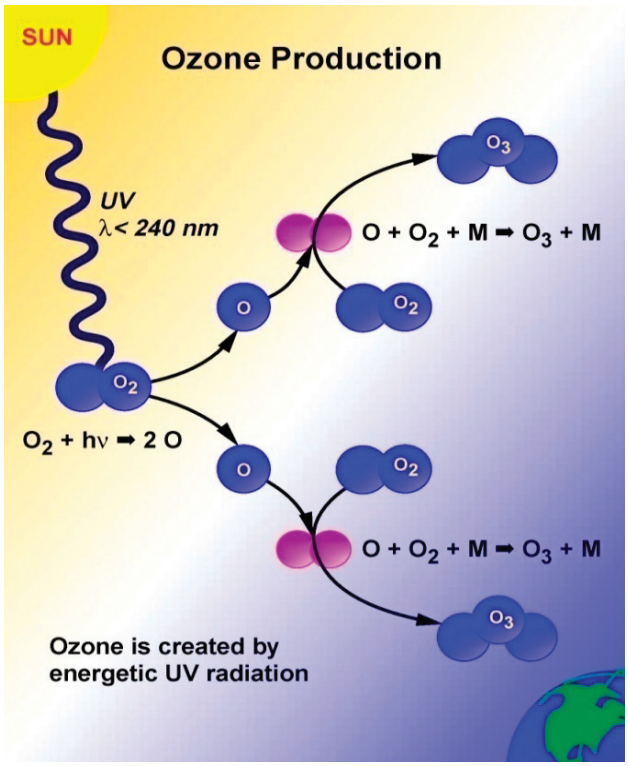

Figure 2. Stratospheric ozone synthesis.

161.3 K, the ozone becomes liquid in deep blue color. It turns into solid at 80.6 K by acquiring dark purple color (Lunin *et al.,* 1998). The risk of ozone detonation is a function of its thermodynamic instability ($\Delta G°298 = -163$ kJ/mol), moreover its decomposition to diatomic oxygen is a thermodynamically conducive process with heat of reaction $\Delta H°298 = -138$ kJ/mol (Perry & Green, 1989).

The creation of ozone in the atmosphere is running photochemically at altitude between 20 and 30 km under the influence of solar UV radiation (wavelength <240 nm). Thereby the ozone concentration is uniformly in the range 10–20 ppm (Figure 2).

For industrial purposes, ozone is synthesized by using pure oxygen by thermal, photochemical, chemical, electrochemical methods, in all forms of electrical discharge

Table 1. Equilibrium constant (K_e) of reaction (2) depending on the temperature

T, K	1500	2000	3000	4000	5000	6000
K_e, M	$1{,}662.10^{-11}$	$4{,}413.10^{-7}$	$1{,}264.10^{-2}$	2.104	48.37	382.9

and under action of a particles stream (Batakliev *et al.,* 2014). The synthesis of ozone is carried out by the following reactions shown in the scheme:

$$O_2 + (e^-, h\nu, T) \rightarrow 2O\ (O_2^*) \quad (1)$$

$$O_2 + O + M \leftrightarrow O_3 + M \quad (2)$$

$$O_2^* + O_2 \rightarrow O_3 + O \quad (3)$$

Where: M is each third particle.

At low temperatures, the ozone consists mainly of molecular oxygen and at higher temperatures of atomic oxygen. There is no area of temperatures at normal pressure wherein the ozone partial pressure is significant. The maximum steady-state pressure, observed at temperature of 350 K, is only 9.10^{-7} bar. The values of the equilibrium constant of reaction (2) at different temperatures are presented in Table 1 (Hon & Yan, 1993).

At high temperatures, when the concentration of atomic oxygen is high, the equilibrium of reaction (2) is moved to the left and the ozone concentration is low. At low temperatures, the equilibrium is shifted to the right but because of the low atomic oxygen concentration the ozone content is negligible. For synthesis of significant ozone concentrations it is always necessary to have the following conditions: 1) low temperature and 2) formation of superequilibrium concentrations of atomic oxygen. Ozone could be formed at low temperatures every time when a process of oxygen dissociation is running. Photochemical synthesis of ozone occurs upon irradiation of gaseous or liquid oxygen by UV radiation with wavelength λ<210 nm (Deninno & McCarthy, 1997). It was suggested (Claudia *et al.,* 1994), that the formation of ozone in presence of radiation with wavelength in the range of $175<\lambda<210$ may be associated with the formation of excited oxygen molecules:

$$O_2 + h\nu \rightarrow (O_2^*) \quad (4)$$

$$O_2^* + O_2 \rightarrow O_3 + O \quad (5)$$

$$O_2 + O + M \leftrightarrow O_3 + M \quad (6)$$

The photochemical ozone synthesis has an important role in atmospheric processes, but it is not easy to apply it for industrial application because of the high energy costs (32 kWh/kg ozone) for generating high-energy shortwave radiation. Nowadays the industrial synthesis of ozone happens mostly by means of electric discharge methods consisting of passing oxygen containing gas through high-voltage (8–10 kV) electrodes. That way, as result of collisions between oxygen molecules and accelerated electrons, part of the kinetic energy is transformed in dissociation energy of O-O bond and formation of excited oxygen molecules at the same time (Rakovsky *et al.,* 2007; Lunin *et al.,* 1998). It is an important precondition before the final step when two molecules of oxygen create one oxygen atom and one ozone molecule:

$O_2 + e \rightarrow 2O\ (O_2^*)$ (7)
$O_2 + O + M \rightarrow O_3 + M$ (8)
$O_2^* + O_2 \leftrightarrow O_3 + O$ (9)

Catalytic ozone decomposition in gas phase

The process of ozone decomposition on the surface of solids is of great interest because of its industrial application. Along with the known gas cycles depleting the atmospheric ozone, the ozone decomposition plays a significant role over aerosols, which their quantity is always a risk due to the anthropogenic factor. The growth of ozone used in chemical industries set up the task for destruction of the residual ozone on heterogeneous environmentally friendly catalysts. In humid environments, under certain temperatures and gas flow rates, this catalytic process, as well as the reaction mechanism, has not been yet fully studied and clarified. The ozone has a great number of advantages as oxidizing agent and, in that ability, it has been used in different scientific investigations done with neutralization of volatile organic contaminants (Skoumal *et al*., 2006; Bianchi *et al*., 2006) as in presence of catalyst the ozonation efficiency is rising (Ma *et al*., 2004; Zhao *et al*., 2008).

The noble metal catalysts and the oxide catalysts based on transition metals have been widely used as catalytic systems for ozone decomposition (Hata *et al*., 1988; Tchihara, 1988; Kobayashi *et al*., 1988; Terui *et al*., 1990; Terui *et al*., 1991; Oohachi *et al*., 1993). The main metals used by the authors were Pt, Pd, Rh and Ce, as well as, metals or metal oxides of Mn, Co, Fe, Ni, Zn, Ag and Cu. The significant price of the noble metals increases the application of metal oxide catalysts having carriers with high specific surface such as γ-Al_2O_3, SiO_2, TiO_2, ZrO_2 and charcoal. Many researchers focused on the development, study and application of catalysts for ozone decomposition based on supported or mixed metal oxides because of the expensive cost of metals as platinum, gold and palladium. In this connection have been the most considerably investigated the oxides of Mn, Co, Cu, Fe, Ni, Si, Ti, Zr, Ag and Al (Oyama, 2000; Einaga & Futamura, 2004; Radhakrishnan *et al*., 2001; Zavadskii *et al*., 2002). It was found that oxide compounds based on transition metals exhibit highest catalytic activity in ozone decomposition (Batakliev *et al*., 2017), and especially the catalysts based on manganese oxide (Batakliev *et al*., 2008). The effect of nickel content in the catalyst was investigated in our paper (Batakliev *et al*., 2017) in terms to elucidate the catalytic activity, stability and mechanical strength of the mixed metal oxides generated by thermal treatment of co-precipitated Ni-Cu-Al samples as catalyst precursors in the reaction of ozone decomposition. The impact of the silver present as a promoter on the catalytic activity was also examined. It could be suggested that during ozone decomposition on transition metal oxides such as NiO-CuO-Al_2O_3 there is formation of intermediate ionic particles possessing either superoxide or peroxide features. The formation of charged chemisorbed oxygen species is accompanied by oxidation of an appropriate number of cations in the oxide crystal lattice to a higher state. In this case it will be the oxidation of Ni^{2+} to Ni^{3+} ions, *scilicet*:

$O_3 + Ni^{2+} \rightarrow O^{2-} + Ni^{3+} + O_2$ (10)
$O_3 + O^{2-} + Ni^{3+} \rightarrow O_2^{2-} + Ni^{3+} + O_2$ (11)
$O_2^{2-} + Ni^{3+} \rightarrow Ni^{2+} + O_2$ (12)

The probable reaction scheme of ozone decomposition consists of electron transfer from the Ni^{2+} center to ozone, resulting in formation of higher oxidation Ni^{3+} species and peroxide particles O_2^{2-}, followed by reduction of Ni^{3+} species by desorption of peroxide particle to form oxygen ($O_2^{2-} \rightarrow O_2 + 2e^-$).

The dissociation of ozone molecules over the surface of metal oxide catalyst based on manganese, nickel and copper oxides was performed by means of kinetic study concerning the equation solution for γ coefficient and activation energy outcome of the process (Batakliev *et al*., 2008). The excellent activity of this catalyst was confirmed by the high values of the coefficient γ found out to be in the range $(2.5–3.5)\times10^{-4}$. Even in humid environment, the decline of catalytic activity did not exceed 20% measured by coefficient values. Following the changes of γ at two different flow rates in the temperature range of 258–323K and using the Arrhenius equation, the calculated activation energy of ozone decomposition reaction was 5 kJ.mol^{-1}. It means that between ozone molecules and catalytic surface appear weak Van der Waals forces and there is running of physisorption during the reaction. Desorption of intermediate species and oxygen molecules is going relatively lightly in expense of the energy shed by catalyst crystal lattice. In another article concerning redox catalytic process in the presence of heterogeneous catalyst (Batakliev *et al*., 2013), the calculated activation energy of ozone decomposition reaction on the surface of manganese oxide catalyst supported on titanium was 11 kJ.mol^{-1}. This value, as the previous cited one, is similar to reported literature data for manganese based catalysts (Radhakrishnan *et al*., 2001). Catalytic cycle of ozone decomposition on MnO_x/TiO_2 catalyst is proposed in Figure 3. This mechanism is based on similar scheme of catalytic ozone decomposition described notably in a paper (Radhakrishnan *et al*., 2001) and in several articles (Reed *et al*., 2005; Xi *at al*., 2005). The transformation of the manganese site from species (I) to (III) is indicative of an oxidation reaction. The structure numbered (II) in Figure 3 is likely a transition state for this first step in the ozone decomposition process. The transformation of species (III) to species (VI) in the proposed catalytic cycle is represented by the redox reaction: $O_3+Mn^{4+}+O^{2-}\rightarrow O_2+O_2^{2-}+Mn^{4+}$. The transition states for this reaction are species (IV) and (V) presented in the catalytic cycle. Finally, the transformation of species (VI) to (I) in the catalytic cycle consist of desorption step and the redox reaction for this step is: $Mn^{4+}+O_2^{2-}\rightarrow O_2+Mn^{2+}$.

Chemical reactions proceeding over heterogeneous α-alumina supported silver catalyst via the dissociative adsorption of O_3 that produces surface chemisorbed atomic oxygen in concentrations sufficiently high to promote oxidation have been described in another article

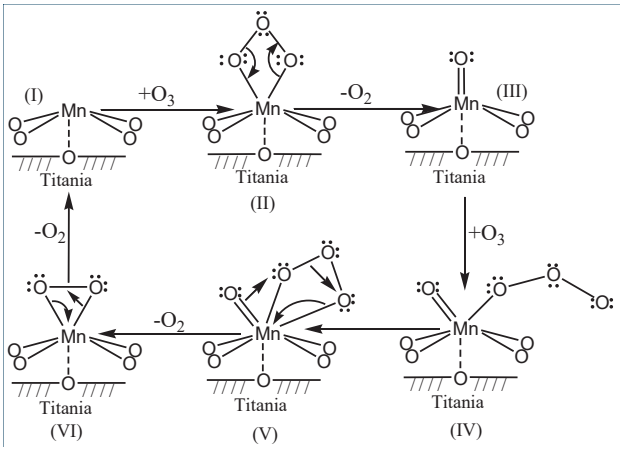

Figure 3. Catalytic cycle of ozone decomposition on MnO_x/TiO_2 catalyst.

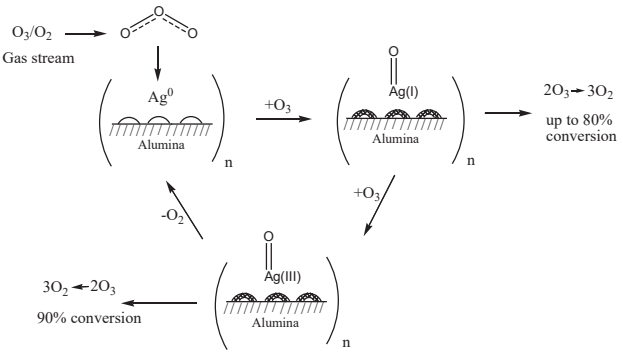

Figure 4. Mechanism of catalytic ozone decomposition on Ag/α-Al_2O_3 catalyst.

(Batakliev *et al.*, 2015). Catalytic scheme of ozone decomposition on Ag/Al_2O_3 catalyst was suggested in Figure 4. The transformation of the silver site from Ag^0 to Ag^{1+} oxidation state is indicative of the occurrence of an oxidation reaction. In this step the ozone conversion is up to 80%. During the next step the Ag^{1+} active site changes its valence state to Ag^{3+} and the ozone conversion becomes already 90%. In the final step of this catalytic cycle the silver active site is reduced and it returns back to the initial coordination state. The ability of silver to provide electrons during the reaction and its high concentration on the catalytic surface increase the probability of the supposed mechanism.

Ion-exchange preparation method of catalysts doped with transition metal was successfully applied for synthesis of materials tested in ozone decomposition reaction (Boevski *et al.*, 2011; Ma *et al.*, 2017). Considering the negative impact of water vapor over catalyst performance due to H_2O molecules adsorption (Batakliev *et al.*, 2008), the authors have studied the activity of cryptomelane-type manganese oxide octahedral molecular sieve (OMS-2) modified with cerium, cobalt and iron transition metal ions in destruction of ozone under high relative humidity. In fact, it has been reported that the structure, morphology, valence state of manganese species, and lattice parameters of OMS-2 can be tuned through single or/and multiple substitution of tunnel K^+ ions and framework Mn ions by different metal ions, such as Cu^{2+}, Ni^{2+}, Co^{2+}, Fe^{3+}, Cr^{3+} and Nb^{5+} (Pahalagedara *et al.*, 2014; Genuino *et al.*, 2015; Sun *et al.*, 2013). ICP-OES and XAFS results confirmed that Co^{3+} and Fe^{3+} replace Mn^{3+} in the cryptomelane structure and Ce^{4+} mainly exchanges the K^+ in the tunnel and partially replaces the Mn^{4+} in the framework of the cryptomelane structure. By using H_2-TPR experiments it was studied the reducibility of the catalysts. The final reduction of MnO_2 was found likely to be MnO with Mn_2O_3 and Mn_3O_4 as intermediates (Bai *et al.*, 2015). The mixed valence states as Mn^{4+} and Mn^{3+} in transition metal oxide samples are significant for electron transfer carrying out in the redox reactions of ozone decomposition catalytic cycle (Wang *et al.*, 2015). Mechanism of ozone decomposition process on the surface of transition metal doped OMS-2 has been presented on the following reaction scheme:

$$O_3 + [Mn^{3+}] \rightarrow O_2 + O^-_{ads}[Mn^{4+}] \quad (13)$$

$$O_3 + O^-_{ads}[Mn^{4+}] \rightarrow 2O_2 + [Mn^{3+}] \quad (14)$$

Plenty of Mn^{3+} active sites located on the catalytic surface could lead to formation of more surface oxygen vacancies, being a precondition for effective ozone decomposition (Jia *et al.*, 2016).

Sub-micrometer spherical $MnCO_3$ has been prepared via a facile co-precipitation method without additive agents at room temperature and characterized by several physical methods (Jia & Zhang, 2018). As-prepared $MnCO_3$ has showed better catalytic activity in ozone decomposition reaction than α-MnO_2 that is usually synthesized by a hydrothermal method (Dong *et al.*, 2014; Su *et al.*, 2013). By XPS analysis of the catalyst after ozonation, the authors have found amorphous MnO_x layer on the $MnCO_3$ surface playing role of active component in the catalytic ozone decomposition whereas the crystalline $MnCO_3$ serves to support stabilizing MnO_x surface phase. The chemical state of Mn was determined to rise from 2.15 to 2.32 during ozone treatment. *In-situ* Raman spectroscopy has been used to detect intermediates when $MnCO_3$ was exposed to the O_2 or O_3/O_2 flow. When the $MnCO_3$ was exposed to the O_3/O_2 flow, a distinct peak at 872 cm^{-1} appeared which could be ascribed to the O-O stretching mode of aggregated peroxide species (Jia *et al.*, 2016).

Catalytic activity of nanocomposites containing mono- and bimetallic Mn(II), Co(II), Cu(II), and Zn(II) complexes with Schiff bases [(salicyl-aldiminopropyl (L1) and 2-hydroxy-4-methoxybenzophenoniminopropyl (L2)] immobilized on silica in the reaction of ozone decomposition has been studied (Rakitskaya *et al.*, 2018). Using nanosilica as precursor for γ-aminopropylsilica synthesis, the authors have received immobilized Schiff bases (salicyl-aldiminopropyl and 2-hydroxy-4-methoxybenzophenoniminopropyl) through some well-known methods (Rakitskaya *et al.*, 2004) (Figure 5).

Monometallic [$M(L)_2$] and bimetallic [Mn-M2-L] complexes have been obtained by adsorption of metal ions from ethanol, acetone or mixture of ethanol-acetone solutions. Best catalytic activity in ozone decomposition reaction has been found for the following complexes: [$Mn(L2)_2$], [Mn-Cu-L2] and [$Mn(L1)_2$].

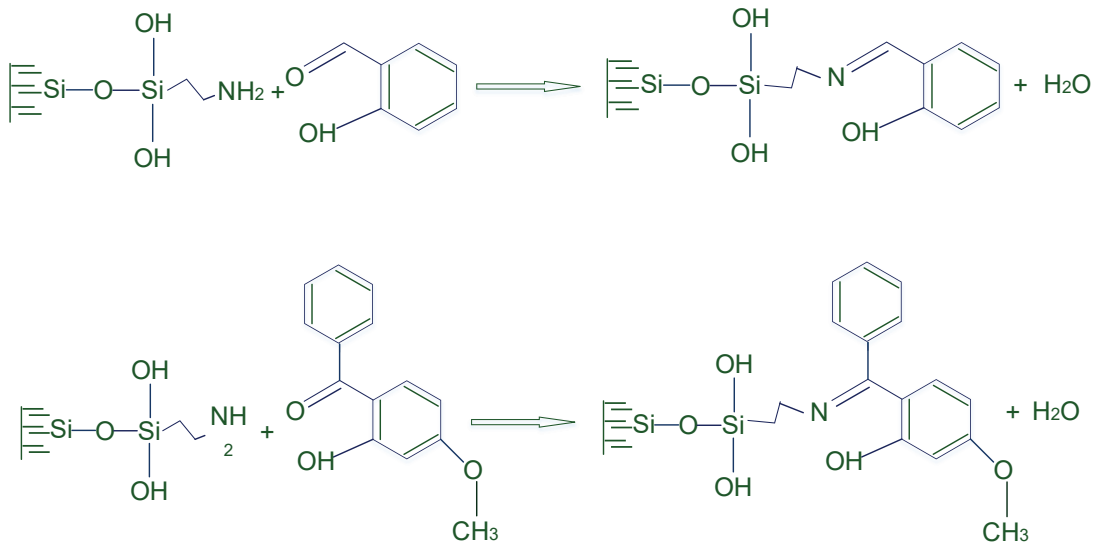

Figure 5. Scheme of immobilized Schiff bases fusion.

In another recent study, nitric acid-treated birnessite-type MnO_2 has been designed for humid ozone decomposition (Liu *et al.*, 2018). Detailed catalysts characterization showed that the higher amount of acid sites and oxygen vacancies together with their improved water-resistant properties facilitates adsorption and subsequent decomposition of humid O_3 over the H-MnO_2. The sample treated by nitric acid (H-MnO_2) exhibited stable O_3 conversion of ~50% within 24 h under 50% of relative humidity (115 ppm of O_3, 600 l g^{-1} h^{-1} of space velocity, 25 °C). The O_3 decomposition efficiency has been much higher over the H-MnO_2 than the pristine MnO_2 indicating that acid treatment could greatly enhance O_3 destruction. The authors ascribed the loss of K^+ cations to the exchange of H^+ into the catalyst layered structure during HNO_3 solution treatment. HNO_3 treatment greatly increased the S_{BET} to 228 m^2 g^{-1} that might be caused either by destabilization of the layered structure after proton exchange (Boppana *et al.*, 2013). XPS analysis has been made to define the oxidation state of surface manganese atoms as well as the nature of O 1s peaks. The Mn $2p_{3/2}$ peaks have given indication that Mn existed in a mixture of Mn^{3+} and Mn^{4+}. Based on the rule of electroneutrality, the higher Mn^{3+}/Mn^{4+} ratio would imply existence of more oxygen vacancies. Therefore, it has been suggested that the oxygen vacancies increased via acid treatment. Water adsorption experiments were performed on a thermogravimetric analyzer over pristine and acid-treated MnO_2. The normalized amount of water adsorption was calculated to be 1.48 mgH_2O/m^2 of catalyst and 0.32 mgH_2O/m^2 of catalyst for pristine and acid-treated MnO_2, respectively, indicating that the acid-treated MnO_2 was much more water-resistant than the pristine MnO_2.

A mechanism involving acid sites and oxygen vacancies for gaseous O_3 decmposition has been illustrated in Figure 6. Ozone molecule is first adsorbed on the surface acid site via latter oxygen atom through hydrogen bond. Then another uttermost oxygen atom of the O_3 molecule

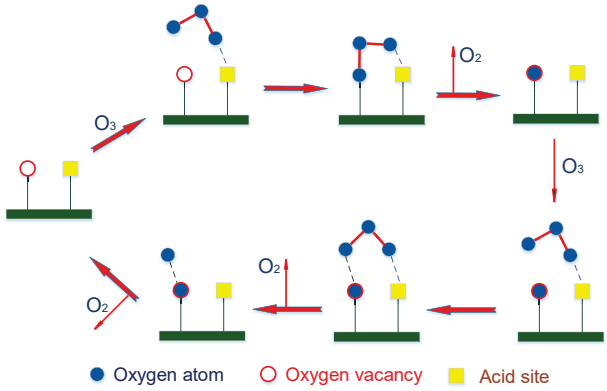

Figure 6. Alleged reaction pathway for gaseous O_3 decomposition.

fall down into an oxygen vacancy site, followed by formation of an O^{2-} species with release of an oxygen molecule into gas phase, and consequently, the acid site is regenerated. After that another one O_3 molecule creates hydrogen bond with surface acid site and the relevant oxygen atom interacts with the formed O^{2-} species to produce peroxide (O_2^{2-}) with simultaneous release of an oxygen molecule. Finally, the O_2^{2-} decomposes desorbing an oxygen molecule and the oxygen vacancy site is therefore regenerated.

The enhancement of the ratio Mn^{3+}/Mn^{4+} due to formation of oxygen vacancies has changed the charge distribution on α-MnO_2 nanofiber catalyst, resulting in an increment of ozone adsorption on the catalytic surface (Zhu *et al.* 2017). DFT calculation revealed that these vacancies could be accepted as active centers for ozone adsorption and afterwards decomposition. The authors have presented possible mechanism referring to such type active site for dry ozone decomposition, see Figure 7. The redox process consisted of three important steps: creation of active oxygen species O^{2-} by electron transfer effect,

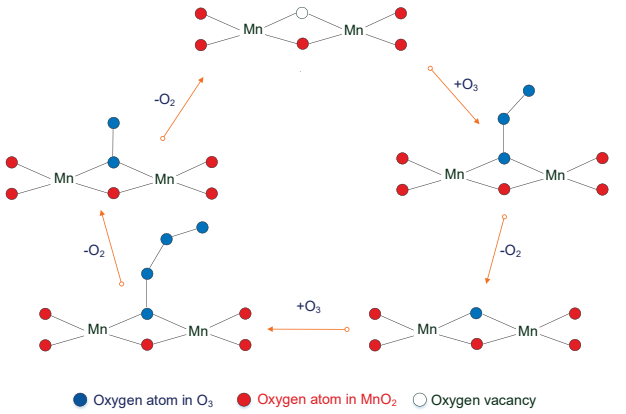

Figure 7. Mechanism of ozone decomposition on α-MnO_2 nanofiber catalyst under dry O_3/O_2 gas flow.

then second step oxidation by ozone generating peroxide species O_2^{2-}, followed finally by their reduction on manganese metal site and release of oxygen molecule.

Efficient catalytic composite system for ozone destruction has been reported notwithstanding the removed amount of ozone was barely 20 ppm O_3/air (Gong *et al.*, 2018). The ozone conversion at high relative humidity levels (ca. 90%) has been found to be above 96%. The excellent performance has been attributed to the highly active ultrafine Cu_2O nanoparticles heterogeneously nucleated on rGO. Cu_2O/rGO composite has exhibited the best catalytic activity in the decomposition of ozone, and this efficiency remained 100% after 10 h of continuous operation in dry air conditions. To explore ozone decomposition mechanism of the highly active Cu_2O/rGO catalyst, the surface states of used Cu_2O/rGO (still active) and that of used pure Cu_2O (deactivated) have been determined by XPS analysis. It was suggested that surface Cu(I) oxidation would not be the main reason for catalyst deactivation. Instead, the generated surface adsorbed oxygen species, during ozone decomposition, cover the active sites of the catalyst surface thus leading to the deactivation of the catalyst. It has been reported that graphene having defects and introduced into the catalyst could promote charge transport and favor activating of reactive molecular species (Gao *et al.*, 2013). The high catalytic activity of Cu_2O/rGO composite was attributed to some synergistic effect between the rGO and ultrafine Cu_2O solid phases that is likely to facilitate the needed electron density transfer in the catalytic process.

Ozone decomposition on copper oxide (CuO_x) with granular activated carbon (GAC) as a support catalyst has been studied in research article (Azhariyah *et al.*, 2018). CuO_x/GAC catalyst with size of 60–100 mesh and loading percentage of 2 wt% was found to have the highest conversion value being reached 100% but at relatively low ozone concentration of 36 ppm. The same Granular Activated Carbon as well as Natural Zeolite (NZ), and Green Sand (GS) have been used for catalytic supports in ozone decomposition reaction (Azhariyah *et al.*, 2018). Active sites comparison has been made using CuO_x and ZnO as metal oxides synthesized over the Granular Activated Carbon. CuO_x/GAC and ZnO/GAC with 2wt% active component in the catalyst structure have showed the highest catalytic activity decomposing 100% of 0.388 mg O_3/min.

If Cu-loaded materials for heterogeneous catalytic ozonation have been prepared by electroless plating-calcination, the deposition rate of metal could be controlled through adjusting the preparation conditions or additive agents in electroless plating process. Moreover, electroless plating might deposit Cu uniformly and densely on the surface of support materials that would result in better catalytic activity compared with those prepared by impregnation (Ren & Lai, 2016). Furthermore, it has been reported that adhesion between the Cu coating and support material obtained by electroless plating would also be much stronger than that of impregnation (Ren *et al.*, 2018). The authors suggested much better electroless plating-calcination comparing to the impregnation-calcination related with Cu-loaded material preparation for applying in catalytic ozonation process. The Cu/Al_2O_3 catalyst synthesized by electroless plating-calcination had uniform and dense deposition of the copper oxide phases on the support surface. Catalytic activity results confirmed the advantage of electroless plating-calcination preparation method showing higher performance of the new Cu/Al_2O_3 catalyst in COD removal during catalytic ozonation of 500 mg/l ρ-nitrophenol in aqueous solution.

According to defined by UV-Vis spectral analysis intermediates, it has been proposed ρ-nitrophenol degradation pathway as result of ozone treatment in presence of Cu/Al_2O_3 catalyst (Figure 8).

Transition metals-modified zeolite has been investigated as environmental catalyst for indoor air ozone decomposition (Mohamed *at al.*, 2018). In terms of O_3 removal efficiency, zeolite-based samples were ranked as follows: Fe-ZSM-5>Cu-ZSM-5>parent ZSM-5. The results revealed about 90% of 13 g/m^3 initial O_3 concentration removal efficiency for Fe-ZSM-5 and 70% for Cu-ZSM-5 as compared to nearly 40% for the parent zeolite. The samples activity has been explained by presence of free Fe and Cu catalytic sites where the exchanged metal ions are coordinated to six-member oxygen rings of aluminum tetrahedra. Removal of the extra-lattice oxygen atoms during high temperature catalyst pre-treatment could result in surface reduction. The following ozone oxidation of these transition metal active centers usually creates highly reactive oxygen species (Mortier, 1982). Some transition metal oxides are able to get involved at redox processes and could be used as reliable catalysts in ozone decomposition reaction. Mechanism based on redox couples including Cu^{+}-Cu^{2+} and Fe^{2+}-Fe^{3+} has been proposed:

$$O_3 + \{M^{n+} - Z\} \rightarrow O_2 + O^{-}\{M^{n+1} - Z\} \quad (15)$$

$$O_3 + O^{-}\{M^{n+1} - Z\} \rightarrow 2O_2 + \{M^{n+} - Z\} \quad (16)$$

where: M is Cu or Fe and Z is zeolite type ZSM-5.

The reported relatively good activity in ozone destruction of zeolite-based catalysts has been attributed to formation of framework Al-O-M (M: Cu or Fe) as well as to

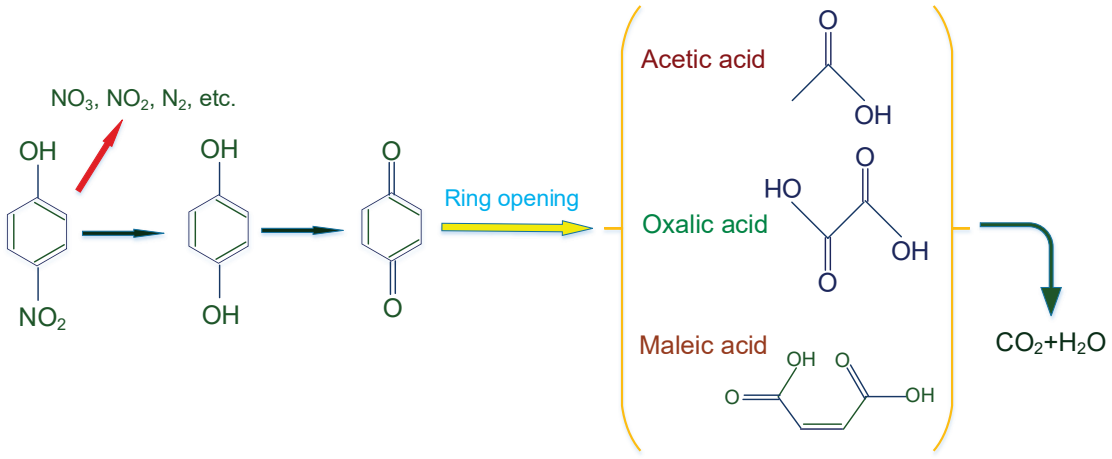

Figure 8. Proposed reaction pathway for the degradation of PNP by O_3 + Cu/Al_2O_3 prepared by electroless plating-calcination system.

alleged synergistic effect between zeolite and metal active sites improving ozone conversion on the catalytic surface.

Simultaneous catalytic decomposition of formaldehyde and ozone over manganese cerium oxides at room temperature has been examined depending on relative humidity of the gas stream passing by continuous-flow fixed-bed reactor under atmospheric pressure (Zhang *et al.*, 2018). The catalytic activity of $MnCeO_x$ catalyst has been compared with the solo MnO_x and CeO_2 catalysts to clarify the promotional effect of the formation of Mn-Ce solid solution on the catalytic activities. Investigation of the oxygen mobility and oxygen vacancies of the catalysts was carried out by O_2-TPD analysis. The spectral peaks have been attributed to physical adsorption of O_2 molecules, molecular oxygen species adsorbed on surface oxygen vacancy (O_I : O_2^-, O_2^{2-}), atomic oxygen species adsorbed on surface oxygen vacancy (O_{II} : O^-, O^{2-}, O^*), and lattice oxygen on the catalyst surface (O_{III}), respectively. In humid environment, the presence of water vapor creates surface hydroxyl groups resulting in the complete oxidation of most formaldehyde in the flow stream over $MnCeO_x$ catalyst at room temperature. That process is fed from the interaction between adsorbed water molecules with surface oxygen species generated from decomposition of ozone on the catalyst surface. *In situ* DRIFT spectrum of HCHO adsorption on $MnCeO_x$ catalyst has shown that after ozone inducement the absorbance at 3654 cm^{-1}, assigned to the OH stretching vibration ν(OH) of structural hydroxyl groups, significantly increases due to surface hydroxyl groups regeneration as result of HCHO and O_3 reaction on the catalyst surface. The absorbance of surface adsorbed water also continuously increased along with the reaction time growing and the absorbance at 3267 cm^{-1} was assigned to the OH stretching vibration ν(OH) of carboxylic acids.

NiO_x, CoO_x and MnO_x transition metal oxide catalysts have been allowed to the decomposition of toxic by-products as ozone (O_3) and nitrogen oxides (NO_x), formed in non-thermal plasma processes for indoor air treatment (Chen *et al.*, 2018). The 5 wt% MnO_x/Al_2O_3 catalyst was impregnated with different trichloro(alkyl)silanes in order to improve the ozone removal efficiency at 60% relative humidity in the air environment. As a ceramic material made from metal oxide, Al_2O_3 is hydrophilic in nature thank to the presence of hydroxyl groups on its surface (Kujawa *et al.*, 2015). The hydrophilic surface of alumina can be changed to a hydrophobic property by a surface modification treatment. Organosilanes such as methyl-, linear alkyl-, aromatic, and perfluorinated alkylsilanes are the most widely used materials for hydrophobic surface modification (Esmaeilirad *et al.*, 2016). Trichloro(alkyl) silanes possess three major parts: an organo-functional group, a linker and hydrolysable groups, which can be hydrolyzed and condensed to oligomers during the modification process. Stable covalent bonds could be created between the hydrolysable groups of the modifying agent and the hydroxyl groups on the substrate. The aliphatic hydrocarbon substituent changes the surface character of a ceramic material from hydrophilic to hydrophobic. A new mechanism based on some previous research (Tidahy *et al.*, 2007) for O_3 decomposition on the surface of γ-Al_2O_3 supported transition metal oxide catalyst was alleged:

$$O_3 + M^{n+} \rightarrow O^{2-} + M^{(n+2)+} + O_2 \quad (17)$$

$$O_3 + O^{2-} + M^{(n+2)+} \rightarrow O_2^{2-} + M^{(n+2)+} + O_2 \quad (18)$$

$$O_2^{2-} + M^{(n+2)+} \rightarrow O_2 + M^{n+} \quad (19)$$

The process of NO oxidation by ozone in presence of TiO_2 catalyst has been investigated at diverse NO inlet concentrations, gas flow rates and reactor temperatures (Jõgi *et al.*, 2016). Independent of reaction conditions and presence of catalyst, NO was totally oxidized to NO_2 when the inlet O_3 concentration reached the value of the inlet NO concentration. Further rise of inlet O_3 concentration resulted in oxidation of NO_2 to N_2O_5. The effect of TiO_2 catalyst appeared at higher reactor temperatures where the presence of TiO_2 increased the oxidation efficiency of NO_2 to N_2O_5 promoted by the presence of oxygen species created on the surface by catalytic decomposition of ozone. The oxidation of NO to NO_2 has been reported to be almost stoichiometric i.e. one O_3 molecule spun out

for one NO molecule (Mok, 2006). Further oxidation of NO_2 to N_2O_5 was less efficient and required either surplus amount of ozone or more continuous reaction time (Skalska *et al.*, 2012). The catalytic gas phase oxidation of NO_2 to N_2O_5 at 100 °C was limited by the formation of NO_3. The authors suggested that the additional formation of NO_3 takes place by the reaction between NO_2 and oxygen atoms stored on the TiO_2 surface: $NO_2+O \rightarrow NO_3$. These stored oxygen atoms are most likely formed as result of the ozone decomposition on TiO_2 surface: $O_3(g) \rightarrow O_2(g)+O$.

Catalytic ozone decomposition in gas-solids circulating fluidized-bed (CFB) riser has been investigated using computational fluid dynamics modeling (Kong *et al.*, 2013). The reaction was implemented on iron-impregnated fluid catalytic cracking particles and it was defined as a one-step first-order reaction: $O_3 \xrightarrow{\text{catalyst}} 1.5O_2$. During the fluidization process in a CFB, a catalytic ozone decomposition into diatomic oxygen required low concentrations of ozone so that the gas density and temperature changes caused by the reaction in the CFB could be overlooked. The simulation results have been compared with experimental data and the reaction rate was modified by using an empirical coefficient to provide better simulation results than the original reaction rate. It was found that particle size has great effect on the reaction rate redounded by the contact surface area in gas-solids interface.

Effective copper and manganese grafting over commercial titanium dioxide was reported to increase significantly the photocatalyst ozone decomposition rate (Patzsch&Bloh, 2018). Iron grafting appeared to be the most universal method of improving the photocatalytic ozone removal rate as even extremely low iron grafting ratios of 0.002 at.% were found to be sufficient to dramatically improve the catalyst performance. The means of ozone on NO_x-based air pollution is considerable because of the NO_2 formation by ozone initiated oxidation reactions. Direct NO_x abatement on titanium dioxide is quite challenging as the reaction involves several toxic intermediates, which may be released in the process (Bloh *et al.*, 2014). González-Elipe and co-workers shown that ozone can be photocatalytically decomposed on UV illuminated titanium dioxide surfaces (González-Elipe *et al.*, 1981). Mechanism of the redox process, including some short-lived intermediates and confirmed by EPR spectroscopy, is presented below:

$$OH^- + h^+ \rightarrow OH^\bullet + e^- \quad (20)$$
$$O_3 + e^- \rightarrow O_3^- \quad (21)$$
$$O_3 + OH^\bullet \rightarrow O_4^- + H^+ \quad (22)$$
$$O_3^- + O_3 \rightarrow O_2 + O_4^- \quad (23)$$
$$2O_3^- \rightarrow O_2 + 2O_2^- \quad (24)$$
$$O_4^- \rightarrow O_2 + O_2^- \quad (25)$$

This study has showed that ozone decomposition efficiency as simple and inexpensive method could improve the overall air cleaning properties of the photocatalyst. The authors explored the strategy of transition-metal grafting to increase the ozone-photo-degradation rate of titanium dioxide based photocatalysts. This grafting process has been reported to enhance the UVA as well as the visible light activity of many photocatalysts as the transition metal ions are strongly adsorbed onto the host crystals where they form small isolated ions or clusters facilitating this way charge carrier separation and electron transfer kinetics (Irie *et al.*, 2008; Liu *et al.*, 2012; Nishikawa *et al.*, 2013). It should be mentioned that the photocatalysts modified with Cu, Mn and Fe ions have been tested in ozone decomposition reaction applying relatively low inlet ozone concentration of 1 ppm.

Zinc oxide, as active phase, and granular activated carbon, as support, have been combined in catalyst for gas phase ozone destruction (Pradyasti *et al.*, 2018). The reaction was performed at room temperature and atmospheric pressure using fixed bed reactor. Crystal phase analysis of the catalysts before and after calcination at 300 °C has been studied by X-ray diffraction (XRD). The catalyst structure was found to be $ZnCO_3$ prior to thermal treatment and ZnO-after thermal treatment. Impurities located on the catalytic surface have been removed by HCl and NaOH processing, improving that way the activity of the ZnO/GAC catalyst in ozone decomposition reaction. Another application of activated carbon (AC) used as MnO_x catalyst support has been reported in a paper depicting the effects of Mn loading on the catalytic structure and ozone decomposition activity (Wang *et al.*, 2014). The catalytic activity was linked with the morphology and MnO_x content. The catalyst having 1.1wt% MnO_x exhibited better performance in ozone destruction because of its porous lichen-like structure compared to the compact morphology and ticker MnO_x layer of 11wt% MnOx/AC catalytic sample.

Catalytic ozone decomposition in water

In recent article (Li *et al.*, 2018), a Fe-based catalyst has been used as a heterogeneous catalyst for ozonation of industrial wastewater and some key operational parameters (pH and catalyst dosage) have been studied. It has been found indication of significantly improved mineralization of organic pollutants in wastewater. TOC removal was reported to be 78.7% at catalyst concentration of 200 g/l and 31.6% at ozonation without presence of catalyst. The Fe-based catalyst has promoted 70% ozone conversion into molecular oxygen in aqueous solution. Through characterization by SEM-EDS, XRD and XPS, it was suggested that FeOOH being on the catalyst surface was the main contributor to catalytic efficiency. Initial pH is one of the most important factors influencing the efficiency of ozonation in water. The authors claim that COD removal is much higher at pH 6 and 8 than that at pH 6.81 and 9, which indicated that COD treatment was much better in weak acid and weak base solutions. However, the Fe-based catalyst could be positively effective at pH 6–9 (Oputu *et al.*, 2015; Ghasemi *et al.*, 2016; Hadavifar *et al.*, 2016). Meanwhile, high pH means the presence of a significant concentration of hydroxyl anions (OH^-) that was confirmed to be an initiator for the decomposition of ozone reflecting in formation of OH radicals

(Staehelin&Hoigne, 1982). Hydroxyl radicals have been detected through EPR technology directly and $NaHCO_3$ scavenging experiments indirectly. It was verified that $HO^{\bullet}$ is a great contributor to mineralization of organic pollutants. The Fe-based catalyst was found to promote ozone decomposition in aqueous solution, which could be responsible for generation of $HO^{\bullet}$.

Synergistically, catalytic effect between $Mn^{4+/3+}$ and $Ce^{4+/3+}$ redox couples in manganese-cerium mixed oxides supported on practicable mesoporous γ-Al_2O_3 has been described in terms of catalyst surface properties and performance as well as reaction mechanism and kinetics during catalytic ozonation of bromaminic acid (BAA) in water solution (Wu *et al.*, 2018). The contribution of $Mn^{4+/3+}$ and $Ce^{4+/3+}$ redox couples to oxygen vacancies formation is presented on Figure 9(A). These oxygen vacancies could work as catalytic active sites for adsorption of ozone molecules that further would decompose via electron transfer from surface $Ce^{3+}$and Mn^{3+} species to create strong $HO^{\bullet}$ and $O_2^{\bullet-}$ radicals as depicted on Figure 9(B). Possible degradation pathway of 1-amino-4-bromoanthraquinone-2-sulfonic acid via Mn-CeO_x/γ-Al_2O_3-catalyzed ozonation was suggested in Figure 10.

BAA degradation mechanism through Mn-CeO_x/γ-Al_2O_3 catalyzed ozonation was based on important information about intermediates generation obtained by monitoring pH changes during single and catalytic ozonation as well as on intermediates identification by LC-MS analysis. The authors reported that during catalyzed ozonation the larger final pH of the solution is mainly due to generation of $HO^{\bullet}$ and $O_2^{\bullet}$ radicals, which could mineralize the acidic intermediates effectively. The adsorption of water molecules onto surface Lewis acid sites leads to their dissociation into protonated surface hydroxyl groups OH_2^+ bonded on catalyst surface, see Figure 9(B). Then the aqueous ozone molecules can interact with Brønsted acid $S–OH_2^+$ (S refers to catalyst surface) forming surface complex $S–OH_2^+–O_3$ via hydrogen bonding and/or electrostatic forces, due to the electrophilic and nucleophilic resonance structure of the ozone molecule (Qi *et al.*, 2010; Larachi *et al.*, 2002).

Summary and perspective

This review was focused on the mechanism of gas phase ozone decomposition process mostly considering optional reaction pathways based on short-lived molecular and atomic oxygen species acting as intermediates. The ozone decomposition in water environment could enhance the formation of hydroxyl radicals that play significant role in the process of water pollutants removal. Nowadays, highly efficient ozone decomposition is still representing a technological challenge especially in the presence of

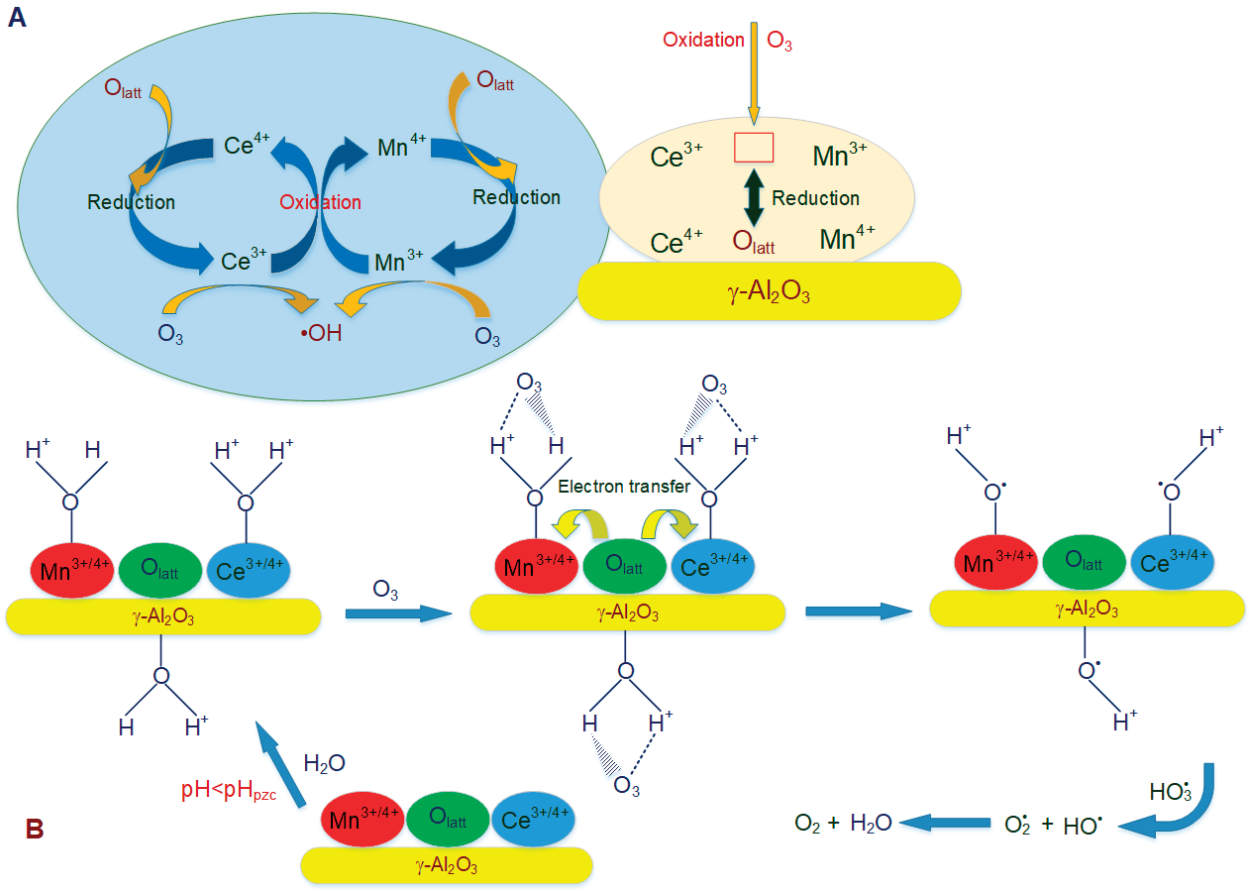

Figure 9. Scheme of Mn–CeO_x synergistic effect in catalytic process (a); and Alleged ozone decomposition mechanism on the surface of Mn–CeO_x/γ-Al_2O_3 catalyst (b).

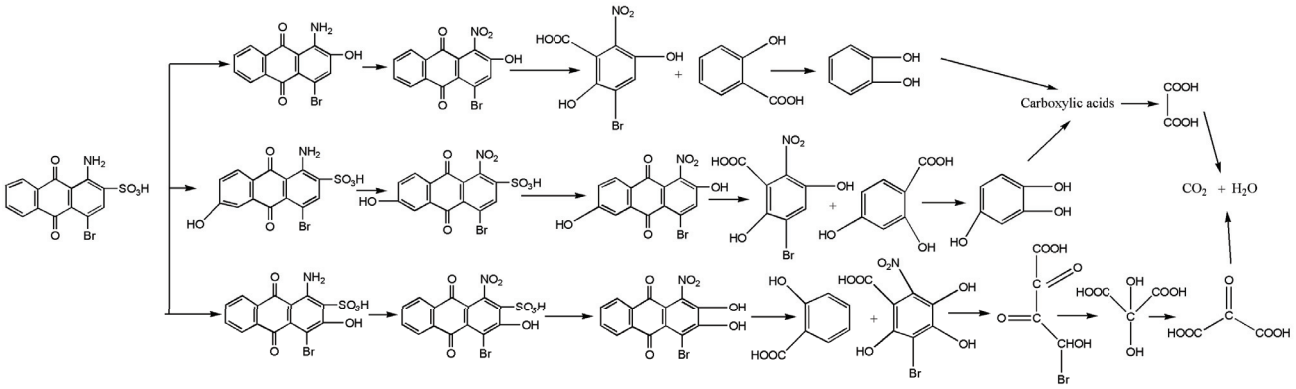

Figure 10. Suggested BAA degradation routes by the Mn-CeO_x/γ-Al_2O_3-catalyzed ozonation.

high humidity levels. The effect of water vapor is probably a result of thin film formation on the catalytic surface thus making the diffusion of ozone to the catalytic active centers more difficult. The synthesis of mixed oxide solid solution based on transition metals could create strong synergistic effect and give rise to larger number of adsorbed ozone molecules participating in preferable low temperature redox catalytic cycle that makes a great contribution to its superior activity. The physical characterization of metal oxide catalysts forming solid solution disclosed significant profusion of oxygen vacancies and surface lattice oxygen species improving the catalytic adsorption and redox properties. The main perspective in ozone decomposition research remains the *"in situ"* detection of all intermediate species generated and participating in the catalytic cycle of the reaction process using appropriate physical methods that should be applied with innovative and reliable experimental set-up. Deep kinetics investigations, including probable new models, have to be used in order to clarify the ozone degradation pathway on the surface of metal oxide catalysts.

REFERENCES

Azhariyah AS, Pradyasti A, Bismo S. (2018). Preparation and characterization of copper oxide catalyst with activated carbon support for ozone decomposition in industrial environment. *IOP Conf. Series: Earth and Environmental Science* **105**: 012012.

Azhariyah AS, Pradyasti A, Dianty AG, Bismo S. (2018). Comparative study of activated carbon, natural zeolite, and green sand supports for CuO_x and ZnO sites as ozone decomposition catalyst. *IOP Conf. Series: Earth and Environmental Science* **334**: 012075.

Bai B, Li J, Hao J. (2015). 1D–MnO_2, 2D–MnO_2 and 3D–MnO_2 for low–temperature oxidation of ethanol. *Appl Catal B Environ* **164**: 241–250.

Batakliev T, Rakovsky S, Zaikov G.E. (2008). Investigation of metal oxide catalyst in ozone decomposition. *Oxidation Communications* **31** (1): 145–150.

Batakliev T, Georgiev V, Anachkov M, Rakovsky S, Zaikov GE. (2014). Ozone decomposition. *Interdiscip Toxicol* **7**(2): 47–59.

Batakliev T, Georgiev V, Karakashkova P, Gabrovska M, Nikolova D, Anachkov M, Rakovsky S. (2017). Gas phase ozone decomposition over co-precipitated Ni-based catalysts. *Bulg Chem Commun* **49**(Special Issue L): 24–29.

Batakliev T, Tyuliev G, Georgiev V, Eliyas A, Anachkov M, Rakovsky S. (2015). Ozone decomposition reaction over α-alumina supported silver catalyst: comparative study of catalytic surface reactivity. *Ozone Sci Eng* **37**: 216–220.

Boevski I, Genov K, Boevska N, Milenova K, Batakliev T, Georgiev V, Nikolov P, Sarker DK. (2011). Low temperature ozone decomposition on Cu^{2+}, Zn^{2+} and Mn^{2+} – exchanged clinoptilolite. *CR ACAD BULG SCI* **64**(1): 33–38.

Bianchi CL, Pirola C, Ragaini V, Selli E. (2006). Mechanism and efficiency of atrazine degradation under combined oxidation processes. *Appl Catal B Environ* **64**: 131–138.

Bloh JZ, Folli A, Macphee DE. (2014). Photocatalytic NO_x abatement: why the selectivity matters. *RSC Adv* **4**: 45726–45734.

Boppana VBR, Yusuf S, Hutchings GS, Jiao F. (2013). Nanostructured alkaline–cation–containing δ–MnO_2 for photocatalytic water oxidation. *Adv Funct Mater* **23**: 878–884.

Chen C, Zhao B, Weschler CJ. (2012). Assessing the influence of indoor exposure to "outdoor ozone" on the relationship between ozone and short-term mortality in US communities. *Environ Health Perspect* **120**: 235–240.

Chen L, Ondarts M, Outin J, Gonthier Y, Gonze E. (2018). Catalytic decomposition performance for O_3 and NO_2 in humid indoor air on a MnO_x/Al_2O_3 catalyst modified by a cost-effective chemical grafting method. *J Environ Sci* **74**: 58–70.

Claudia C, Mincione E, Saladino R, Nicoletti R. (1994). Oxidation of Substituted 2-Thiouracils and Pyramidine-2-Thione with Ozone and 3,3-Dimethyl-1,2-Dioxiran. *Tetrahedron* **50**(10): 3259–3272.

Deninno MP, McCarthy KE. (1997). The C-14 radiolabelled synthesis of the cholesterol absorption inhibitor CP-148,623. A novel method for the incorporation of a C-14 label in enones. *Tetrahedron* **53**(32): 11007–11020.

Dong Y, Kun L, Jiang P, Wang G, Miao H, Zhang J, Zhang C. (2014). Simple Hydrothermal Preparation of Alpha–, Beta–, and Gamma–MnO_2 and Phase Sensitivity in Catalytic Ozonation. *RSC Adv.* **4**(74): 39167–39173.

Einaga H, Harada M, Futamura S. (2005). Structural Changes in Alumina-supported Manganese Oxides during Ozone Decomposition. *Chem. Phys. Lett.* **408**: 377.

Esmaeilirad A, Rukosuyev MV, Jun MBG, Van Veggel FCJM. (2016). A cost-effective method to create physically and thermally stable and storable superhydrophobic aluminum alloy surfaces. *Surf. Coat. Technol.* **285**: 227–234.

Gao E, Wang W. (2013). Role of graphene on the surface chemical reactions of $BiPO_4$–rGO with low OH–related defects, *Nano* **5**: 11248–11256.

Genuino HC, Seraji MS, Meng YT, Valencia D, Suib SL. Combined experimental and computational study of CO oxidation promoted by Nb in manganese oxide octahedral molecular sieves. (2015). *Appl Catal B Environ* **163**: 361–369.

Ghasemi Z, Younesi H, Zinatizadeh AA. (2016). Preparation, characterization and photocatalytic application of TiO_2/Fe-ZSM-5 nanocomposite for the treatment of petroleum refinery wastewater: optimization of process parameters by response surface methodology. *Chemosphere* **159**: 552–564.

Gong S, Chen J, Wu X, Nan N, Chen Y. (2018). *In-situ* synthesis of Cu_2O/reduced graphene oxide composite as effective catalyst for ozone decomposition. *Catal Commun* **106**: 25–29.

González-Elipe AR, Soria J, Munuera G. (1981). Photo-decomposition of ozone on TiO_2. *Zeitschrift Für Phys Chem* **126**: 251–257.

Hadavifar M, Younesi H, Zinatizadeh AA, Mahdad F, Li Q, Ghasemi Z. 2016. Application of integrated ozone and granular activated carbon for decolorization and chemical oxygen demand reduction of vinasse from alcohol distilleries. *J Environ Manag* **170**: 28–36.

Hata K, Horiuchi M, Takasaki T. (1988). Preparation of high performance metal catalyst. Jap Pat CA, 108, 61754u.

Irie H, Miura S, Kamiya K, Hashimoto K. (2008). Efficient visible light-sensitive photocatalysts: grafting Cu(II) ions onto TiO_2 and WO_3 photocatalysts. *Chem Phys Lett* **457**: 202–205.

Jia JB, Zhang PY, Chen L. (2016). Catalytic decomposition of gaseous ozone over manganese dioxides with different crystal structures. *Appl Catal B Environ* **189**: 210–218.

Jia J, Zhang P, Chen L. (2016). The Effect of Morphology of A–MnO_2 on Catalytic Decomposition of Gaseous Ozone. *Catal Sci Technol* **6**(15): 5841–7.

Jia J, Zhang P. (2018). Catalytic Decomposition of Airborne Ozone by $MnCO_3$ and its Mechanism, *Ozone Sci Eng* **40**(1): 21–28.

Jõgi I, Erme K, Raud J, Laan M. (2016). Oxidation of NO by ozone in the presence of TiO_2 catalyst, *Fuel* **173**: 45–51.

Kobayashi M, Mitsui M, Kiichiro K. (1988). Chemical composition of metal oxide catalysts. Jap Pat CA, 109, 175615a.

Kong L, Zhu J, Zhang C. (2014). Catalytic Ozone Decomposition in a Gas-Solids Circulating Fluidized-Bed Riser. *Chem Eng Technol* **37 (3)**: 435–444.

Kujawa J, Cerneaux S, Kujawski W. (2015). Highly hydrophobic ceramic membranes applied to the removal of volatile organic compounds in pervaporation. *Chem Eng J* **260**: 43–54.

Lai D, Karava P, Chen Q. (2015). Study of outdoor ozone penetration into buildings through ventilation and infiltration. *Build Environ* **93**: 112–118.

Larachi F, Pierre J, Adnot A, Bernis A. (2002). Ce 3d XPS study of composite $Ce_xMn_{1-x}O_{2-y}$ wet oxidation catalysts. *Appl Surf Sci* **195**: 236–250.

Li X, Chen W, Ma L, Wang H, Fan J. (2018). Industrial wastewater advanced treatment via catalytic ozonation with a Fe-based catalyst, *Chemosphere* **195**: 336–343.

Liu G, Yin L-C, Wang J, Niu P, Zhen C, Xie Y, Cheng H–M. (2012). A red anatase TiO_2 photocatalyst for solar energy conversion. *Energy Environ Sci* **5**: 9603.

Liu Y, Yang W, Zhang P, Zhang J. (2018). Nitric acid-treated birnessite-type MnO_2: An efficient and hydrophobic material for humid ozone decomposition. *Appl Surf Sci* **442**: 640–649.

Lunin VV, Popovich MP, Tkachenko SN. (1998). Physical Chemistry of Ozone. Moscow State University Publisher, 480 p. [in Russian].

Ma J, Sui MH, Chen ZL, Li NW. (2004). Degradation of Refractory Organic Pollutants by Catalytic Ozonation—Activated Carbon and Mn-Loaded Activated Carbon as Catalysts. *Ozone Sci Eng* **26**(1): 3–10.

Ma J, Wang C, Hong H. (2017). Transition metal doped cryptomelane–type manganese oxide catalysts for ozone decomposition. *Appl Catal B Environ* **201**: 503–510.

Mohamed EF, Awad G, Zaitan H, Andriantsiferana C, Manero M–H. (2018). Transition metals-incorporated zeolites as environmental catalysts for indoor air ozone decomposition. *Environ Technol* **39**(7): 878–886.

Mok YS, Yoon EY. (2006). Effect of Ozone Injection on the Catalytic Reduction of Nitrogen Oxides. *Ozone Sci Eng* **28**: 105–110.

Mortier J. (1982). *Compilation of extra framework sites in zeolites*, Guildford: Butterworth Sci. Ltd., 67 p.

Nishikawa M, Hiura S, Mitani Y, Nosaka Y. (2013). Enhanced photocatalytic activity of $BiVO_4$ by co-grafting of metal ions and combining with $CuBi_2O_4$. *J Photochem Photobiol A Chem* **262**: 52–56.

Oohachi K, Fukutake T, Sunao T. (1993). Method for synthesis of iron oxides. Jap Pat CA, 119, 119194g.

Oputu O, Chowdhury M, Nyamayaro K, Fatoki O, Fester V. (2015). Catalytic activities of ultra-small beta-FeOOH nanorods in ozonation of 4-chlorophenol. *J Environ Sci* **35**: 83–90.

Oyama ST. (2000). Chemical and Catalytic Properties of Ozone. *Catal Rev Sci Eng* **42**: 279.

Pahalagedara LR, Dharmarathna S, King'ondu CK, Pahalagedara MN, Meng YT, Kuo CH, Suib SL. (2014). Microwave-Assisted Hydrothermal Synthesis of α-MnO_2: Lattice Expansion via Rapid Temperature Ramping and Framework Substitution. *J Phys Chem C* **118**: 20363–20373.

Patzsch J, Bloh J. (2018). Improved photocatalytic ozone abatement over transition metal-grafted titanium dioxide. *Catal Today* **300**: 2–11.

Perry RH, Green D. (1989). *Perry's Chemical Engineer's Handbook*, McGraw-Hill, New York, 147 p.

Pradyasti A, Azhariyah AS, Karamah EF, Bismo S. (2018). Preparation of zinc oxide catalyst with activated carbon support for ozone decomposition. *IOP Conf Ser Earth Environ Sci* **105**: 012013.

Qi F, Chu W, Xu B. (2016). Comparison of phenacetin degradation in aqueous solutions by catalytic ozonation with $CuFe_2O_4$ and its precursor: Surface properties, intermediates and reaction mechanisms. *Chem Eng J* **284**: 28–36.

Radhakrishnan R, Oyama ST, Chen J, Asakura A. (2001). Electron Transfer Effects in Ozone Decomposition on Supported Manganese Oxide. *J Phys Chem B* **105**(19): 4245–4253.

Rakitskaya T, Truba A, Radchenko E, Golub A. (2018). Mono- and Bimetallic Complexes of Mn(II), Co(II), Cu(II), AND Zn(II) with Schiff Bases Immobilized on Nanosilica as Catalysts in Ozone Decomposition Reaction, *Chem Chem Technol* **12**(1): 1–6.

Rakyts'ka T., Pidmazko A., Golub O. (2004). Compositions Based on Pl(II) and Cu(II) Compounds, Halide Ions, and Bentonite for Ozone Decomposition. *Ukr Khim Zh* **70**: 16 [in Ukrainians].

Rakovsky SK, Zaikov GE. (2007). *Kinetic and mechanism of ozone reactions with organic and polymeric compounds in liquid phase – 2nd edition*, Nova Sci. Publ., Inc. New York.

Reed C, Xi Y, Oyama ST. (2005). Distinguishing between reaction intermediates and spectators: a kinetic study of acetone oxidation using ozone on a silica-supported manganese oxide catalyst. *J Catal* **235**: 378–392.

Ren Y, Lai B. (2016). Comparative study on the characteristics, operational life and reactivity of Fe/Cu bimetallic particles prepared by electroless and displacement plating process. *RSC Adv* **6**: 58302–58314.

Ren Y, Li J, Peng J, Ji F, Lai B. (2018). Strengthening the catalytic activity for ozonation of Cu/Al_2O_3 by an electroless plating–calcination process. *Ind Eng Chem Res* **57**: 1815–1825.

Qi F, Xu B, Chen Z, Zhang L, Zhang P, Sun D. (2010). Mechanism investigation of catalyzed ozonation of 2-methylisoborneol in drinking water over aluminum (hydroxyl) oxides: Role of surface hydroxyl group. *Chem Eng J* **165**: 490–499.

Skalska K, Miller JS, Wilk M, Ledakowicz S. (2012). Nitrogen Oxides Ozonation as a Method for NO_x Emission Abatement. *Ozone Sci Eng* **34**: 252–258.

Skoumal M, Cabot PL, Centellas F, Arias C, Rodriguez RM, Garrido JA, Brillas E. (2006). *Appl Catal B Environ* **66**: 228–240.

Staehelin J, Hoigne J. (1982). Decomposition of ozone in water–rate of initiation by hydroxide ions and hydrogen–peroxide. *Environ Sci Technol* **16**: 676–681.

Su D, Ahn H–J, Wang G. (2013). Hydrothermal synthesis of α-MnO_2 and β-MnO_2 nanorods as high capacity cathode materials for sodium ion batteries. *J Mater Chem A* **1**: 4845–4850.

Sun M, Yu L, Ye F, Diao GQ, Yu Q, Hao ZF, Zheng YY, Yuan LX. (2013). Transition metal doped cryptomelane-type manganese oxide for low-temperature catalytic combustion of dimethyl ether. *Chem. Eng. J.* **220**: 320–327.

Tchihara S. (1988). Cobalt catalyst for decomposition of ozone. Jap Pat CA, 108, 192035h.

Terui S, Sadao K, Sano N, Nichikawa T. (1990). Synthesis of supported silver oxide catalysts. Jap Pat CA, 112, 20404p.

Terui S, Sadao K, Sano N, Nichikawa T. (1991). Investigation on Pd and Rh catalysts supported on colloidal polyurethane for ozone destruction. Jap Pat CA, 114, 108179b.

Tidahy HL, Siffert S, Wyrwalski F, Lamonier J–F, Aboukaïs A. (2007). Catalytic activity of copper and palladium based catalysts for toluene total oxidation. *Catal Today* **119**: 317–320.

Wang C, Ma J, Liu F, He H, Zhang R. (2015). The Effects of Mn^{2+} Precursors on the Structure and Ozone Decomposition Activity of Cryptomelane-Type Manganese Oxide (OMS–2) Catalysts. *J Phys Chem C* **119**: 23119–23126.

Wang M, Zhang P, Li J, Jiang C. (2014). The effects of Mn loading on the structure and ozone decomposition activity of MnOx supported on activated carbon. *Chinese J Catal* **35**: 335–341.

Wiley-VCH. (1991). *Ullmann's Encyclopedia of Industrial Chemistry*. John Wiley and Sons, New York.

Wu Z, Zhang G, Zhang R, Yang F. (2018). Insights into Mechanism of Catalytic Ozonation over Practicable Mesoporous Mn-CeO_x/γ-Al_2O_3 Catalysts. *Ind Eng Chem Res* **57**: 1943–1953.

Xi Y, Reed C, Lee Y–K, Oyama ST. (2005). Acetone oxidation using ozone on manganese oxide catalysts. *J Phys Chem B* **109**: 17587–17596.

Zavadskii AV, Kireev SG, Muhin VM, Tkachenko SN, Chebkin VV, Klushin VN, Teplyakov DE. (2002). Thermal Treatment Influence over Hopcalite Activity in Ozone Decomposition. *J Phys Chem* **76**: 2278 [in Russian].

Zhang Y, Chen M, Zhang Z, Jiang Z, Shangguan W, Einaga H. (2019). Simultaneously catalytic decomposition of formaldehyde and ozone over manganese cerium oxides at room temperature: Promotional effect of relative humidity on the $MnCeO_x$ solid solution. *Catal Today* **327**: 323–333.

Zhao L, Ma J, Sun ZZ. (2008). Oxidation products and pathway of ceramic honeycomb-catalyzed ozonation for the degradation of nitrobenzene in aqueous solution. *Appl Catal B Environ* **79**: 244–253.

ISSN: 1337-6853 *(print version)* | 1337-9569 *(electronic version)*

Interdiscip Toxicol. 2020; **Vol. 13**(1): 13–20.
doi: 10.2478/intox-2020-0002

sciendo

interdisciplinary toxicology

ORIGINAL ARTICLE

Toxicological effects of methyl eugenol and fenitrothion on hematological, hepatic, renal, and oxidative stress-related biochemical characteristics of white albino rats

Yehia M. M. SALIM [1], Ismail R. EL-GENDY [2], Atef M. K. NASSAR [1]

[1] Plant Protection Department, Faculty of Agriculture, Damanhour University, Egypt
[2] Plant Protection Research Institute, Agricultural Research Centre, Giza, Egypt

ITX130120A02 • Received: 22 November 2019 • Accepted: 27 January 2020

ABSTRACT

The present study aimed to investigate the possible adverse effects of methyl eugenol (ME), a potent kairomone, and fenitrothion insecticide that are used extensively in male annihilation programs worldwide during the management of fruit flies. Therefore, the side effects of ME, fenitrothion (FEN) and their mix (ME+FEN) were tested in a 28 days-inhalation study on white albino rats. Rats were grouped and exposed to 1/20 LC_{50} of ME, FEN, and their mixture. Then hematological components, hepatic and renal parameters, and oxidative stress enzymes were measured. Results revealed significant decrease effects on mean cell hemoglobin and mean cell hemoglobin concentration (up to 18% decrease of control), red blood cell (28%), acetylcholinesterase (39%), and total lipids (36%) levels. On the other hand, lactate dehydrogenase (increased to 29.5% of control), uric acid (109%), creatinine (140%), γ-glutamyl transferase (159%), and oxidative stress-related enzymes (glutathione peroxidase (149%), glutathione reductase (170%), glutathione-S-transferase (34%), and superoxide dismutase (88%)) values were increased compared to results of control group. Adverse effects of ME, FEN, and their mixture might trigger an alarm for farmers who directly or indirectly inhale these chemicals continuously in the field. More importantly, safe alternatives to agricultural chemicals, including pesticides, should be enforced.

KEY WORDS: occupational exposure; fenitrothion; methyl eugenol; inhalation toxicity

Introduction

Worldwide and during pest management practices tons of pesticides are being applied. According to FAOSTAT, 4,088,167.77 tons of pesticides were applied on agricultural crops worldwide (FAOSTAT, 2019). Among these pesticides, the pheromone and kairomones are used in traps to deter or attract insects. This approach is coined as environmentally-safe (Bhagat *et al.,* 2013). The kairomones such as methyl eugenol (ME) have been used extensively in many male annihilation programs (Ghanim *et al.,* 2010; Keng & Nishida, 2012). The ME, 3,4-dimethoxyallylbenzene is the main constituent of many plant species including basil, tarragon, fennel, marjoram, mace, allspice, star anise, and anise (Keng & Nishida, 2012; NTP, 2000; Smith *et al.,* 2002). Also, it is used as a synthetic flavoring substance in non-alcoholic beverages, condiments, and hard and soft candy (Smith *et al.,* 2002). In agriculture, it is used solely or in combination with the organophosphate insecticides as an insect attractant (Benford *et al.,* 2010; IARC, 2013; Vargas *et al.,* 2010).

Although ME was declared as generally safe (GRAS) by the Food and Drug Administration as a food additive (NTP, 2000). Several studies described the adverse effects of the alkoxyallylbenzenes group of chemicals including ME, where it was reported as a DNA-reactive compound that induces cancer (neoplastic lesions) in the livers of rodents and mice (Burkey *et al.,* 2000; Thompson *et al.,* 1990; Williams, 2010; Williams *et al.,* 2008). It was reported as cytotoxic to cultured hepatocytes isolated from rats and mice *via* causing unscheduled DNA synthesis (UDS) in both species in a dose-dependent manner (Burkey *et al.,* 2000; Martelli *et al.,* 1994). Also, the glutathione-S-transferase isozymes (GSTs) were inhibited by ME as illustrated by studies on rats and humans (Rompelberg *et*

Correspondence address:
Prof. Atef M.K. Nassar, PhD.
Plant Protection Department, Faculty of Agriculture
Damanhour University, Damanhour
El-Beheira, P.O. Box 59, Egypt.
E-MAIL: atef.nassar@dmu.edu.eg

al., 1996). After a 14-weeks study, liver and testis weight were increased significantly when rats were given daily doses from 300 to 1000 mg/kg of ME. Also, the authors reported a decreased mean packed red cell volume and increased platelet counts, alanine aminotransferase, and sorbitol dehydrogenase activities after the administration of ME (Luo & Guenthner 1995; Rompelberg *et al.* 1996). In another 2-years study, ME induced a high incidence of atrial thrombosis in female mice treated with 75 mg/kg or higher doses (Yoshizawa *et al.,* 2005).

Moreover, oral administration of ME induced erythrocyte microcytosis and thrombocytosis, and caused an increase in the activities of alanine aminotransferase and sorbitol dehydrogenase and bile acid concentration in male and female rats, suggesting hepatocellular injury, cholestasis or altered hepatic function (Abdo *et al.,* 2001). Additionally, ME triggered hypoproteinemia and hypoalbuminemia in both male and female rats. In mice, it increased incidences of adrenal gland cortical hypertrophy and/or cytoplasmic alteration in the submandibular salivary glands, adrenal glands, testis, and uterus were considered secondary to the chemical-related effects observed in the liver and glandular stomach of rats (Abdo *et al.,* 2001). But it was reported that ME might elicit DNA repair synthesis in cultured rat and mouse hepatocytes (Burkey *et al.,* 2000).

In parallel to the abovementioned, fenitrothion (FEN), *O,O*-dimethyl-*O*-(3-methyl-4-nitrophenyl) phosphorothioate is an organophosphorus insecticide that is widely used as a mixture with ME in traps to control the Bactrocera insects (Ghanim *et al.,* 2010; Keng & Nishida, 2012). It is a broad-spectrum non-systemic insecticide with high selective toxicity to insects compared to mammals and moderate toxicity, with an oral LD_{50} of 330 mg/kg, to rats (Briggs, 1992; Vásquez-Castro *et al.,* 2012). FEN is being sprayed worldwide against a wide range of insects on rice, cereals, fruits, vegetables, stored grains, cotton and forests, and public health disease vectors (Wang *et al.,* 2012; WHO, 2010). Therefore, it might be considered as a hazard compound to mammals (Khan *et al.,* 1990). FEN was reported to have lower toxicity to mammals relative to insects because of the enhanced detoxification system (NRCC, 1975). It's well documented that FEN acts by inhibiting the activity of the acetylcholinesterase enzyme, which highlights acute neurotoxicity (Wang *et al.,* 2012). In addition, several studies reported toxicity of FEN to mammals via different routes of administration with a limited number of studies that investigated its inhalation toxicity. For example, FEN at 6.7, 20, and 60 pg/l of air for 2 hr/day for 30 consecutive days reduced body weight, food intake, muscle fasciculations, erythrocyte content and brain cholinesterase activity (Breckenridge *et al.,* 1982).

When young Japanese children inhaled FEN at 0–44 ng/kg/day, they suffered severe health effects (Kawahara *et al.,* 2005). In another study, it was reported that single inhalation exposure of rats to 500 mg/m^3 of FEN showed no serious pulmonary toxicity but minor modifications of lung alveolar tissues (Chevalier *et al.,* 1984). Exposure of rabbits to fenitrothion as thermal fog at 10 l/ha for 30 days significantly reduced the body weight (13.34%) but increased weights of liver, heart, and lungs by 23.37, 20.23 and 14.76%, respectively and reduced the activity of brain, blood, plasma, and erythrocytes cholinesterases (Al-Sarar *et al.,* 2011).

To the best of our knowledge, the inhalation toxicity of the mixture of ME and FEN was not tested. Therefore, the current study aimed to investigate the inhalation toxicity of sublethal doses of methyl eugenol (1/20 LC_{50}), fenitrothion (1/20 LC_{50}), and their mixture on hematology and biochemical parameters of white albino rats after 28 days of exposure.

Materials and methods

Chemicals

Fenitrothion, O,O-dimethyl-O-(4-nitrophenyl) phosphorothioate, (CAS 122–14–5, 99% purity) was obtained from Supelco Analytical (USA). It was diluted in corn oil for the final test concentration. Methyl eugenol (purity 99%) was obtained from Ministry of Agriculture and Land Reclamation, National Pesticides Committee, Egypt. Acetylthiocholine iodide (ATChI; Sigma order #A5751-250MG), 5,5-dithiobis-2-nitrobenzoic acid (DTNB-Ellman's reagent: Sigma order #D218200), brilliant (Coomassie) blue G-250 (Sigma order #B0770-5G), and bovine serum albumin (BSA: Sigma order #A2153-10G) were provided from Sigma-Aldrich, USA.

Animals and treatments

Young, 60-days old, male white albino Sprague Dawley rats (*Rattus norvegicus*) weighing 120±5 g were purchased from the Animal Health Research Center, Cairo, Egypt. Rats were housed in plastic cages in an animal room maintained at 25±2°C and in an alternate 12 hr cycle of light and darkness. They fed on a pellet diet and tap water was provided *ad libitum*. After 2-week acclimatization period, the rats were randomly divided into four groups (6 animals in each group): control (corn oil), FEN (0.25 mg/l air: 1/20 LC_{50} inhalation (EPA, 1996)), ME (240 mg/l air: 1/20 LC_{50} (Beroza *et al.,* 1975)), and FEN+ME at 1:1 ratio. The rats inhaled treatments for 28 days from chipboard blocks (cotton rolls No. 2, medium-sized, with 6×2×2 cm dimensions, Defend, MyDent International, Hauppauge, NY, 11788, USA) that were impregnated by dipping in corn oil, FEN, ME, and FEN+ME concentrations. Blocks were hanged in 45 l plastic cages using metal wire in a way to avoid any direct contact with rats for 8 hr daily. Cages of each group were separated completely from the other groups. Rats in each group were anesthetized with diethyl ether and sacrificed by decapitation at the end of treatment. Initial and final body weights of individual rats in each group were recorded to calculate relative weight changes (Chapman *et al.,* 1959). All rats were handled in accordance with the standard guide for the care and use of laboratory animals of the National Research Council (NRCNA, 2011) and the animal ethics guidelines of Damanhour University.

Hematological parameters

After killing rats, trunk blood was collected gently in sterilized EDTA tubes containing an anticoagulant (ethylenediamine tetra-acetic acid, EDTA) to give a final concentration of 5 mg EDTA/ml blood. Samples were mixed gently and discarded if any clots were seen in the vial. Total red blood cell (RBC) count ($\times 10^6$/µl), hemoglobin (Hb) content (g/dl), hematocrit (HCT) value (%), mean corpuscular volume (MCV; fl), mean cell hemoglobin (MCH; pg), mean corpuscular hemoglobin concentration (MCHC) values (g/dl), total WBC count ($\times 10^3$/µl) and platelet count ($\times 10^3$/µl) were assessed using Sysmex KX-21 hematological analyzer (Sysmex KX21, Japan) in a certified clinical laboratory.

Biochemical parameters

Blood samples were collected in test tubes without an anticoagulant, allowed to clot at room temperature for 15 min, and then centrifuged at 1390 g (Universal 32R, Hettich Zentrifugen model D-78532, Germany) for 10 min for serum separation. Serum was used for the following assays. The AChE activity was quantified following a modified method of Ellman *et al.* (Ellman *et al.,* 1961). Blood glucose (Trinder, 1969), uric acid (Barham & Trinder, 1972), total protein (Gornall *et al.,* 1949), total lipids (Zöllner & Kirsch, 1962), alkaline phosphatase (ALP) (Belfield & Goldberg, 1971), glutathione-S-transferase (GST) (Habig *et al.,* 1974), glutathione peroxidase (GP) (Paglia & Valentine, 1967), glutathione reduced (GR) (Beutler *et al.,* 1963), superoxide dismutase (SOD) (Nishikimi *et al.,* 1972), and creatinine (Bartels *et al.,* 1972) were measured using BioDiagnostic kits (Diagnostic research and Reagents, Giza, Egypt). Lactate dehydrogenase (LDH) activity (Burtis *et al.,* 2005) was determined using BioSystems Kit (BioSystems S.A., Costa Brava, Barcelona, Spain). Determination of γ-glutamyl transferase (GGT) activity was done using Spectrum Kit (MDSS, GmbH, Schiffgraben, Germany) (Heersink *et al.,* 1980). The replicates were measured in triplicates.

Statistical analysis

Toxicological data were analyzed using the general linear model (GLM) procedure of the Statistical Analysis System (SAS) (Version 9.3, Cary, NC, USA, 2016). Means were compared using Scheffe's *post-hoc* Multiple Comparison ($p \leq 0.05$) (SAS, 2016).

Results and discussion

Mortality and relative bodyweight

During the study period, there was no mortality or severe clinical signs of toxicity in treated rats. Body weight changes were reported, and relative weights of internal organs liver, kidney, heart, brain, spleen, lungs, and testes were reported (Table 1). Weekly percentages of change of body weight were significantly different between the control group and treated groups. FEN, ME, and ME+FEN showed an increased body weight compared to the control, but they had similar % of change. For the relative organ weight, kidney and spleen had similar percentages to the control group. The ME+FEN treatment increased the liver relative weight compared to the other treatments. The FEN reduced the heart and brain relative weights compared to control, ME, and ME+FEN groups that were similar. Lung relative weights were reduced after treatments of ME+FEN, ME, and FEN compared to the control. The ME significantly reduced the relative weights of testes of treated rats compared to control, ME+FEN, and FEN groups that had similar results.

Hematology

Application of pheromones mixed with insecticides would reduce the amounts of pesticides that are required to control plant pests and were coined as a safe approach. The ME, an alkenylbenzene pheromone, is used as a mixture with organophosphate insecticides in the annihilation programs against fruit flies. Possible adverse effects on hematological parameters of rats that inhaled ME, FEN and their mix were reported herein. Results in Table 2 showed that the numbers of white blood cells (WBCs) were increased significantly in rats that inhaled ME (mean WBC's equal to 11.70×10^3/µl), FEN (15.22×10^3/µl), and ME+FEN (15.35×10^3/µl) compared to the control group (9.25×10^3/µl). Moreover, both FEN and FEN+ME treatments revealed increased numbers of WBCs compared to the ME group. Similarly, platelets numbers were increased in blood samples of the three treated groups of rats after the treatment with ME (667.8×10^3/µl), FEN (677.3×10^3/µl), and ME+FEN (650.3×10^3/µl) compared to control (452.5×10^3/µl), but they were not different from each other.

On the other hand, numbers of red blood cells (RBCs), hemoglobin (HGB), and hematocrit (HCT) values were

Table 1. Mean relative organ weights ± SE of liver, lung, kidney, heart, brain, spleen, and testes of white albino rats inhaled methyl eugenol (ME), fenitrothion (FEN), and their mixture (ME+FEN) for 28 days.

Treatments	% of Change / Week	Liver	Kidney	Heart	Brain	Spleen	Lung	Testes
Control	12.89^{c}±0.58	3.16^{bc}±0.14	0.74^{a}±0.06	0.39^{a}±0.05	0.72^{a}±0.05	0.26^{a}±0.05	0.86^{a}±0.08	1.15^{a}±0.10
FEN	19.05^{a}±0.82	3.59^{ab}±0.16	0.76^{a}±0.07	0.33^{b}±0.02	0.62^{b}±0.04	0.26^{a}±0.04	0.73^{b}±0.06	1.08^{a}±0.12
ME	15.27^{ab}±0.58	3.28^{b}±0.14	0.72^{a}±0.06	0.39^{a}±0.05	0.77^{a}±0.05	0.28^{a}±0.05	0.70^{bc}±0.08	0.63^{b}±0.10
ME+FEN	15.16^{ab}±0.58	3.71^{a}±0.14	0.78^{a}±0.06	0.38^{a}±0.05	0.72^{a}±0.05	0.30^{a}±0.05	0.67^{c}±0.08	1.17^{a}±0.10

n=6 rats, SE; standard error, means with the same superscript letter were not significantly different, $p<0.05$, % of body weight change/week = ((final body weight-initial body weight)/ initial body weight)/no of weeks × 100, and relative organ weight = (organ weight/final body weight) × 100

Table 2. Mean ± SE values of total white blood cell (WBC) counts (×10³/µl), platelets (PLT No.) number (×10³/µl), total red blood cell (RBC) count (×10⁶/µl), hemoglobin (HGB) content (g/dl), hematocrit (HCT) value (%), mean cell hemoglobin (MCH; pg), mean corpuscular hemoglobin concentration (MCHC) values (g/dl), and mean corpuscular volume (MCV; fl) of white albino rats inhaled methyl eugenol (ME), fenitrothion (FEN), and their mixture (ME+FEN) for 28 days.

Treatments	WBC (×10³/µl)	PLT No. (×10³/µl)	RBC (×10⁶/µl)	HGB (g/dl)	HCT (%)	MCH (pg)	MCHC (g/dl)	MCV (fl)
Control	9.25^{c}±0.44	452.5^{b}±31.52	5.09^{a}±0.23	13.05^{a}±0.32	35.43^{a}±0.80	26.02^{a}±1.34	36.99^{a}±1.66	70.49^{a}±4.81
ME	11.70^{b}±0.39	667.8^{a}±28.20	3.78^{b}±0.20	9.52^{b}±0.29	31.20^{b}±0.72	25.30^{a}±1.20	30.59^{ab}±1.48	83.55^{a}±4.31
FEN	15.22^{a}±0.44	677.3^{a}±31.52	3.74^{b}±0.23	7.85^{c}±0.32	28.75^{b}±0.80	21.25^{a}±1.34	27.42^{b}±1.66	77.68^{a}±4.81
ME+FEN	15.35^{a}±0.44	650.3^{a}±31.52	3.96^{b}±0.23	8.45^{bc}±0.32	29.05^{b}±0.80	21.39^{a} ±134	29.22^{b}±1.66	73.58^{a}±4.81

Means were statistically compared using the Scheffe's *post-hoc* multiple comparison method at $p \leq 0.05\%$. Means with the same superscript letter are not significantly different. Each treatment was replicated 6 times and each replicate was measured 3 times.

Table 3. Mean ± SE values of glucose, uric acid, creatinine, total protein, and total lipids contents and acetylcholinesterase (AChE; nM ATChI/min), alkaline phosphatase (ALP), γ-glutamyl transferase (γ-GT), and lactate dehydrogenase (LDH) enzyme activities of serum of white albino rats inhaled methyl eugenol (ME), fenitrothion (FEN), and their mixture (ME+FEN) for 28 days.

Treatments	AChE	Glucose (mg/dl)	Uric Acid (mg/dl)	Creatinine (mg/dl)	Total Protein (g/dl)	ALP (IU/l)	γ-GT (U/l)	LDH (U/l)	Total Lipids (mg/dl)
Control	1.22^{a}±0.03	63.81^{c}±2.95	1.69^{c}±0.20	1.07^{c}±0.121	8.30^{a}±0.36	184.40^{c}±5.90	64.56^{c}±6.72	132.90^{a}±11.74	770.20^{a}±17.37
ME	0.97^{b}±0.03	117.13^{b}±2.64	2.42^{bc}±0.18	1.38^{c}±0.109	6.05^{b}±0.32	278.65^{b}±5.27	113.25^{b}±6.01	149.05^{a}±10.50	408.08^{d}±15.53
FEN	0.83^{b}±0.03	149.84^{a}±2.95	3.54^{a}±0.20	2.57^{a}±0.121	5.34^{b}±0.36	313.69^{a}±5.90	167.05^{a}±6.72	172.02^{a}±11.74	500.00^{c}±17.37
ME+FEN	0.75^{b}±0.03	149.96^{a}±2.95	3.07^{ab}±0.20	1.91^{b}±0.121	6.32^{b}±0.36	336.96^{a}±5.96	134.04^{b}±6.72	163.12^{a}±11.74	623.74^{b}±17.37

Means were statistically compared using the Scheffe's *post-hoc* multiple comparison method at $p \leq 0.05\%$. Means with the same superscript letter are not significantly different. Each treatment was replicated 6 times and each replicate was measured 3 times

decreased relative to the control group (Table 2). In addition, inhalation of sub-lethal doses of FEN and ME+FEN caused a reduction in mean corpuscular hemoglobin concentration (MCHC) compared to control. However, their effects were not different from the ME group that was not different from the control group. Results also revealed no difference between treated groups and the control group in the mean corpuscular hemoglobin (MCH) and mean cell volume (MCV).

The results reported herein showed that exposure to ME and fenitrothion as separate treatments or mixed caused hematological adverse effects to rats. Inhalation of ME, FEN, and ME+FEN significantly increased numbers of WBCs and platelets but numbers of RBCs and HGB, HCT, and MCHC values were decreased significantly relative to the control group. In previous studies, ME significantly reduced the size of RBCs (erythrocyte microcytosis) and elevated numbers of platelets (thrombocytosis) in male and female rats (Abdo *et al.,* 2001). In a 90-days study, rats fed ME daily at 18 mg/kg b.w. showed a decrease in mean packed red cell volume and increased platelet counts (Gardner *et al.,* 1996; Luo & Guenthner, 1995; Rompelberg *et al.,* 1996). Also hematocrit value, WBCs, and lymphocytes percentages were increased in blood samples of rats orally given FEN at ¼ of LD_{50} (60 mg/kg bw) for 12 days (Al-Sahhaf, 2006).

Effects on acetylcholinesterase (AChE)

The activity of acetylcholinesterase enzyme (AChE) was depleted significantly after rats have been inhaling ME, FEN, and ME+FEN (Table 3). Results showed a significant reduction in the enzyme activity compared to the control group, but it was not different from each other. Inhalation of ME, FEN, and ME+FEN reduced AChE activity by 21, 32, and 39% of the control, respectively (Figure 1). The organophosphate insecticides are known as inhibitors of acetylcholinesterase (Farghaly *et al.,* 2010). In addition, ME was reported in the current study as an inhibitor of AChE. However, rare studies were conducted on the inhalation of fenitrothion and/or methyl eugenol. Current results might be compared to that of the study of exposure of rabbits to thermal fogging of FEN at 10 l/ha for 30 days, which showed a significant reduction of cholinesterase activity of brain, blood, plasma, and erythrocytes (Al-Sarar *et al.,* 2011). To highlight the suppressive effect of FEN on AChE activity, some results of other studies with different routes of administration were reported. The oral doses between 2.5 and 10 mg/kg b.w. of FEN for 30 days caused a decrease in tissue esterase activity (Trottier *et al.,* 1980). It was noticed that the hepatic ChE was the most inhibited enzyme compared to other esterases (Trottier *et al.,* 1980). After a 13-week study, administering oral doses of 30 mg/kg of FEN to male and female rats inhibited the plasma, erythrocyte, and brain ChE activity (Ecobichon *et al.,* 1980; Yoshida *et al.,* 1997). Similar inhibition of plasma cholinesterase (ChE) after administering of 1/30 and 1/60 LD_{50} of FEN doses to rats for 28 days was reported (Elhalwagy *et al.,* 2008).

Effects on glucose content

Glucose contents were increased significantly after the treatment with ME, FEN, and ME+FEN compared to control. The mean values were 63.81±2.95, 117.13±2.64, 149.84±2.95, and 149.96±2.95 mg/dl, respectively (Table 3). However, there was no difference between both FEN and ME+FEN, but both treatments were significantly different

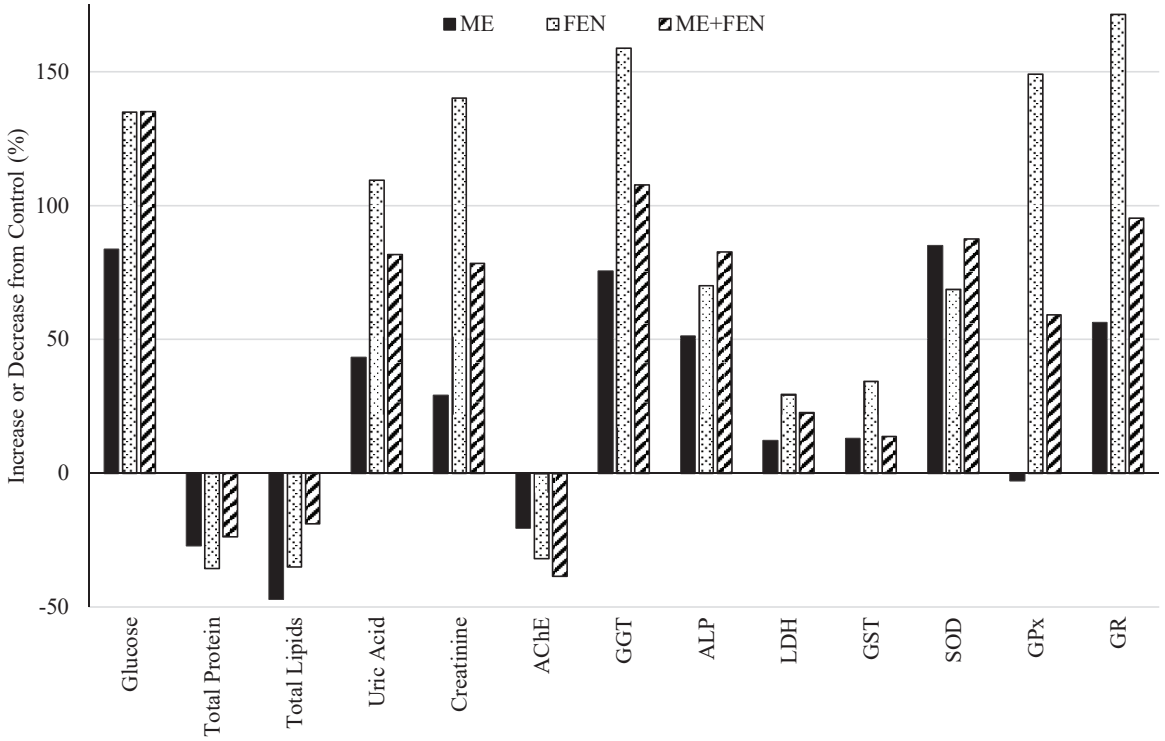

Figure 1. Average percentages of increase or decrease of biochemical parameters of control group after the inhalation study for 28 days. Relative decrease or increase from control = (Treatment Reading – Control Reading)/Control Reading) × 100

from ME. Glucose contents were severely increased by 84, 135, and 135% of control after rats have been inhaling ME, FEN, and ME+FEN (Figure 1), respectively.

Effects on renal characteristics

Kidney functions were impaired as revealed by the elevated levels of creatinine in serum (Table 3 and Figure 1). Creatinine results were affected significantly by ME, FEN treatments, and their mixture. Levels of creatinine were 1.07±0.121, 1.38±0.109, 2.57±0.121, and 1.91±0.121 mg/dl for control, ME, FEN, and ME+FEN, respectively. FEN treatment showed the greatest increase in creatinine followed by ME+FEN, while ME was not different from the control. Creatinine levels were increased by ME, FEN treatments, and their mixture by 29, 140, and 78% of control, respectively (Figure 1). It was reported that oral doses of FEN at ¼ of LD_{50} (60 mg/kg b.w.) for 12 d increased cholesterol and creatinine causing renal damage (Al-Sahhaf, 2006).

In addition, levels of uric acid were increased from 1.69±0.20 (control) to 2.42±0.18, 3.54±0.20, and 3.07±0.20 mg/dl after ME, FEN, and ME+FEN treatments, respectively (Table 3). The ME, FEN, and ME+FEN treatments increased uric acid contents by 43, 109, and 78% of control, respectively (Figure 1). The FEN treatment increased uric acid content compared to control and ME groups, which were not different from each other and ME was not different from the mixture treatment (ME+FEN). Yet, the effect of ME on uric acid was similar to that of ME+FEN.

Effects on hepatic biochemical parameters

The liver was the most affected organ by repeated oral administration of FEN (Trottier *et al.,* 1980). As well, ME caused tumors in liver cells of rats and mice (Burkey *et al.,* 2000; Thompson *et al.,* 1990). Besides, ME was minimally cytotoxic to hepatocytes isolated from rats and mice and caused UDS in both species in a dose-dependent manner (Burkey *et al.,* 2000; Martelli *et al.,* 1994). Current results showed that total protein contents were significantly different between control and ME, FEN, and ME+FEN treatments from 8.30±0.36 g/dl to 6.05±0.32, 5.34±0.36, and 6.32±0.36, respectively (Table 3). However, there were no differences between ME, FEN, and ME+FEN inhalation treatments. Total protein contents were decreased relative to control by 36% as a result of FEN treatment (Figure 1). Additionally, ME induced hypoproteinemia and hypoalbuminemia evidenced by the decreased concentrations of total protein in both male and female rats due to the induced liver and glandular stomach toxicity (Abdo *et al.,* 2001).

Alkaline phosphatase (ALP) activity was increased significantly after rats had inhaled ME, FEN, and ME+FEN compared to the control group. Both FEN and ME+FEN doses revealed elevated adverse effects on ALP compared to ME. The ALP activity was increased significantly after rats inhaled ME, FEN, and ME+FEN by 51, 70, and 83% of control, respectively (Figure 1). γ-Glutamyl transferase (γ-GT) activity values were 64.56±6.72, 113.25±6.01, 167.05±6.72, and 134.04±6.72 U/l for control, ME, FEN, and ME+FEN, respectively (Table 3). All three treatments

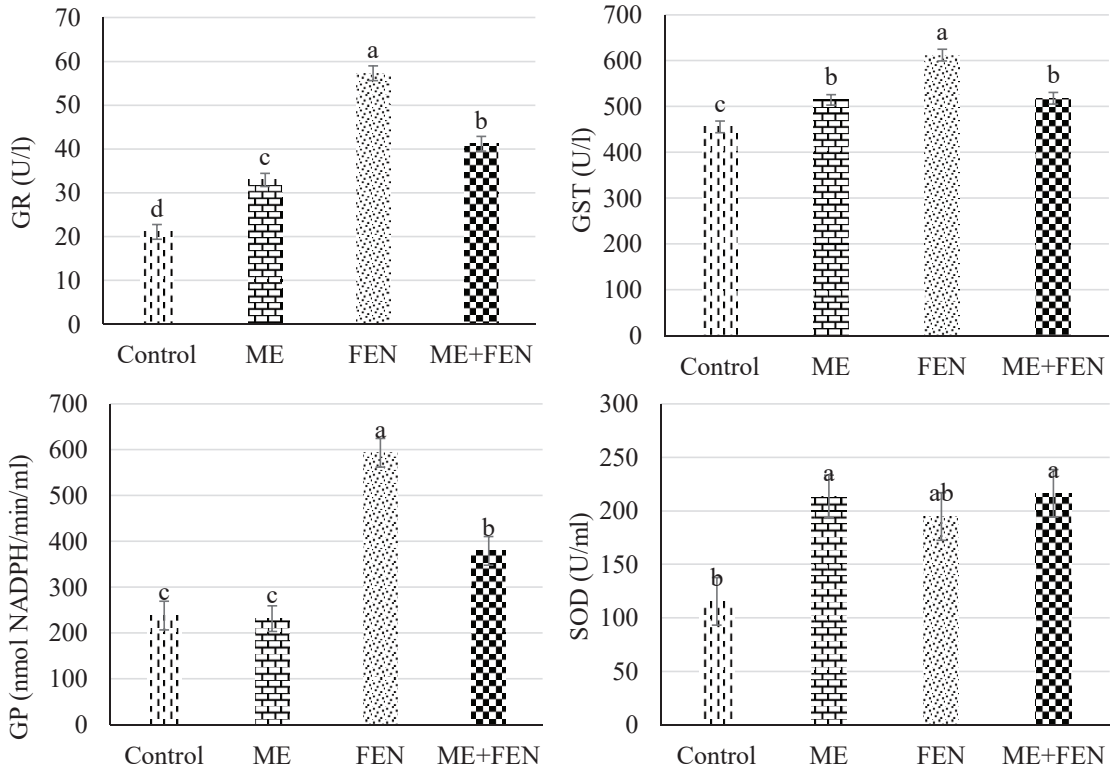

Figure 2. Mean ± SE activity values of glutathione-S-transferase (GST; U/l), superoxide dismutase (SOD; U/ml), glutathione peroxidase (GP; nM NADPH/min/ml), and glutathione reductase (GR; U/l) of serum of white albino rats inhaled methyl eugenol (ME), fenitrothion (FEN), and their mixture (ME+FEN) for 28 days. Means were statistically compared using the Scheffe's *post-hoc* multiple comparison method at $P \leq 0.05\%$. Columns with the same superscript letter are not significantly different. Each treatment was replicated 6 times and each replicate was measured 3 times.

significantly increase γ-GT activity compared to control. Rats that inhaled FEN showed the greatest activity of γ-GT followed by ME and ME+FEN treatments.

Inhalation of ME, FEN, and ME+FEN significantly decreased total lipid contents with mean values of 408.08, 500, and 623.74 mg/dl, respectively, compared to the control (770.20 mg/dl) (Table 3). The ME group showed the least amount of total lipids followed by FEN and ME+FEN groups. The ME, FEN, and ME+FEN treatments caused a significant decrease in the total lipids content by 47.02, 35.08, and 19.02% of control, respectively (Figure 1). In literature, it was reported that FEN, in a dose-dependent manner from 5 to 20 mg/100 g, caused lipid accumulation with the alteration of the ratio of various components of phospholipids and neutral lipids in various organs of rats (Roy *et al.,* 2004). Lactate dehydrogenase (LDH) activity tended to increase after inhalation of ME, FEN, and ME+FEN, but there was no significant difference between treatments and control group (Table 3). The elevated activity of LDH by FEN could be due to cell lysis or membrane damage and indicates significant pulmonary injury (Khan *et al.,* 1990), but the current study reported a tendency of increase in the activity of LDH.

Effects on oxidative stress enzymes

Oxidative stress enzymes glutathione-S-transferase (GST), glutathione peroxidases (GP), glutathione reductase (GR), and superoxide dismutase (SOD) activities were increased after the ME, FEN, ME+FEN treatments (Figure 2). FEN caused a significant increase in the GST activity compared to ME and ME+FEN treatments that showed similar effects but had greater GST activity compared to the control group. Similarly, FEN insecticide caused the greatest increase in GP activity (593.33 nM NADPH/min/ml) and followed by ME+FEN (379.34) and ME (231.5) treatments, respectively, compared to the control group (238.2 nM NADPH/min/ml). The GR activity (U/l) was significantly increased in the serum of rats that inhaled FEN (57.28), ME+FEN (41.20), and ME (32.95) in an ascending order compared to the control (21.10). In addition, SOD activity (U/l) was increased significantly after ME+FEN (216.35), ME (213.46), and FEN (194.72) in ascending order but not different from each other. FEN treatment tended to increase the SOD activity compared to the control group but not significantly different.

It was noticed that the FEN insecticide caused the highest increase in GR activity where it was increased in the serum of rats by 170% of control (Figure 1). Additionally, the GP activity values were increased up to 150% of control. The SOD activity was increased significantly after ME+FEN, ME, and FEN inhaling by 85, 69, 88% of control, respectively. In previous studies, the GST isozymes in rat and human samples were inhibited by ME (Rompelberg *et al.,* 1996). Fenitrothion was reported to has lower toxicity to mammals relative to insects due to the enhanced detoxification system through dealkylation by glutathione

dealkyltransferase (NRCNA, 2011). It was suggested that GSH, GP, SOD, and GST play a key role in the defense against induced oxidative stress in isolated hepatocytes when incubated with FEN (El-Shenawy, 2010).

Conclusions

Annihilation systems as part of the integrated pest management practices might cause inhalation toxicity to farmers. The ME and FEN are used extensively in the pheromone-baited traps in agricultural fields. Therefore, the inhalation of ME, FEN, and their mix (ME+FEN) might incite hematological and biochemical parameters (AChE, glucose, lipids, hepatic, renal, and oxidative stress enzymes) in rats. The studied parameters were altered significantly compared to the control group. Significant decreases in mean cell hemoglobin and mean cell hemoglobin concentration, red blood cell, AChE, and total lipids levels were reported. On the other hand, lactate dehydrogenase, uric acid, creatinine, γ-glutamyltransferase, and oxidative stress-related enzymes (glutathione peroxidase, glutathione reductase, glutathione-S-transferase, and superoxide dismutase values were increased compared to the results of the control group. Therefore, handling safe-labeled chemicals should be carefully done.

Acknowledgments

The author would like to thank the staff members of Pesticides Residue Analysis and Toxicity (PRATL) Laboratory for granting access to perform various assays required to complete this work.

REFERENCES

Abdo KM, Cunningham ML, Snell ML, Herbert RA, Travlos GS, Eldridge SR, Bucher JR. (2001). 14-Week toxicity and cell proliferation of methyleugenol administered by gavage to F344 rats and B6C3F1 mice. *Food Chem Toxicol* **39**: 303–316.

Al-Sahhaf Z. (2006). Toxicity of sumithion in albino rats: hematological and biochemical studies. *J Appl Sci* **6**: 2959–2962.

Al-Sarar AS, Hafiz AM, Bayoumi A, Hussein HI, Abo Bakr Y. (2011). Impact of Fenitrothion Thermal Fogging on some Biological and Biochemical Parameters in New Zealand Rabbits as Non-target Organisms. *Int J Agric Biol* **13**: 435–438.

Barham D, Trinder P. (1972). An improved colour reagent for the determination of blood glucose by the oxidase system. *Analyst* **97**: 142–5.

Bartels H, Böhmer M, Heierli C. (1972). Serum kreatininbestimmung ohne enteiweissen. *Clin Chim Acta* **37**: 193–197.

Belfield A, Goldberg DM. (1971). Revised assay for serum phenyl phosphatase activity using 4-amino-antipyrine. *Enzyme* **12**: 561–73.

Benford D, Bolger PM, Carthew P, Coulet M, Dinovi M, Leblanc J-C, Renwick AG, Setzer W, Schlatter J, Smith B, Slob W, Williams G, Wildemann T. (2010). Application of the Margin of Exposure (MOE) approach to substances in food that are genotoxic and carcinogenic. *Food Chem Toxicol* **48**: S2–S24.

Beroza M, Inscoe MN, Schwartz PH, Keplinger ML, Mastri CW. (1975). Acute toxicity studies with insect attractants. *Toxicol Appl Pharmacol* **31**: 421–429.

Beutler E, Duron O, Kelly BM. (1963). Improved method for the determination of blood glutathione. *J Lab Clin Med* **61**: 882–8.

Bhagat D, Samanta SK, Bhattacharya S. (2013). Efficient management of fruit pests by pheromone nanogels. *Sci Rep* **3**: 1–8.

Breckenridge C, Pesant M, Durham HD, Ecobichon DJ. (1982). A 30-Day Toxicity study of inhaled fenitrothion in the albino rat. *Toxicol Appl Pharmacol* **62**: 32–43.

Briggs SA. (1992). *Basic Guide to Pesticides; Their Characteristics and Hazards*. Hemisphere Publishing Crop., Washington, Philadelphia, London.

Burkey JL, Sauer J-M, McQueen CA, Sipes IG. (2000). Cytotoxicity and genotoxicity of methyleugenol and related congeners. A mechanism of activation for methyleugenol. *Mutat Res* **453**: 25–33.

Burtis C, Ashwood E, Bruns D, Saunders W. (2005). *Tietz Textbook of Clinical Chemistry and Molecular Diagnostics*, 4th ed, Elsevier Saunders, St. Louis, Missouri.

Chapman D, Castillo R, Campbell J. (1959). Evaluation of protein in food determination of protein and food efficiency ratio. *Can J Biochem Physiol* **37**: 676–786. https://doi.org/10.1139/y59-074

Chevalier G, Hénin JP, Vannier H, Canevet C, Côté MG, Le Bouffant L. (1984). Pulmonary toxicity of aerosolized oil-formulated fenitrothion in rats. *Toxicol Appl Pharmacol* **76**: 349–55.

Ecobichon DJ, Comeau AM, Cameron PH. (1980). Chronic toxicity of technical fenitrothion in male rats. *Toxicol Appl Pharmacol* **56**: 409–417. https://doi.org/10.1016/0041-008X(80)90075-7.

Elhalwagy ME, Darwish NS, Zaher EM. (2008). Prophylactic effect of green tea polyphenols against liver and kidney injury induced by fenitrothion insecticide. *Pestic Biochem Physiol* **91**: 81–89.

Ellman GL, Courtney KD, Andres V, Featherstone RM. (1961). A new and rapid colorimetric determination of acetylcholinestrase activity. *Biochem Pharmacol* **7**: 88–95.

El-Shenawy NS. (2010). Effects of insecticides fenitrothion, endosulfan and abamectin on antioxidant parameters of isolated rat hepatocytes. *Toxicol In Vitr* **24**: 1148–1157. .

EPA. (1996). *Reregistration Eligibility Decision Fenitrothion*. List A. Case # 0445. Washington, USA. Available from: https://archive.epa.gov/pesticides/reregistration/web/pdf/0445.pdf

FAOSTAT. (2019). Pesticides Use. Available from: http://www.fao.org/faostat/en/#compare.

Farghaly M, Taha H, Soliman S, Fathy U, Bedair A. (2010). Effect of refining processes on magnitude and nature of fenitrothion and pirimiphos-methyl residues in maize oil and bioavailability of their cake residues on rats. *Egypt J Chem* **53**: 923–938.

Gardner I, Bergin P, Stening P, Kenna JG, Caldwell J. (1996). Immunochemical detection of covalently modified protein adducts in livers of rats treated with methyleugenol. *Chem Res Toxicol* 9: 713–721. https://doi.org/10.1021/TX950211V.

Ghanim N, Moustafa S, El-Metwally M, Afia Y, Salman M, Mostafa M. (2010). Efficiency of some insecticides in male annihilation technique of peach fruit fly, *Bactrocera zonata* (Saunders) under Egyptian conditions. *Egypt Acad J Biol Sci F Toxicol Pest Control* **2:** 13–19.

Gornall AG, Bardawill CJ, David MM. (1949). Determination of serum proteins by means of the biuret reaction. *J Biol Chem* **177**: 751–66.

Habig WH, Pabst MJ, Jakoby WB. (1974). Glutathione S-transferases the first enzymatic step in mercapturic acid formation. *J Biol Chem* **249**: 7130–7139.

Heersink W, Hafkenscheid JCM, Siepel H, Enjongekryg J Van der, Dijt CCM. (1980). Temperature-converting factors for enzymes: Comparison of methods. *Enzyme* **25**: 333–341.

IARC. (2013). *Methyleugenol*. In: Some chemicals present in industerial and consumer products, food and drinking-water. IARC Monograph on the Evaluation of Carcinogenic Risk to Humans, Volume 101. pp. 407–433.

Kawahara J, Horikoshi R, Yamaguchi T, Kumagai K, Yanagisawa Y. (2005). Air pollution and young children's inhalation exposure to organophosphorus pesticide in an agricultural community in Japan. *Environ Int* **31**: 1123–1132.

Keng H, Nishida R. (2012). Methyl eugenol: Its occurrence, distribution, and role in nature, especially in relation to insect behavior and pollination. *J Insect Sci* **12**: 56.

Khan FM, Abidi P, Anwer J, Ray PK, Anand M. (1990). Pulmonary biochemical assessment of fenitrothion toxicity in rats. *Bull Environ Contam Toxicol* **45**: 598–603.

Luo G, Guenthner TM. (1995). Metabolism of allylbenzene 2′,3′-oxide and estragole 2′,3′-oxide in the isolated perfused rat liver. *J Pharmacol Exp Ther* **272**: 588–96.

Martelli A, Canonero R, Cavanna M, Ceradelli M, Marinari UM. (1994). Cytotoxic and genotoxic effects of five in primary cultures of rat and human hepatocytes. *Mutat Res Lett* **323**: 121–126.

Nishikimi M, Appaji Rao N, Yagi K. (1972). The occurrence of superoxide anion in the reaction of reduced phenazine methosulfate and molecular oxygen. *Biochem Biophys Res Commun* **46**: 849–854.

NRCC. (1975). *Fenitrothion: The effects of its use on environmental quality and its chemistry.* National Research Council of Canada, 162 pp, 14104 of the Environmental Secretariat Volume 15.

NRCNA. (2011). *Guide for the care and use of Laboratory Animals.* National Research Council of the National Academics. The National Academics Press, Washington, DC.

NTP. (2000). National Toxicology Program. U.S. Environmental Protection Agency and the National Institute of Environmental Health Sciences, NIH. Available from: http://ntp-server.niehs.nih.gov/htdocs/liason/LowDoseWebPage.html

Paglia DE, Valentine WN. (1967). Studies on the quantitative and qualitative characterization of erythrocyte glutathione peroxidase. *J Lab Clin Med* **70**: 158–69.

Rompelberg CJ, Ploemen JHTM, Jespersen S, Greef J van der, Verhagen H, Bladeren PJ van. (1996). Inhibition of rat, mouse, and human glutathione S-transferase by eugenol and its oxidation products. *Chem Biol Interact* **99**: 85–97.

Roy S, Roy S, Sharma CB. (2004). Fenitrothion-induced changes in lipids of rats. *Biomed Chromatogr* **18**: 648–654.

SAS. (2016). Statistical Analysis System. Version 9.3. SAS Institute Inc. Cary, NC, USA

Smith RL, Adams TB, Doull J, Feron VJ, Goodman JI, Marnett LJ, Portoghese PS, Waddell WJ, Wagner BM, Rogers AE, Caldwell J, Sipes IG. (2002). Safety assessment of allylalkoxybenzene derivatives used as flavouring substances - methyl eugenol and estragole. *Food Chem Toxicol* **40**: 851–870.

Thompson D, Constantin-Teodosiu D, Egestad B, Mickos H, Moldeus P. (1990). Formation of glutathione conjugates during oxidation oxidation of eugenol by microsomal fractions of rat liver and lung. *Biochem Pharmacol* **39**: 1587–1595.

Trinder P. (1969). Determination of glucose in blood using glucose oxidase with an alternative oxygen acceptor. *Ann Clin Biochem* **6**: 24–27.

Trottier B, Fraser AR, Planet G, Ecobichon DJ. (1980). Subacute toxicity of technical fenitrothion in male rats. *Toxicol* **17**: 29–38.

Vargas RI, Shelly TE, Leblanc L, Piñero JC. (2010). Recent advances in methyl eugenol and cue-lure technologies for fruit fly detection, monitoring, and control in hawaii. *Vitam Horm* **83**: 575–595.

Vásquez-Castro JA, de Baptista GC, Gadanha CD, Trevizan LRP. (2012). Insecticidal effect and residual action of fenitrothion and esfenvalerate on *Sitophilus oryzae* and *S. zeamais* (Coleoptera: Curculionidae) in stored maize and wheat . *ISRN Agron* **2012**: 1–11.

Wang D, Naito H, Nakajima T. (2012). *The Toxicity of fenitrothion and permethrin*. In: Perveen, F. (Ed.), Insecticides - Pest Engineering. InTech, pp. 85–98.

WHO. (2010). WHO Specification and evaluation for public health pesticides. Fenitrothion: O,O-dimethyl O-4-nitro-m-tolyl phosphorothioate. Available from: https://www.who.int/whopes/quality/Fenitrothion_specs_eval_WHO_Jan_2010_ok.pdf

Williams GM, Iatropoulos MJ, Enzmann H, Deschl UF. (2008). *Carcinogenicity of Chemicals: Assessment and Human Extrapolation.* In: Wallace Hayes, A. (Ed.), Principles and Methods of Toxicology. Taylor and Francis, Philadelphia, pp. 1265–1316.

Williams GM. (2010). Chemicals with carcinogenic activity in rodent liver. *Compr Toxicol* **9**: 221–250.

Yoshida A, Harada T, Maita K. (1997). A safety study on rat's eye after 13-week oral administration with fenitrothion. *J Toxicol Sci* **22**: 89–97.

Yoshizawa K, Kissling GE, Johnson JA, Clayton NP, Flagler ND, Nyska A. (2005). Chemical-induced atrial thrombosis in ntp rodent studies. *Toxicol Pathol* **33**: 517–532.

Zöllner N, Kirsch K. (1962). Colorimetric method for determination of total lipids. *J Exp Med* **135**: 545–55.

Interdiscip Toxicol. 2020; **Vol. 13**(1): 21–27.
doi: 10.2478/intox-2020-0003

sciendo

interdisciplinary toxicology

ORIGINAL ARTICLE

Effect of Vipoxin (*V. amm. meridionalis*) and its components on neuromuscular transmission

Yana GORANOVA [1], Silviya STOYKOVA [2,3], Ivan SAMNALIEV [1], Vasil ATANASOV [2,3]

[1] Research Laboratory of Military Toxicology, Department "Disaster Medicine and Toxicology" Military Medical Academy, Sofia, Bulgaria
[2] Emergency Toxicology Clinic, Department "Disaster Medicine and Toxicology" Military Medical Academy, 3, Sofia, Bulgaria
[3] Laboratory of Biocoordination and Bioanalytical Chemistry, Department of Analytical Chemistry, Faculty of Chemistry and Pharmacy, Sofia University, Sofia, Bulgaria

ITX130120A03 • Received: 12 December 2018 • Accepted: 08 March 2020

ABSTRACT
Vipoxin is the main toxic component isolated from the venom of long-nosed viper *Vipera ammodytes meridionalis,* which population is widely distributed on the Bulgarian area. The neurotoxin consists of two subunits – unstable and toxic phospholipase A_2 (PLA_2) and non-toxic acidic component without enzymatic activity (Vipoxin's acidic components, VAC). In the current study, the action of neurotoxic complex was examined by neurophysiological *in vivo* experimental model on anaesthetized rats. Vipoxin produces neuromuscular blockade in a dose-dependent manner with non-depolarizing post-junctional site of action. It was found that isolated PLA_2 displays significantly lower blocking activity in comparison with Vipoxin when both have been applied in equimolar concentration. That implies the stabilizing role of VAC and its significance for the toxicity of the whole complex. The Vipoxin-induced neuromuscular blockade is completely reversed when antivenom is administrated.

KEY WORDS: snake venom; Vipoxin; *in vivo* neurotoxicity; neuromuscular transmission

Introduction

Snake venoms are a cocktail of different compounds such as proteins with enzymatic and non-enzymatic activity, polypeptides and inorganic components that have evolved to assist in the capture and digestion of prey, as well as for use in defense against potential enemy. Each of these compounds may possess one or more different function as anticoagulant, hemolytic and cytolytic activities, necro-, myo-, nephro-, cardio- or neurotoxicity that could not be directly correlated with the enzymatic activity (Kini & Evans, 1989, Joseph *et al*., 2011).

Skeletal neuromuscular junction is one of the major targets of snake venom in the somatic nervous system (Utkin & Krivoshein, 2016). Particularly, attention needs to be paid to neurotoxins, which can be classified according to their site of action as pre- or post-synaptic (Gawade, 2004). Pre-synaptic neurotoxins with varying phospholipase A_2 activities were identified in the venoms of the four major families of venomous snakes – *Crotalidae, Elapidae, Hydrophiidae* and *Viperidae* (Harris, 1997, Kuruppu *et al*., 2008). A triphasic effect on acetylcholine release could be seen when the blockade of transmission is produced by these toxins (Su & Chang, 1984). Post-synaptic neurotoxins are known to be antagonists of the nicotinic receptor in the skeletal muscle (Gong *et al*., 1999). Depending on their sequence, post-synaptic toxins are subdivided into short- and long-chain toxins (Phui Yee *et al*., 2004). These toxins display different binding kinetics and different affinity for subtypes of nicotinic receptors. Post-synaptic neurotoxins are identified only in venoms of snakes from the families *Elapidae* and *Hydrophiidae*. (Hodgson & Wickramaratna, 2002). Effects of neurotoxins are manifested as interference of neuromuscular signal transmission and can vary from subtle alteration of neurotransmitter release to complete neuromuscular block. The activity of neurotoxins can be exerted at the pre-synaptic elements, post-synaptic or both (Harris, 1984). There are different kinds of venom, which contain both pre- and post-synaptically active toxins.

Correspondence address:
Yana Goranova
Research Laboratory of Military Toxicology,
Department "Disaster Medicine and Toxicology"
Military Medical Academy,
3, G. Sofiiski Str., 1606 Sofia, Bulgaria.
TEL.: ++3592-92-25960 • FAX +3592-92-25966
E-MAIL: goranovay@gmail.com

For example, a post-synaptic toxin Daboia Neurotoxin isolated from the venom of Russell's viper *Daboia russelii* contains phospholipase A_2 with pre-synaptic site of action. Venom of kraits (*Bungarus* spp.) consists of several different types of neurotoxins (Kini, 2003), in addition to the alpha-bungarotoxin (post-synaptic) and beta-bungarotoxin (pre-synaptic) already described (Lee *et al*., 1977, Rugulo *et al*, 1986). Venom of kraits also contains kappa-bungarotoxin that binds to the neuronal nicotinic acetylcholine receptors at the post-synaptic level in central cholinergic synapses in autonomic ganglia (Ranawaka *et al*., 2013). The main toxic component of the South American rattlesnake – the β-neurotoxin crotoxin (*Crotalus durissus terrificus*) may cause blockade via a post-synaptic action involving stabilization of the desensitized form of the nicotinic acetylcholine receptor (Sampaio *et al.,* 2010).

The family *Viperidae* is the most diverse family of venomous snakes (Tasoulis & Isbister, 2017). Most vipers have numerous heavily keeled scales and possess a large, flattened triangular head. The venom fangs are large, which permit deep penetration during envenomation of prey. They are found throughout Europe, Africa, Asia and America (Lewis & Gutmann, 2004).

Vipoxin is the main toxic component isolated from the venom of long-nosed Bulgarian viper – *Vipera ammodytes meridionalis* (Tomovic, 2006). It is a complex of two subunits – a basic and toxic phospholipase A_2 enzyme (EC 3.1.1.4, $sPLA_2$) and an acidic non-enzymatic component (Vipoxin's acidic components, VAC) with 62% amino-acid sequence identity (Mancheva *et al.,* 1987). This toxin is the first reported example of a high structural similarity between an enzymatic and non-enzymatic subunit and it is a unique example of regulation of toxic function generated by molecular evolution that is of great pharmacological interest. The complex formation between the two subunits is necessary for the physiological function of Vipoxin (Noetzel *et al*., 2002). The function of VAC is to stabilize the neurotoxin's quaternary structure, required for Vipoxin's toxic and enzymatic activities, similarly to the role of the acidic component of crotoxin (Atanasov *et al*. 2012). According to the published preliminary data, the neurotoxic complex of Vipoxin appeared able to block the post-synaptic membrane, whereas phospholipase A_2 manifested a pre-synaptic action that was possibly due to its enzymatic activity (Tchorbanov *et al*., 1978). In the present study, we are trying to investigate the mechanism of neuromuscular blockage *in vivo* as well as to answer the question about the difference in the toxic action of Vipoxin and its PLA_2.

Material and methods

Animals and surgical procedures, *in vivo* experiments

Experiments were carried out on 18 male albino "Wistar" rats (180–220 g) obtained from the Laboratory Animal Farm of Military Medical Academy (Sofia, Bulgaria). Prior to the experiments they have been housed with 6 animals per cage. Temperature was kept at 18–22 °C, humidity was maintained at 50–65% and 12 h light-dark cycle was available. Rats were allowed to standard rodent food and tap water *ad libitum.* The animals were anaesthetized by intraperitoneal injection of 1.5 g/kg 20% urethane applied 45 min before the beginning of experiment to minimize any pain and discomfort caused.

Experimental surgical protocol for cannulation of femoral vein and intravenous administration of the testing compounds was used (Goranova *et al*., 2018). This provides prolonged monitoring within the framework of 60–120 min and toxicological evaluation of the testing compounds and observation. The trachea was cannulated with an endotracheal tube connected to rodent ventilator with artificial ventilation. Tetanic responses of the *m. extensor digitorum longus* (EDL) evoked by *n. ischiadicus* stimulation.

Experiments were carried out in accordance with the Regulation № 20/2012 "Minimal requirements for protection and humanely attitude to the experimental animals, Bulgarian Food Safety Agency, Animal Health and Welfare and Feed Control Directorate, Animal Welfare Unit (Member State authorities for Directive 2010/63/EU).

The scientific examination *in vivo* of experimental animals, has been conducted in accordance with the principles of ICLAS/FELASA and the Ordinance for a humanely attitude towards the experimental animals, with regard to which Military Medical Academy (Sofia, Bulgaria) has received the necessary license-permit received by the National Commission. /License-permit from the National Commission 13/06.02.2013/ Standpoint № 6/ expiration date: 06.02.2018/

Toxins

Vipoxin was isolated from crude air-dried venom from Bulgarian long-nosed viper *Vipera ammodytes meridionalis* (purchased from the Thracian Herpetological Society, Stara Zagora, Bulgaria) by ion-exchange chromatography on SP-Sephades C-50 (Pharmacia, Sweden) using linear gradient from 0.05 M up to 0.4 M Tris-citrate buffer, pH 7.3 (Tchorbanov & Aleksiev, 1981; Atanasov *et al*., 2009). It was dialyzed and lyophilized before separation of its component using charged chromatography with carboxymethylcellulose. The homogeneity of the basic and acidic subunits was verified by SDS-PAGE (Laemmli, 1970). Total protein content was determined according to Smith *et al.* (1985). Enzymatic activity was assayed as described by Cho *et al.* (1988) and Holzer & Mackessy (1996).

Doses, *in vivo* experiments

Vipoxin was administered intravenously in three different doses – 1/5, 1/10, and 1/20 of LD_{50} (7.8 mg/kg b.w.). LD_{50} (rats) of the neurotoxin was calculated using conversion factor between animals (Nair & Jacob, 2016) based on previously published LD_{50} (mice) (Atanasov *et al*., 2012). PLA_2 and VAC were also applied intravenously in the dose equimolar to 1/5 LD_{50} of Vipoxin and 1/10 LD_{50} (rats) of Vipoxin, respectively (the number of repetitions is 3 for each dose administered). To reconstitute the

Vipoxin complex, the PLA_2 subunit was incubated with the same molar concentration of VAC (1:1 molar ratio as in the native Vipoxin) for 30 min at 4 °C (Atanasov *et al*., 2012). To analyze the effect of antivenom (100AE, 1:100, Bul Bio, Bulgaria), it was injected intravenously without further dilution.

Devices

Measuring system for investigation of neuromuscular conduction and contractile function on rat skeletal muscle was used (Experimetria, Ltd., Hungary). The system is designed to study on neuromuscular connection in *in vivo* condition on small laboratory animals (rats and guinea pigs). It mainly consists of microprocessor controlling modular square wave stimulator. SPEL Advanced Haemosys Software is an integral part of the compact research system and has been developed to monitor, save and analyze all measuring online and offline data. The contractile response is measured following either direct muscle stimulation, or by nerve stimulation. Parameters of the electrical stimulus were: PP (pulse period) – 45 s, PW (pulse width) – 1 ms, TD (train delay) – 0, TN (train numbers) – 0, DE (delay) – 5 ms, pressure – 3 V. Tetanic responses were elicited by 50 Hz trains of stimuli for five seconds.

Red blood cells (RBC) morphology and complete blood count

The effect of Vipoxin and its components to RBC morphology was assessed by examination of stained blood smears. To make a visual evaluation of RBC, 50 µl whole blood (K_2EDTA) was collected from the treated animal in the end of the neuromuscular transmission experiment. The staining of blood smears was accomplished according to the Pappenheim procedure using Giemsa and May-Grünwald dyes (Penev & Dukova-Peneva, 2007). Visualization of RBC morphology was performed using light microscope Motik 1820 (Motik, China, 1000×, oil immersion). Complete blood count was measured using analyzer "Erma Inc".

Results and discussion

Neuromuscular transmission

Neuromuscular synaptic transmission involves sequence of events, in which every single step is a possible target for neurotoxic activity. Acetylcholine is neurotransmitter synthesized from inactive precursors within the pre-synaptic nerve terminal (Bowman, 1995). Arrival of action potential in pre-synaptic motor axon terminals cause to open of voltage gated Ca^{2+} channels and Ca^{2+} moves down its electrochemical gradient into the nerve terminal. The elevation of unbound Ca^{2+} leads to fusion of the vesicles with the pre-synaptic membrane. Acetylcholine is released into the synaptic cleft as a response to an action potential and bounds to the acetylcholine receptors on the post-synaptic membrane (Sakmann, 1992). This opens ion channels in the post-synaptic membrane that allow the flow of positive-charged ions down the concentration gradient and consequently depolarization of the post-synaptic membrane occurs. If the response reaches threshold, a regenerative action potential is generated on the post-synaptic membrane, which ultimately results in muscle contraction. The action of acetylcholine is terminated rapidly by the enzyme acetylcholinesterase and the process repeats (Lewis & Gutmann, 2004).

Snake venoms contain potent toxins that are capable of inhibiting neuromuscular transmissions on pre-synaptic (β-neurotoxins) and post-synaptic (α-neurotoxins) sites. The pre-synaptic neurotoxicity is associated with PLA_2 activity found in the venoms. Finding that after a relatively short time period (*i.e.* approximately 30 min) the inhibitory effects of the β-neurotoxins cannot be reversed by the addition of antivenom is of clinical interest (Hodgson & Wickramaratna, 2002). It is known that some β-neurotoxins (taipoxin, notexin) cause irreversible pre-synaptic damage and depletion of pre-synaptic vesicles one hour after injection of venoms (Bowman, 2006, Cull-Candy *et al*., 1976).

Vipoxin is one of the few known multichain neurotoxins with post-synaptic toxicity. The results obtained in previously *in vitro* experiment in 1978 showed that the toxin isolated from *Vipera ammodytes meridionalis* is an α-neurotoxin that acts on the postsynaptic membranes preventing the binding of acetylcholine to its receptor and blocking the neuromuscular transmission of skeletal muscles (Tchorbanov *et al*., 1978). In this way, the toxin exerts its lethal action similar to another multimeric post-synaptic snake venom α-bungarotoxin. When isolated from the complex, the vipoxin's PLA_2 manifests a presynaptic action. Evidently, the complex formation changes the target of the pharmacological action of the neurotoxin and Vipoxin is "targeted" to the post-synaptic site (Banumathi *et al*., 2001).

In the current study, we assessed *in vivo* effects on the neuromuscular transmission of native Vipoxin in rats, isolated from the venom of Bulgarian long-nosed viper *Vipera ammodytes meridionalis*, and its subunits – PLA_2 and VAC, each applied alone as well as reconstituted complex Vipoxin (a mixture of preliminary separated PLA_2 and VAC in 1:1 molar ratio, incubated for 30 min at 4 °C).

In blank experiment (control), the tetanic responses of EDL after nerve stimulation were 95±5% of control group (n=3) after 60 min of *n. ischiadicus* stimulation were induced.

In our experiments Vipoxin produces a dose-depended blockade of the tetanic responses of the EDL to nerve stimulation. 75% inhibition of neuromuscular transmission was recorded at higher dose of Vipoxin 1/5 LD_{50} (rats) (Figures 1A, B). In contrast, when PLA_2 was applied in equimolar dose of 1/5 LD_{50} (rats) Vipoxin, causes only 15% depression of neuromuscular transmission (Figures 1A, B). The reconstituted Vipoxin demonstrates 40% depression of neuromuscular transmission, that is practically the same effect as native Vipoxin in the same dose used, which means that the Vipoxin complex is completely restored (Figure 1A). These findings support the presumption that the integrity of the neurotoxin is

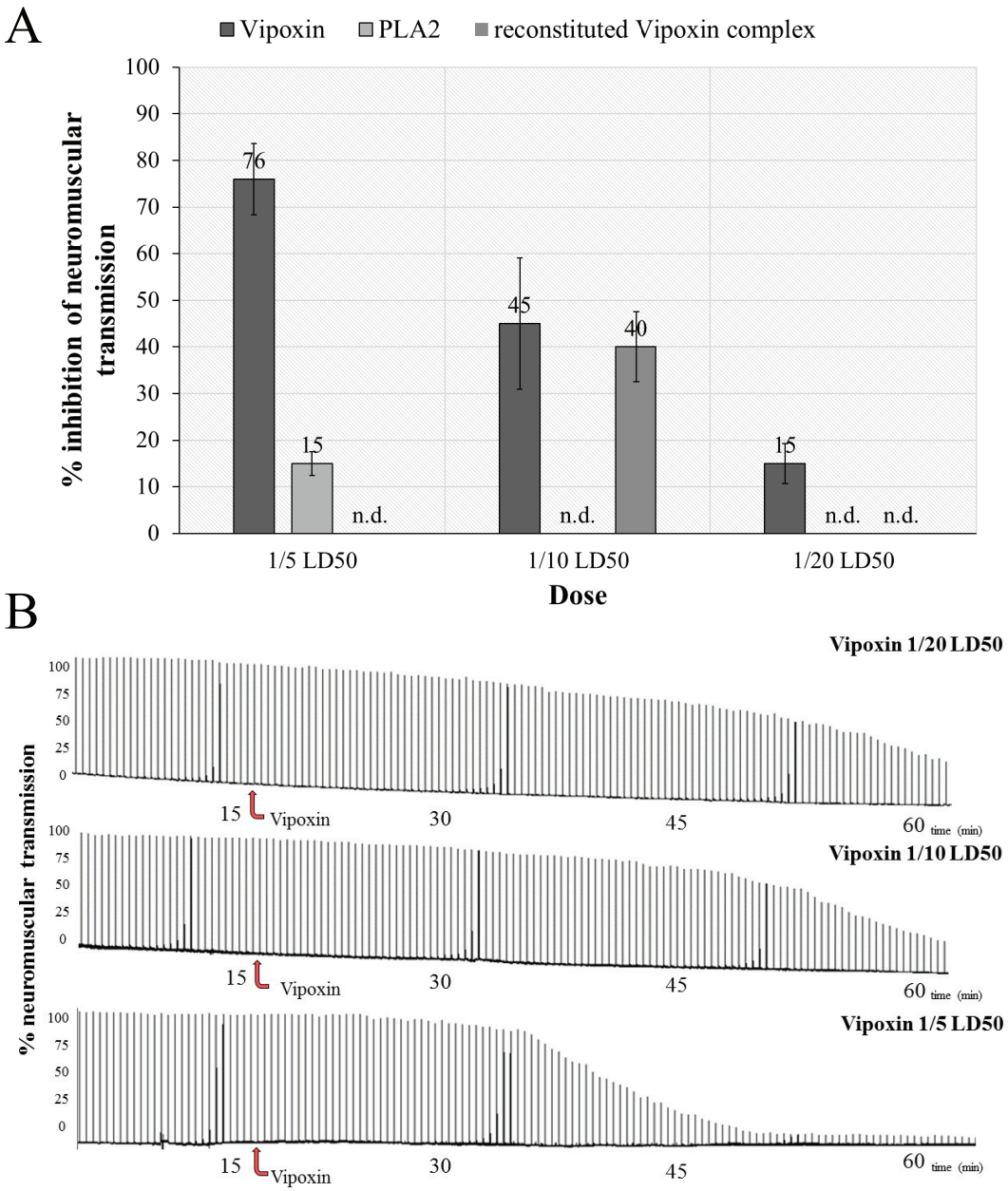

Figure 1. A) Evaluation of inhibitory effect of Vipoxin, PLA_2 and reconstituted Vipoxin complex (PLA_2 and VAC in ratio 1:1) on neuromuscular transmission at 60 min. All compounds tested were used at doses equimolar to 1/5, 1/10 and 1/20 LD_{50} Vipoxin. Each experiment was performed in triplicate (three independent analysis). B) Representative mechanograms of neuromuscular transmission following application of neurotoxin Vipoxin at doses to 1/5, 1/10 and 1/20 LD_{50}. Administration of compound tested was labeled and indicated by a bent arrow.

important for its toxic activity and raise questions about the VAC role on the whole complex.

The onset of neuromuscular block was gradual in all of the doses and testing compounds used. The depressions in the tetanic responses became detectable approximately 14 min (8–20 min) after intravenous injection of the testing compounds. The presence of a fade response during the blockade of nerve-evoked tetanic responses of the EDL has been observed for all Vipoxin and reconstituted complex doses applied.

The muscle response to tetanic stimulation is sustained during normal neuromuscular transmission and a pure depolarizing block, whereas during a non-depolarizing block fade occurs and the response is not sustained. A possible explanation for the fade response is that under tetanic stimulation the acetylcholine, available in pre-synaptic stores, bursts into synaptic cleft and starts to stimulate post-synaptic cholinergic receptors. The process continues until a depletion of stores occurs followed by a period of equilibrium, meanwhile mobilization and synthesis of acetylcholine is achieved. However, even in condition of this equilibrium a tetanic stimulation of the nerve (50 Hz) maintain muscle response due to incongruity between the release of acetylcholine (much higher) and

its amount necessary to evoke a response. When a non-depolarizing neuromuscular blocking agent provokes reduction of the "margin of safety" of the post-synaptic membrane the decrease in release of acetylcholine during tetanic stimulation produces fade (Miller, 2010).

The results obtained from this study well correlate to the data about acute toxicity of Vipoxin and its PLA_2 confirming that native Vipoxin is more toxic in comparison to PLA_2 and the VAC is of importance for toxicity of the whole complex (Atanasov *et al*., 2012). It can be concluded that Vipoxin is the carrier of the toxic effects on the skeletal muscles and neuromuscular transmission particularly.

There is a dose-response relationship between the amount of Vipoxin and the reducing of the neuromuscular transmission. This finding explains the clinical signs followed envenoming by Bulgarian viper and the corresponding effects on the skeletal muscles.

Here, for the first time, we have tested the effect of the antivenom (commercial product; fraction from horse hyperimmune plasma) on the neuromuscular transmission after Vipoxin-induced inhibition. It was found that the neuromuscular activity is successfully recovered when the antivenom have been applied (Figure 2). In our experimental protocol, the specific treatment started immediately when the neuromuscular block was registered. In the future project, the antidote effects of the same antivenom will be assessed after postpone application.

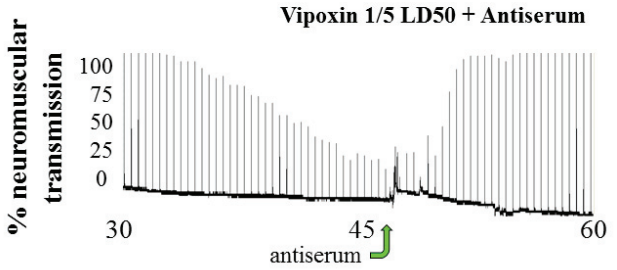

Figure 2. Representative mechanogram of effect of antivenom (applicated 30 min after neurotoxin) on neuromuscular blockade caused by 1/5LD50 Vipoxin (administered at 15 min).

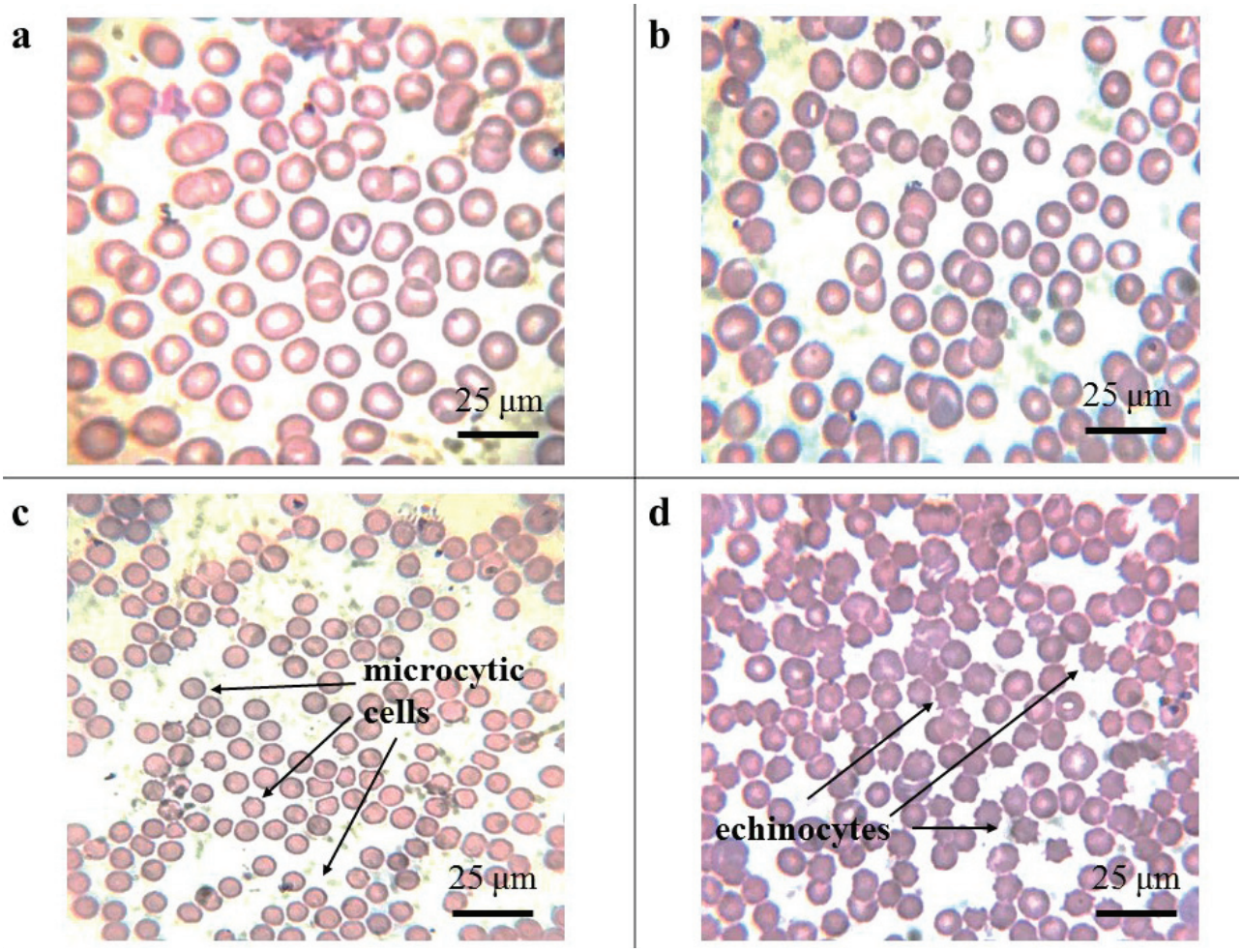

Figure 3. Representative images of effect of Vipoxin at doses of 1/5, 1/10 and 1/20 LD_{50} on morphology of RBC (blood smears): **(a)** normal erythrocytes control; (b) RBC treated with Vipoxin at dose 1/20 LD_{50} where no morphology deviation was observed; (c) RBC treated with 1/10 LD_{50} Vipoxin – an increased number of microcytic cells suggesting initial membrane lysis can be observed; (d) RBC treated with Vipoxin at dose 1/5 LD_{50} – registration of numerous echinocyte formation.

Red blood cells morphology and complete blood count

Normocytic RBCs are biconcave, disc-shaped, anuclear cells. Their morphology has five important parameters: shape, size, color, inclusions and arrangement. The abnormalities of RBC morphology are source of the key information in establishing a differential diagnosis. In our experiment, no deviation in RBC morphology was observed in the control sample (Figure 3a) and at the lowest dose of Vipoxin 1/20 LD_{50} (rats) used (Figure 3b). When the dose of 1/10 LD_{50} (rats) Vipoxin was applied (Figure 3c) an increased number of macrocytic cells was observed, whereas when the highest dose of 1/5 LD_{50} (rats) Vipoxin was applied numerous echinocyte formations were found (Figure 3d). It should be mentioned that macrocytosis supposes an initial membrane lysis. The presence of echinocytes in this case may be used as a diagnostic and hemolytic prognostic factor. The effect on RBC morphology due to Vipoxin's PLA_2 subunit have been studied (Stoykova *et al*., 2013) and apparently, it was found that echinocytes formation is a main result of PLA_2 enzymatic activity.

Conclusion

The effect of Vipoxin (the main toxin isolated from the long-nosed Bulgarian viper – *Vipera ammodytes meridionalis*) on the neuromuscular transmission and its ability to cause disturbance in physiological functions of the neuromuscular synapse was studied for the first time using neurophysiological *in vivo* experiment. A relation between the doses of the neurotoxin Vipoxin and the extent of reduction of neuromuscular transmission was registered. The comparison between the effects of PLA_2 and recombinant Vipoxin (complex of PLA_2 and VAC) on the neuromuscular transmission showed that recombinant Vipoxin possesses the same potential as the native Vipoxin. Vipoxin induces neuromuscular block with non-depolarizing post-junctional site of action. Applying of antivenom reverses the neuromuscular transmission when the Vipoxin-induced blockade is realized. The dose-responded changes on RBC's morphology was observed during the experiments displaying *in vivo* hemolysis of the cells.

REFERENCES

Atanasov VN, Danchev D, Mitewa M, Petrova S. (2009). Hemolytic and anticoagulant study of the neurotoxin Vipoxin and its components – basic phospholipase A_2 and an acidic inhibitor *Biochemistry (Moscow)* **74**(3): 276–280.

Atanasov VN, Stoykova S, Goranova Y, Mitewa M, Petrova S. (2012) Acute toxicity of vipoxin and its components: is the acidic component an "inhibitor" of PLA_2 toxicity? *Interdiscip. Toxicol.* **5** (4): 169–172.

Banumathi S, Rajashankar RK, Nötzel C, Aleksiev B, Singh PT, Genov N, Betzel Ch. (2001). Structure of neurotoxic complex Vipoxin at 1.4 Å resolution. *Acta Cryst D57,* 1552–1559.

Bowman CW. (1995). Physiology of the Neuromuscular Junction, in *Muscle Relaxants* (Fukushima K and Ochiai R eds) pp. 117–127, Springer, Tokyo.

Bowman CW. (2006). Neuromuscular block. *Br J Pharmacol* **147**: S277–S286.

Cho W, Markowitz MA, Kézdy FJ. (1988). A new class of phospholipase A_2 substrates: kinetics of the phospholipase A_2 catalyzed hydrolysis of 3-(acyloxy)-4-nitrobenzoic acids. *J Am Chem Soc* **110**: 5166–5171.

Cull-Candy GS, Fohlman J, Gustavsson D, Lüllmann-Rauch R, Thesleff S. (1976). The effects of Taipoxin and Notexin on the function and fine structure of the murine neuromuscular junction. *Neuroscience* **1**: 175–180.

Gawade PS. (2004). Snake venom neurotoxins: Pharmacological classification. *J Toxicol Toxin Rev* **23** (1): 37–96.

Gong N, Armugam A, Jeyaseelan K. (1999). Postsynaptic short-chain neurotoxins from *Pseudonaja textilis*, cDNA cloning, expression and protein characterization. *Eur J Biochem* **265**: 982–989.

Goranova Y, Samnaliev I, Nikolov S, Zlatev O, Kesov G, Iordanov V, Atanasov V. (2019). Experimental surgical protocol for continuous femoral venous access in the rat. *BJVM* **22**(3): 322–329.

Harris JB, Grubb BD, Maltin CA, Dixon R. (1984). The neurotoxicity of the venom phospholipases A_2, notexin and taipoxin. *Exp Neurol* **161**: 517–526.

Harris JB. (1997). Toxic phospholipases in snake venom: An introductory review. *Symp Zool Soc Lond* **70**: 235–250.

Hodgson CW, Wickramaratna CJ. (2002). *In vitro* neuromuscular activity of snake venoms. *Clin and Exp Pharm and Phys* **29**: 807–814.

Holzer M, Mackessy SP. (1996). An aqueous endpoint assay of snake venom phospholipase A_2. *Toxicon* **34**: 1149–1155.

Joseph B, Raj SJ, Edwin T, Sankarganesh P. (2011). Pharmacognostic and biochemical properties of certain biomarkers in snake venoms. *Asian J Biol Sci* **4**: 317–324.

Kini RM, Evans HJ. (1989). A model to explain the pharmacological effects of snake venom phospholipase A_2. *Toxicon* **27**: 613–635.

Kini RM. (2003). Excitement ahead: structure, function and mechanism of snake venom phospholipase A_2 enzymes. *Toxicon* **42** (8): 827–840.

Kuruppu S, Ian Smith A, Isbister GK, Hodgson WC. (2008). Neurotoxins from australo-papuan elapids: a biochemical and pharmacological perspective. *Crit Rev Toxicol* **38**: 73–86.

Laemmli UK. (1970). Cleavage of Structural Proteins during the Assembly of the Head of Bacteriophage T4. *Nature* **227**: 680–685.

Lee Ch, Dennis Ch, Katz LR. (1977). Characteristics of nondepolarizing neuromuscular block: (I) Post-junctional block by alpha-bungarotoxin. *Canad Anaesth Soc J* **24** (2): 212–219.

Lewis RL, Gutmann L. (2004). Snake venoms and the neuromuscular junction, Disorders of neuromuscular transmission. *Semin Neurol* **24** (2): 175–179.

Mancheva I, Kleinschmidt T, Aleksiev B, Braunitzer G. (1987). Sequence homology between phospholipase and its inhibitor in snake venom. The primary structure of phospholipase A_2 of vipoxin from the venom of the Bulgarian viper (*Vipera ammodytes ammodytes*, Serpentes). *Biol Chem Hoppe-Seyler* **368**: 343–352.

Miller RD. (2010). *Miller's Anesthesia* (7th ed.). Churchill Livingstone, Philadelphia.

Nair AB, Jacob S. (2016). A simple practice guide for dose conversation between animals and human. *J Basic Clin Pharma* **7**: 27–31.

Noetzel C, Chandra V, Perbandt M, Rajashankar K, Singh T, Aleksiev B, Kalkura N, Genov N, Betzel Ch. (2002). Enzymatic activity and inhibition of the neurotoxic complex vipoxin from the venom of *Vipera ammodytes meridionalis*. *Z Naturforsch* **57**: 1078–1083.

Penev M, Dukova-Peneva P. (2007). *Laboratory Hematology*. Artik-2001, Sofia.

Phui Yee JS. Nanling G, Afifiyan F, Donghui M, Lay PS, Armugam A and Jeyaseelan K. (2004). Snake postsynaptic neurotoxins: gene structure, Phylogeny and applications in research and therapy. *Biochimie* **86**: 137–149.

Ranawaka KU, Lalloo GD, de Silva HJ. (2013). Neurotoxicity in snakebite-the limits of our knowledge. *PLOS Negl Trop Dis* **7**(10): e2302.

Rugulo MJ, Dolly O, Nicholis DG. (1986). The mechanism of action of β-bungarotoxin at the presynaptic plasma membrane. *Biochem J* **233**: 519–523.

Sakmann B. (1992). Elementary steps in synaptic transmission revealed by currents through single ion channels. *The EMBO Journal* **11**(6): 2003–2016.

Sampaio CS, Hyslop S, Fontes RM, Prado-Franceschi J, Zambelli OV, Magro JA, Brigatte P, Gutierrez PV, Cury Y. (2010). Crotoxin: Novel activities for a classic β-neurotoxin. *Toxicon* **55**: 1045–1066.

Smith PK, Krohn RI, Hermanson GT, Mallia AK, Gartner FH, Provenzano MD, Fujimoto EK, Goeke NM, Olson BJ, Klenk DC. (1985). Measurement of protein using bicinchoninic acid. *Anal Biochem* **150**: 76–85.

Stoykova S, Goranova Y, Pantcheva Iv, Atanasov V, Danchev D, Petrova S. (2013). Hemolytic activity and platelet aggregation inhibitory effect of vipoxin's basic $sPLA_2$ subunit. *Interdiscip Toxicol* **6**(3): 136–140.

Su MJ, Chang CC. (1984). Presynaptic effects of snake venom toxins which have phospholipase A_2 activity (β-bungarotoxin, taipoxin, crotoxin). *Toxicon* **22**(4): 631–640.

Tasoulis T, Isbister GK. (2017). A review and database of snake venom proteomes. *Toxins (Basel)* **9**: 290.

Tchorbanov B, Aleksiev B. (1981). A simple procedure for the isolation of Vipoxin – a neurotoxin with phospholipase A_2 activity from the venom of the Bulgarian viper (*Vipera ammodytes*). *J App Biochem* **3**: 558–561.

Tchorbanov B, Grishin E, Aleksiev B, Ovchinnikov Yu. (1978). A neurotoxic complex from the venom of the Bulgarian viper (*Vipera ammodytes ammodytes*) and a partial amino acid sequence of the toxic phospholipase A_2. *Toxicon* **16**: 37–44.

Tomovic L. (2006). Systematics of the nose-horned viper (*Vipera ammodytes Linnaeus*, 1758). *Herpetol J* **16**: 191–201.

Utkin YN, Krivoshein AV. (2016). *Snake venoms and envenomation, modern trends and future prospects*. Nova Science Publishers.

Interdiscip Toxicol. 2020; **Vol. 13**(1): 28–38.
doi: 10.2478/intox-2020-0004

sciendo

interdisciplinary toxicology

ORIGINAL ARTICLE

Lead induced impairments in brain mitochondrial metabolic and oxidative enzymes in pregnant and non-pregnant rats: protective effect of α-tocopherol

Sreenivasulu NAGARAJ, Chand Basha DAVULJIGARI, Rajarami Reddy GOTTIPOLU
Department of Zoology, Sri Venkateswara University, Tirupati, Andhra Pradesh, India

ITX130120A04 • Received: 26 September 2018 • Accepted: 15 March 2020

ABSTRACT
Our earlier studies showed that exposure to lead (Pb) caused irreversible perturbations in the cholinergic system and neurobehavioral functions of female rats. In this study, we extended our studies to investigate the role of mitochondrial metabolic and oxidative enzymes in response to Pb exposure in pregnant and non-pregnant rats. Further, we evaluated the protective effect of α-tocopherol against Pb-induced mitochondrial dysfunction in female rats. Pregnant (GD 1 to PND 21) and non-pregnant rats were exposed to 0.2% Pb for the period of 42 days (6 weeks) while alpha (α)-tocopherol (100 mg/kg) was given orally through gavage for a period of 21 days (last 3 weeks) to Pb exposed pregnant and non-pregnant rats. Rats were decapitated on 7th day and 30th-day after the 42 days Pb exposure. Pb exposure decreased the activities of mitochondrial succinate dehydrogenase (SDH), isocitrate dehydrogenase (ICDH), superoxide dismutase (SOD), glutathione peroxidase (GPx) and catalase (CAT) enzymes whereas the glucose-6-phosphate dehydrogenase (G6PDH), and malondialdehyde (MDA) levels increased in the cortex, cerebellum, and hippocampus at both 7th and 30th day points of pregnant and non-pregnant rats. Pb-induced alterations were greater in cortex coinciding with higher Pb levels observed in the cortex than hippocampus and cerebellum. Although the supplementation of α-tocopherol significantly reversed the Pb-induced alterations in the mitochondrial metabolic and oxidative enzymes, the reversal effect on Pb levels in different brain regions was marginal in both pregnant and non-pregnant rats. In conclusion, our data demonstrate that exposure to Pb significantly alters the mitochondrial enzymes in brain region-dependent manner and the effect of Pb was greater in non-pregnant female rats than pregnant rats. Further, the data provide evidence for the protective efficacy of α -tocopherol against Pb-toxicity.

KEY WORDS: lead toxicity; vitamin E; pregnancy; rats; mitochondrial enzymes

Introduction

Lead (Pb) is a ubiquitous environmental and industrial pollutant that has been detected in almost all phases of biological systems (EFSA, 2012). Pb is known to induce a broad range of physiological, biochemical and behavioral dysfunctions in animals and humans (Basha & Reddy, 2015; Gao *et al.,* 2010). Exposure to Pb can result in significant alterations in various organs, the nervous system being an important target (Flora *et al*., 2012). The mean half-life of Pb in blood is approximately 21–28 days, whereas Pb accumulates in bones with a mean half-life of 5–19 days and this burden may be mobilized during pregnancy and readily crosses the placenta into the blood of the developing fetus (Beier *et al.,* 2015; ATSDR, 2007). Neuro-behavioral deficits in children such as impaired cognition, impulsivity, hyperactivity and decreased motor functions, due to exposure to low-level Pb, have been well documented (Liu *et al.,* 2013). Our previous studies also clearly stated that early life exposure to Pb-induced the broad range of neurological problems and these Pb-induced neurobehavioral dysfunctions in young rats persisted in later life (Gottipolu *et al.,* 2014; Basha *et al.,* 2012). However, compared with children, the impact of Pb exposure on women health has been neglected.

Correspondence address:
Dr. Davuljigari Chand Basha
Department of Zoology,
Sri Venkateswara University,
Tirupati, Andhra Pradesh, India-517502.
E-MAIL: drchandbasha2012@gmail.com

One of the possible mechanisms underlying Pb-induced neurotoxicity is its capacity to produce reactive oxygen species (ROS) and oxidative stress, which contributes to the pathogenesis of poisoning by disrupting the pro-oxidant/antioxidant balance in cells (Jia *et al.*,2012). Neurons are particularly vulnerable to free radical attack since impaired defences or exposure to excess free radicals may lead to neuronal death (Gutowicz, 2011; Akitane *et al.*, 1994). Mitochondria are important intracellular target site for Pb toxicity (Sousa & Soares, 2014). Experimental studies confirmed the possible involvement of reactive oxygen species (ROS) in Pb-induced toxicity (Lopes *et al.*, 2016) by increased lipid peroxidation (TBARS) and decreased activities of mitochondrial enzymes, succinate dehydrogenase (SDH), isocitrate dehydrogenase (ICDH), catalase (CAT), glutathione peroxidase (GPx), and superoxide dismutase (SOD) in rat brains (Basha *et al.*, 2012; Pande & Flora 2002; Kuhad & Chopra, 2007).

Vitamin E (vit-E) has been used as antioxidant to prevent the Pb-induced oxidative damage in nervous system (Salehi *et al.*, 2015). Few studies reported that supplementation of vit-E lowered ROS that generate cellular damage in different cell types, prevented the Pb-induced perturbations in aminolevulinic acid dehydratase (ALAD) activity in blood (Rendón-Ramirez *et al.*, 2007), increased the total antioxidant capacity as well as superoxide dismutase (SOD), catalase (CAT) and glutathione peroxidase (GPx) activities (Prasanthi *et al.*, 2010, Machartová *et al.*, 2000). Our previous study also reported the beneficial effects of vit-E against Pb-induced neurobehavioral dysfunctions in female rats (Sreenivasulu *et al.*, 2015). The present study is designed to investigate the adverse effects of Pb on mitochondrial metabolic and oxidative enzymes in different brain regions of pregnant and non-pregnant rats and further examine the beneficial effect of the administration of vit-E on Pb-induced mitochondrial dysfunction in rats.

Materials and methods

Chemicals

Chemicals (lead acetate and α-tocopherol acetate) used in this study were purchased from Sigma Chemical Co. St Louis., USA and all other chemicals were purchased from Merk, India.

Animal exposure

For the present study, non-pregnant (adult) and pregnant female (adult) rats were selected. Pregnant (GD 1 to PND 21) and non-pregnant rats were exposed to 0.2% Pb for the period of 42 days (6 weeks) while alpha (α)-tocopherol (100 mg/kg) was given orally through gavage for a period of 21 days (last 3 weeks) to Pb exposed pregnant and non-pregnant rats (Figure 1). Control rats received only deionized water without Pb. Rats were decapitated on 7th day and 30th-day after the 42 days Pb exposure (*i.e.*, 6 animals of each group were sacrificed for each time point (7th and 30th days). Different brain regions such as cerebral cortex, hippocampus and cerebellum were isolated on ice and used for estimating biochemical analysis and Pb levels. The experiments were carried out in accordance with the guidelines of the Committee for the Purpose of Control and Supervision on Experiments on Animals (CPCSEA), Government of India, and Animal Ethical Committee of S.V. University.

Preparation of brain mitochondrial fraction

Mitochondrial fractions were prepared by following the method of Lai and Clark (1979). The tissues were homogenized in 10 volumes (w/v) of SET buffer (0.25 M sucrose, 10 mM Tris-Hcl, and 1 mM EDTA, pH 7.4). The homogenate was first centrifuged at 800 × *g* for 10 min at 4 °C, and then supernatant was centrifuged at 10,000 × *g* for 20 min. Then the pellet of mitochondrial fraction was suspended in SET buffer.

Estimation of mitochondrial metabolic enzymes

Succinate dehydrogenase (SDH)

SDH activity was estimated by the method of Nachlas *et al.* (1960) as modified by Prameelamma and Swami (1975) with slight modifications. The total reaction mixture contained 0.5 ml of phosphate buffer (pH 7.2), 0.4 ml of sodium succinate, 0.4 ml of INT and 0.2 ml of water in a final volume of 2 ml. The reaction was initiated by addition of 0.2 ml of mitochondrial fraction. The contents

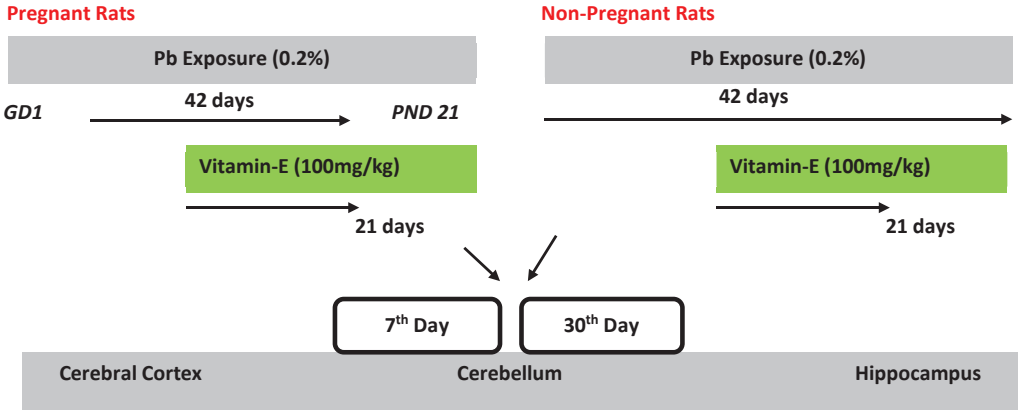

Figure 1. Study design: A schematic representation of exposure.

were incubated for 30 min at 37 °C. After incubation, the reaction was stopped by addition of 5 ml of glacial acetic acid. Later 5 ml of Toluene was added and kept for overnight. The formazan formed was extracted into 5.0 ml of toluene and the colour was measured at 495 nm in spectrophotometer (Hitachi model, U-2001) against toluene blank.

Isocitrate dehydrogenase (ICDH)

Isocitrate Dehydrogenase activity was estimated by the method of Lee and Lardy (1965). The final volume of 2 ml assay mixture contains 0.5 ml of phosphate buffer (pH 7.2), 0.4 ml of Isocitrate, 0.4 ml of INT, 0.1 ml of $MgCl_2$, 0.1ml of ADP and 0.2 ml of NAD. The reaction was initiated by addition of 0.3 ml of mitochondrial fraction. The contents were incubated for 30 min at 37 °C. After incubation, the reaction was stopped by addition of 5 ml of glacial acetic acid. Later 5 ml of Toluene was added and kept for overnight. The formazan formed was extracted into 5.0 ml of toluene and the colour was measured at 545 nm in spectrophotometer (Hitachi model, U-2001) against toluene blank.

Glucose-6-phosphate dehydrogenase (G6PDH)

G6PDH activity was estimated by the method of Bergmeyer and Bruns (1965). The final volume of 2 ml assay mixture contains 0.5 ml of phosphate buffer (pH 7.2), 0.4 ml of Glucose-6-Phosphate, 0.4 ml of INT, 0.1 ml of NADP and 0.2 ml of water. The reaction was initiated by addition of enzyme source. The contents were incubated for 30 min at 37 °C. After incubation, the reaction was stopped by addition of 5 ml of glacial acetic acid. Later 5 ml of Toluene was added and kept for overnight. The formazon formed was extracted into 5.0 ml of toluene and the colour was measured at 545 nm in spectrophotometer (Hitachi model, U-2001) against toluene blank.

Estimation of mitochodrial oxidative marker enzymes

Superoxide dismutase (SOD)

SOD activity was determined by using the epinephrine assay of Misra and Fridovich (1972). At alkaline pH, superoxide anion O_2^- causes the autooxidation of epinephrine to adenochrome; while completing this reaction, SOD decreased the adenochrome formation. One unit of SOD is defined as the amount of extract that inhibits the rate of adenochrome formation by 50%. The reaction mixture in a final volume of 2.0 ml contained 0.05 M carbonate buffer (pH 10.2), 30 mM epinephrine (freshly prepared) and the enzyme extract. The changes in absorbance were recorded at 480 nm, measured at 10 sec intervals for 1 min in a spectrophotometer (Hitachi model, U-2001).

Catalase (CAT)

Catalase activity in the brain mitochondrial fraction was assayed by following the method of Chance and Maehly (1955). The reaction mixture in a final volume of 2.5 ml contained: 0.05 M phosphate buffer (pH 7.0) and appropriate amount of enzyme protein. The reaction was initiated by the addition of 19 mM hydrogen peroxide (H_2O_2). The decomposition of H_2O_2 was followed directly by measuring the decrease in absorbance at 240 nm, at 10 sec intervals for 1 min in a spectrophotometer (Hitachi model, U-2001).

Glutathione peroxidase (GPx)

GP_X activity in the mitochondrial fraction of brain was assayed as described by Rotruck *et al.* (1973). The reaction mixture contained 0.2 ml of EDTA, 0.2 ml of 4 mM sodium azide, 0.2 ml of glutathione reduced, 0.2 ml of H_2O_2, 0.4 ml of 0.32 M sodium pyrophosphate buffer (pH 7.0) and 0.1 ml of enzyme source. Then the reaction mixture was incubated at 37 °C for 10 min. Then the reaction was arrested by adding of 0.5 ml 10% TCA. Then, samples were centrifuged at 2000 rpm for 10 min. To 0.5 ml of supernatant, 3.0 ml of 0.3 M disodium hydrogen phosphate and 1.0 ml of DTNB were added and the reaction was read at 412 nm in spectrophotometer (Hitachi model, U-2001).

Lipid peroxidation

The lipid peroxides were determined by the TBA method of Ohkawa and Yagik (1979). The tissues were homogenized in 1.5%KCl (20% W/V). To 1 ml of tissue homogenate 2.5 ml of 20%TCA was added and the contents were centrifuged at 3,500 g for 10 minutes and the precipitate was dissolved in 2.5 ml of 0.05 M sulphuric acid. To this, 3 ml of thiobarbituric acid (TBA) was added and the samples were kept in a hot water bath for 30 minutes. The samples were cooled and malonaldehyde (MDA) was extracted with 4 ml of n-butanol and the color was read at 530 nm in a spectrophotometer (Hitachi model, U-2001) against the reagent blank. Trimethoxy pentane (TMP) was used as external standard.

Estimation of brain regional Pb levels

Pb levels in different brain regions of control and experimental rats were estimated with atomic absorption spectrophotometer (AAS- Shimadzu-AA 6300) with graphite furnace (GFA-EX7i). After digestion with concentrated nitric acid using a microwave digestion system followed by addition of 30% hydrogen peroxide, samples were brought to a constant volume. The aliquots were used for estimation of Pb levels.

Protein content

Protein content of the tissues was estimated by the method of Lowry *et al.* (1951). 1% (W/V) homogenate was prepared in 0.25 M ice cold sucrose solution. To 0.5 ml of crude homogenate, 1 ml of 10% TCA was added and the samples were centrifuged at 1000 × g for 15 min. The residue was resuspended in 0.5 ml of 1 N NaOH. And 4 ml of alkaline copper sulphate reagent was added followed by 0.4 ml of folin-phenol reagent (1:1 folin: H_2O). The color was measured at 600 nm in a UV–vis spectrophotometer (Hitachi model U-2001) against blank. The protein standard graph was prepared using Bovine serum albumin.

Statistical analysis of the data

The data were subjected to one way analysis of variance (ANOVA) followed by student Newman-Keuls (SNK) *post hoc* test. The 0.05 level of probability was used as the criterion for significance.

Results

The specific activities of superoxide dismutase (SOD), catalase (CAT), glutathione peroxidase (GPx), succinic dehydrogenase (SDH), isocitrate dehydrogenase (ICDH) and glucose-6-phosphate dehydrogenase (G6PDH) enzymes were estimated in the mitochondrial fractions of the cerebral cortex, cerebellum and hippocampus of Pb exposed pregnant and non-pregnant rats (Figures 2 to 7). Exposure to Pb exhibited significant decrease in the specific activities of SOD, GPx, CAT, SDH and ICDH enzymes in all selected brain regions of pregnant and non-pregnant rats at 7th (p<0.001) and 30th (p<0.01) day time intervals, where as G6PDH showed increased levels (45.01%, 19.33% in cortex; 42.71%, 16.65% in hippocampus; 36.32%, 15.27% in cerebellum at 7th (p<0.001) and 30th (p<0.01) day time intervals respectively in non-pregnant rats; 32.30%, 27.32% in cortex; 21.79%, 20.48% in hippocampus; 18.52%, 15.70% in cerebellum at 7th (p<0.001) and 30th (p<0.01) day time intervals respectively in pregnant rats) (Figure 7). The MDA formation was observed as a level of lipid peroxidation in control and experimental rats of different brain regions. Pb-exposure increased the MDA levels in the cortex, cerebellum, and hippocampus compared to controls and the increase was found to be greater in non-pregnant rats (55.66%, 34.44% in cortex; 46.18%, 32.50% in hippocampus; 39.22%, 30.6% in cerebellum at 7th and 30th (p<0.01) time intervals respectively) than pregnant rats (44.10%, 39.18% in cortex; 43.94%, 31.92% in hippocampus; 40.28%, 29.80% in cerebellum at 7th (p<0.001) and 30th (p<0.01) day time intervals respectively) (Figure 8). However, Pb-induced impairments in the specific activities of mitochondrial enzymes and MDA levels were more pronounced in cortex compared to hippocampus and cerebellum. Further, these results clearly show that Pb-induced effect was more pronounced in non-pregnant rats than pregnant rats following exposure to Pb. The concentrations of Pb in different brain regions of non-pregnant and pregnant rats at 7th (p<0.001) and 30th (p<0.01) day after exposure are shown in Table 1. A significant increase was observed in the concentration of Pb levels in all three brain regions of both female rat groups. Among the brain regions, the cortex showed the highest content of Pb compared to cerebellum and hippocampus. Further greater Pb content was observed in non-pregnant rats compared to pregnant rats (Table 1). In addition, we investigated the protective effect of vit-E against Pb induced alterations in brain mitochondrial dysfunction in pregnant and non-pregnant

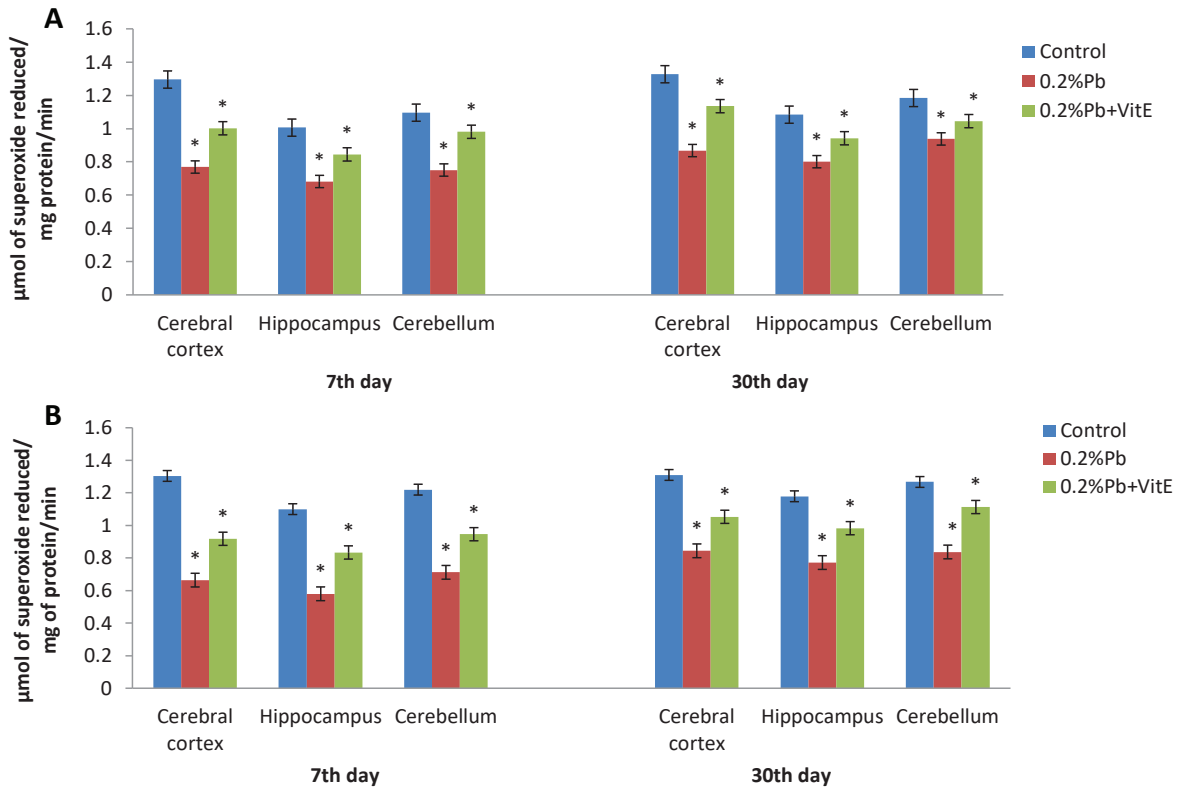

Figure 2. Effect of Pb (0.2%) exposure on superoxide dismutase (SOD) activity (µ moles of superoxide reduced/mg of protein/min) in mitochondrial fractions of cerebral cortex, hippocampus and cerebellum of rats and protective effects of α-tocopherol acetate (vitamin E) (100 mg/kg body wt). A: non-pregnant rats, B: pregnant rats; *p≤0.05.

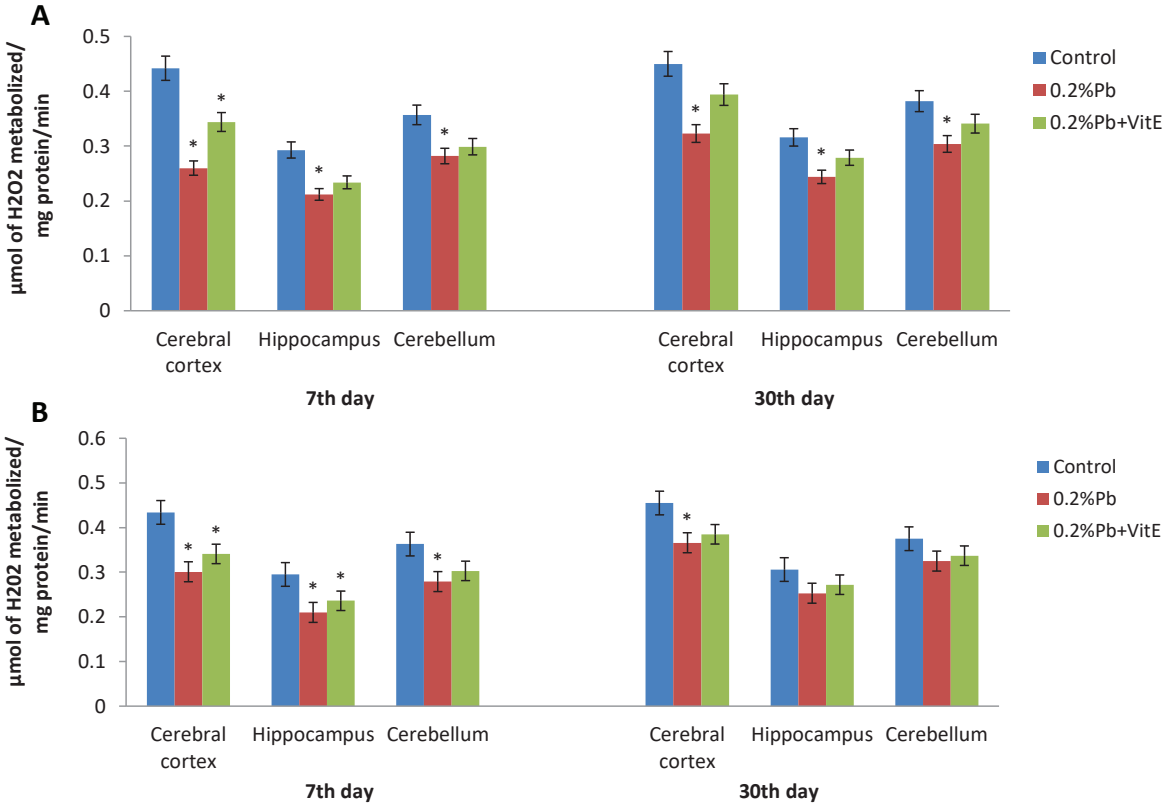

Figure 3. Effect of Pb (0.2%) exposure on catalase (CAT) activity (µ moles of H_2O_2 decomposed/mg protein/hr) in mitochondrial fractions of cerebral cortex, hippocampus and cerebellum of rats and protective effects of α-tocopherol acetate (vitamin E) (100 mg/kg body wt). A: non-pregnant rats, B: pregnant rats; *$p \leq 0.05$.

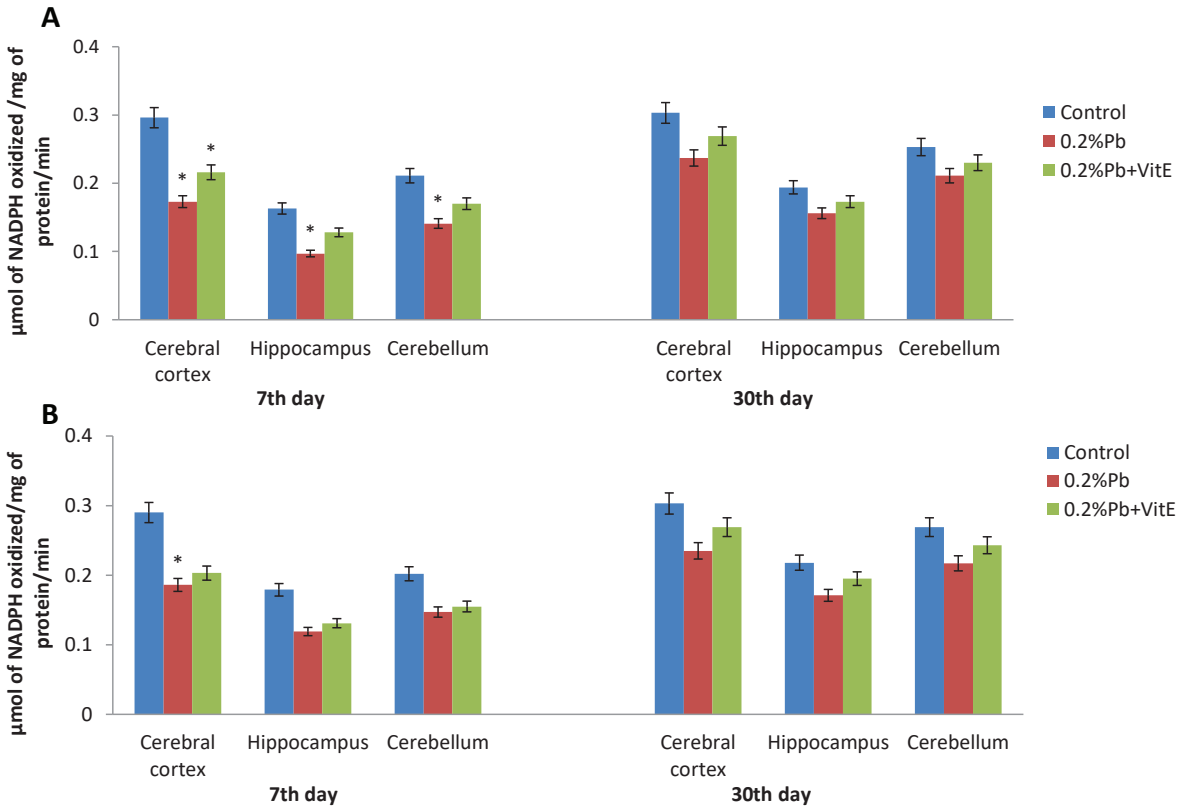

Figure 4. Effect of Pb (0.2%) exposure on glutathione peroxidase (GPx) activity (µ moles of NADPH oxidized/mg protein/min) in mitochondrial fractions of cerebral cortex, hippocampus and cerebellum of rats and protective effects of α-tocopherol acetate (vitamin E) (100 mg/kg body wt). A: non-pregnant rats, B: pregnant rats; *$p \leq 0.05$.

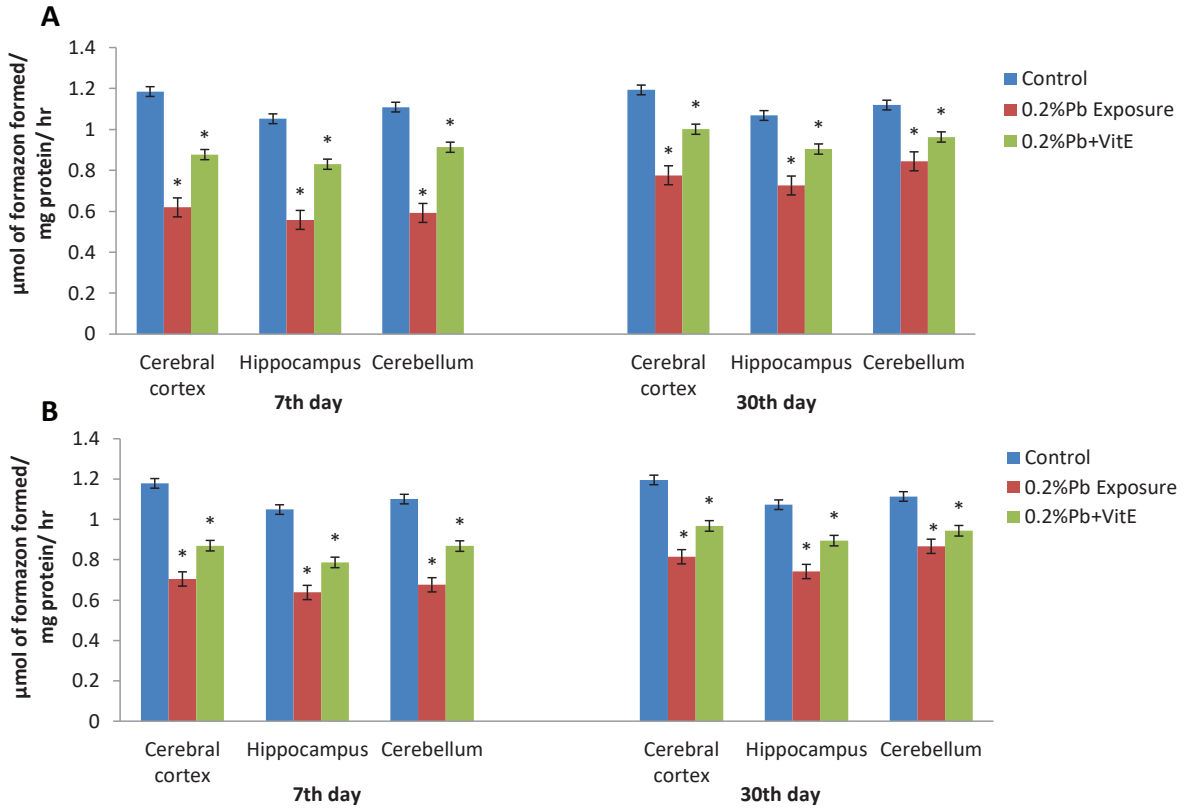

Figure 5. Effect of Pb (0.2%) exposure on succinate dehydrogenase (SDH) activity (µmoles of formazan formed/mg protein/hr) in mitochondrial fractions of cerebral cortex, hippocampus and cerebellum of rats and protective effects of α-tocopherol acetate (vitamin E) (100 mg/kg body wt). A: non-pregnant rats, B: pregnant rats; *$p \leq 0.05$.

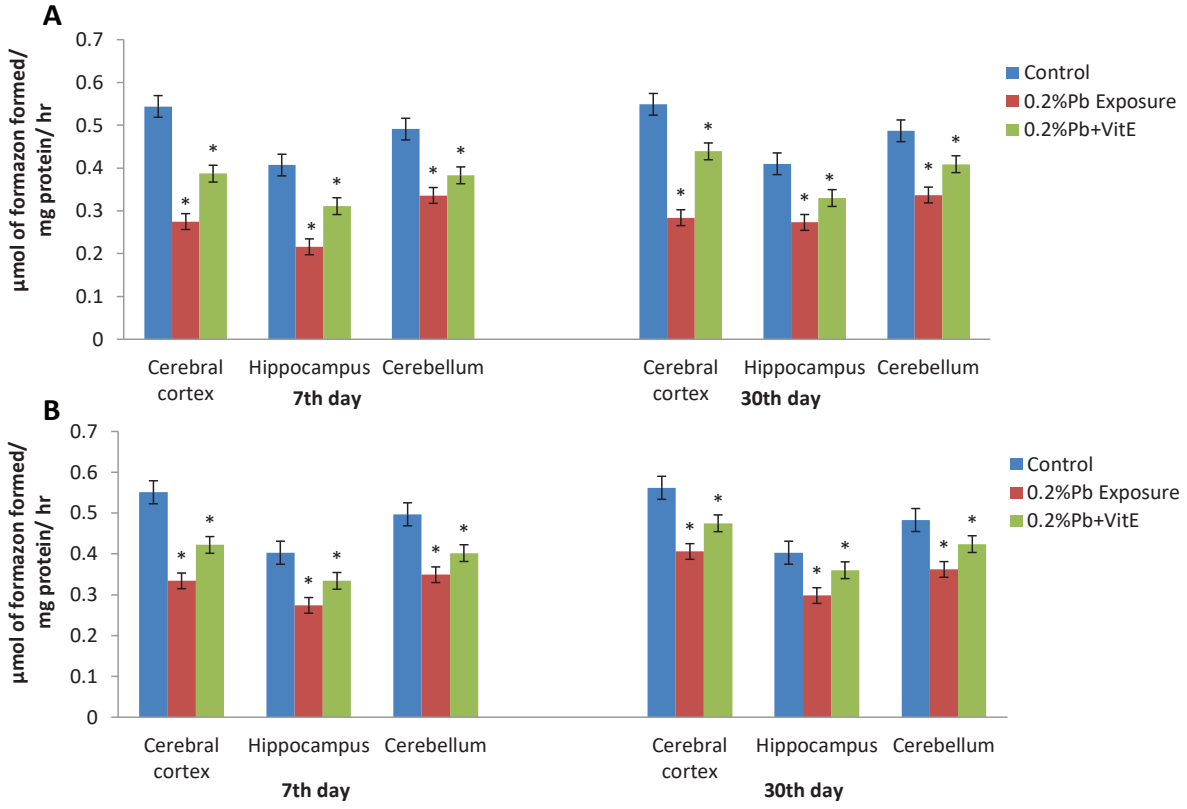

Figure 6. Effect of Pb (0.2%) exposure on isocitrate dehydrogenase (ICDH) activity (µmoles of formazan formed/mg protein/hr) in mitochondrial fractions of cerebral cortex, hippocampus and cerebellum of rats and protective effects of α-tocopherol acetate (vitamin E) (100 mg/kg body wt). A: non-pregnant rats, B: pregnant rats; *$p \leq 0.05$.

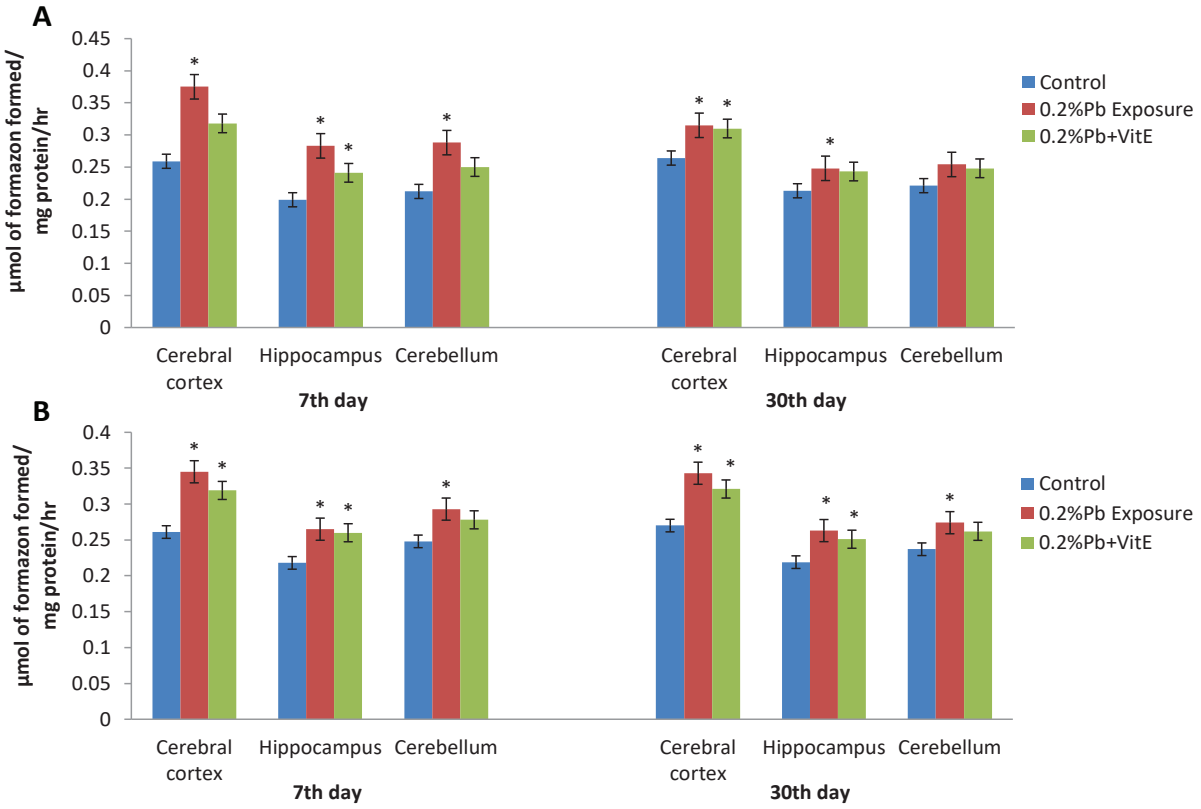

Figure 7. Effect of Pb (0.2%) exposure on glucose-6-phosphate dehydrogenase (G-6PD) activity (µmoles of formazan formed/mg protein/hr) in mitochondrial fractions of cerebral cortex, hippocampus and cerebellum of rats and protective effects of α-tocopherol acetate (vitamin E) (100 mg/kg body wt). A: non-pregnant rats, B: pregnant rats; *$p \leq 0.05$.

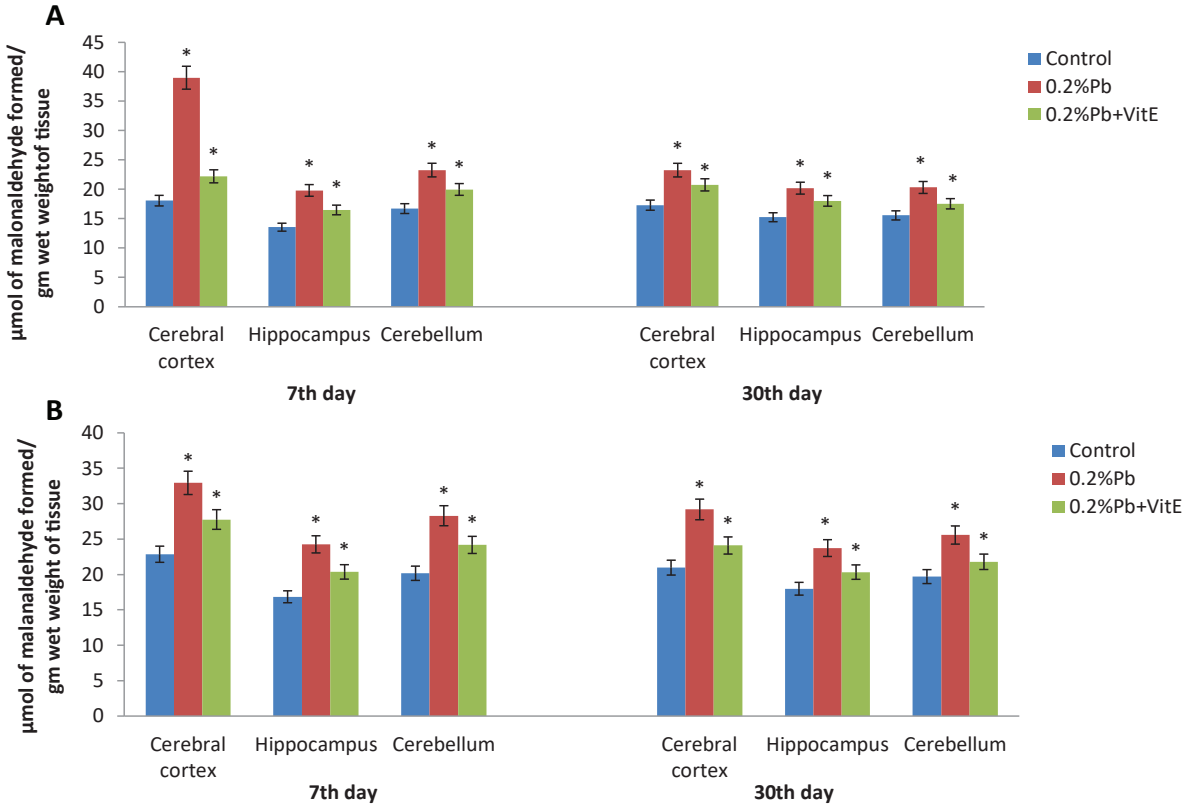

Figure 8. Effect of Pb (0.2%) exposure on malondialdehyde content (MDA) (µ moles of malondialdehyde/gm wet wt. of tissue) in mitochondrial fractions of cerebral cortex, hippocampus and cerebellum of rats and protective effects of α-tocopherol acetate (vitamin E) (100 mg/kg body wt). A: non-pregnant rats, B: pregnant rats; *$p \leq 0.05$.

Table 1. Pb levels (µg/g) estimated in different brain regions in control, Pb exposed and vit-E supplemented rats.

	7th day			30th day		
	Cortex	**Hippocampus**	**Cerebellum**	**Cortex**	**Hippocampus**	**Cerebellum**
Non-Pregnant Rats						
Control	0.014±0.007	0.020±0.001	0.017±0.008	0.007±0.003	0.016±0.007	0.012±0.005
0.2% Pb	0.36±0.008*	0.19±0.006*	0.21±0.007*	0.28±0.006*	0.14±0.005*	0.18±0.007*
0.2% Pb +Vit-E	0.31±0.004*	0.17±0.003*	0.18±0.004*	0.24±0.003*	0.10±0.003*	0.12±0.002*
Pregnant Rats						
Control	0.011±0.005	0.018±0.007	0.013±0.006	0.009±0.0004	0.017±0.0007	0.012±0.005
0.2% Pb	0.29±0.007*	0.17±0.006*	0.18±0.007*	0.19±0.006*	0.12±0.005*	0.14±0.005*
0.2% Pb +Vit-E	0.23±0.003*	0.14±0.002*	0.16±0.003*	0.18±0.003*	0.11±0.003*	0.10±0.003*

The values are mean ± S.D of six separate experiments. Differences between values marked with asterisk (*) within each row are statistically significant at $p<0.05$ level of probability

rats ($p<0.005$). The supplementation of vit-E along with Pb exposure was found to be effective in reducing lipid peroxidation and the activities of mitochondrial enzymes but the reversal effect of vit-E on Pb levels was marginal in both non-pregnant and pregnant rats ($p<0.005$) (Figures 2 to 8 and Table 1).

Discussion

The findings of the present study demonstrate that exposure to Pb causes significant alterations in mitochondrial metabolic and antioxidant enzymes and MDA levels in different brain regions of pregnant and non-pregnant rats. Further, supplementation of vit-E provided a significant protection from Pb-induced oxidative damage in the brain. Mitochondria are the major intracellular target site for Pb-induced ROS and oxidative damage in the brain cells (Ma *et al.,* 2017). Previous studies demonstrated that the deleterious effect of Pb on mitochondrial membranes is associated with changes in fatty acid composition. The damage of the fatty acids alters the function of the enzymes (Armstrong, 2006), particularly mitochondrial dehydrogenases (Ramanathan *et al.,* 2003). In this study, we observed that Pb exposure decreased the mitochondrial SDH and ICDH activities whereas the activity of G6PDH increased in the cortex, hippocampus and cerebellum of pregnant and non-pregnant rats. Similar results were observed by Kilikdar *et al.* (2011) and Jarrar *et al.* (2002) in rats following exposure to Pb. Recently, Ma *et al.* (2017) reported that the addition of Pb into isolated liver mitochondria lead to rapid increase in ROS (H_2O_2) formation suggesting that Pb may impair complex III resulting in increased leakage of electrons and generating more ROS, which ultimately lead to impairments in enzymes and mitochondrial dysfunction. According to Basha *et al.* (2012), exposure to Pb during development decreased heart mitochondrial SDH and ICDH enzyme activities and these alterations persist in the later life of rats. However, a significant decrease observed in both SDH and ICDH activities might also be due to the direct interaction of Pb with -SH groups of these enzymes. The G6PDH enzyme plays an important role in the regulation of sugar metabolism and determines whether glucose shall undergo glycolysis or be utilized via the pentose phosphate pathway (Stanton, 2012). The results of the present investigation have shown an increase in the activity of G6PDH in different brain regions of Pb exposed female rats. The increase in the activity of G6PDH, due to Pb intoxication, might indicate an increased demand to generate reducing power in the form of NADPH (Patra *et al.,* 2011). Gurer and Eracal (2000) reported that Pb-induced perturbations in G6PDH activity depend on the concentration and duration of Pb exposure, and magnitude of oxidative stress inside the cell.

The toxicity of Pb may be mainly due to its high rate of free radical production and decrease in free radical scavenging enzymes (Sandhir *et al.,* 1994). In the present study, we found that exposure to Pb decreased the mitochondrial SOD, CAT and GPx, activities with a concomitant increase in lipid peroxidation in the cortex, cerebellum and hippocampus of pregnant and non-pregnant rats. SOD is the most important enzyme involved in the antioxidant defence and responsible for scavenging the superoxide ions to yield hydrogen peroxide (H_2O_2) and oxygen (Pushpakiran *et al.,* 2004). Previous studies reported that the decreased SOD activity can lead to adverse effects since superoxide anions are extremely toxic to lipids, proteins and DNA (Dobrakowski *et al.,* 2017; Adanylo & Otieza, 1999). Further, it is suggested that Pb-induced deficiency in SOD activity may be due to deficiency of copper and zinc as Pb competes and replaces copper and zinc in their binding sites (Kluska *et al.,* 2018; Prasanthi *et al.,* 2010). GPx is selenium containing metalloenzyme that needs GSH to decompose hydrogen peroxide with the simultaneous oxidation of GSH to GSSG (Sara *et al.,* 2008). We found Pb-induced significant alteration in GPx enzyme activity in the cortex whereas the cerebellum and hippocampus showed marginal alterations. Many studies, either experimental or clinical, have shown much divergence in the influence of Pb on the activity of GPx. Sandhir *et al.* (1994) observed that the differential decrease in GPx activity in different brain regions was due to regional differences in accumulation of Pb. Our previous studies also

showed that Pb exposure significantly decreased the GPx activity in cerebellum and hippocampus regions during development of rats (Reddy *et al.,* 2014; Basha *et al.,* 2012; Prasanthi *et al.,* 2010). Our results clearly showed that Pb exposure significantly decreased the CAT activity in all selected brain regions of pregnant and non-pregnant rats. These antioxidant enzymes are the potential target for Pb-toxicity due to the high affinity of Pb for -SH group or metal co-factor in these enzymes (Armstrong, 2006). However, significant decrease in the levels of these enzymes following Pb exposure could lead to increased susceptibility of the brain tissue to free radical damage.

Free radical damage in specific regions of the brain has been recognized in cases like epilepsy, schizophrenia, Parkinson's or Alzheimer's diseases (Wrangler & Richardson, 1991). The most widely used test for oxidative stress is the measurement of MDA, a product of lipid peroxidation. In the current study, Pb-exposure significantly increased the MDA levels in various brain regions of pregnant and non-pregnant rats. Pb is known to promote oxidative damage in the brain by enhancing peroxidation of membrane lipids (Stohs & Bagchi, 1995), generation of ROS and decrease in the activity levels of antioxidant enzymes (Prasanthi *et al., 2*010). Neurons are particularly vulnerable to free radical attack since impaired defences or exposure to excess free radicals may lead to neuronal death (Akitane *et al.,* 1994). Increased lipid peroxidation is also responsible for altered membrane fluidity (Viani *et al.,* 1991) in the affected tissue. Our results clearly showed that an increased MDA level was accompanied by a reduction in the activities of SOD, CAT and GPx enzymes in various regions of female rats. Pb induced damage in the brain appears to be region specific and this might be due to either differential accumulation of Pb in various regions of the brain or because of differential susceptibility of cells to Pb in each region of the brain (Zawia *et al.,*1996). In this study, Pb exposure resulted in a significant increase in Pb levels in all the three brain regions of both female rat groups. Pb-induced alterations were greater in cortex coinciding with higher Pb levels observed in the cortex compared to hippocampus and cerebellum. From our results it is clear that the alterations observed in the enzyme activities and MDA levels were due to regional differences in the accumulation of Pb. Further, the non-pregnant rats were found to be more sensitive to Pb-induced impairments in mitochondrial enzymes than pregnant rats. This could be attributed to the fact that in pregnant rats part of Pb was accumulated in placenta and transferred to pups whereas in non-pregnant rats Pb will be retained in the body. Gardella (2001) and Bhattachary (1983) also reported that there is a strong correlation between maternal and umbilical cord blood Pb levels indicating the transfer of Pb from mother to foetus. Few other studies also reported that Pb exposed pregnant rats transfer the Pb content to foetus and pups through placenta and maternal milk (Kelman & Walter, 1980; Dietrich, 1991; Patriarca *et al.,* 2000) as a result Pb-induced effect was more pronounced in non-pregnant rats than pregnant rats.

We found that co-administration of vit-E with Pb exposure decreased Pb-induced oxidative damage by reducing the levels of MDA and restoring the levels of metabolic and antioxidant enzymes in different brain regions of female rats. Different studies have shown that vit-E can remove superoxide anion and other free radicals (Traber & Stevens, 2011; Patrick, 2006), which might account for the beneficial effects of its supplementation in Pb-exposed female rats. Moreover, different experimental studies showed that vit-E treatments ameliorated brain injury induced by exposure to Pb. Sajitha *et al.* (2010) observed that Pb exposure causes significant alternations in antioxidant enzymes and increases MDA levels in liver and heart of rats. Further, this study also suggested that vit-E may be a useful preventive agent against the Pb-induced oxidative stress. Al-Attar *et al.* (2011) evaluated the antioxidant and protective effect of vit-E on a mixture of heavy metals (Pb, Hg, Cd and Cu) induced oxidative stress in male mice and suggested that vit-E might be a useful preventive agent against the effect of the studied heavy metals due to its antioxidant properties. Vit-E was found to be effective in decreasing the Pb-induced oxidative stress and lipid peroxide levels in different organs of rats. Interestingly, vitamin E supplementation caused no significant reduction in Pb concentration in all selected brain regions of pregnant and non-pregnant female rats. Similar results were also observed in different studies with vit-E supplementation against Pb-induced oxidative damage in liver, kidney, brain, and blood (Patra *et al.,* 2001; Nascimento & Risso, 2016). Few other studies reported that supplementation of vit-E with chelating agents was very effective in reducing metal concentrations in different organs of rats (Flora *et al.,* 2012, 2003; Patra *et al.,* 2001). In this study, we found vit-E supplementation to be efficient to protect the brain from Pb-induced oxidative damage but not effective to reduce metal concentration in brain regions of female rats. However, the mechanisms of dietary supplementation of vit-E remain to be further examined in Pb exposed humans or animals.

Conclusion

This study demonstrated that the exposure to Pb has a potential to induce significant perturbations in mitochondrial oxidative and antioxidant enzymes in both pregnant and non-pregnant female rats. Further, this study indicated that Pb-induced effect was more pronounced in non-pregnant rats than pregnant rats because of transfer of part of Pb from placenta and milk to pups. Supplementation of vit- E along with Pb might alleviate the brain mitochondrial perturbations from the oxidative stress suggesting that adequate vit-E intake may be useful in treating the Pb induced brain oxidative stress in female rats. However, further studies are required to establish the mechanism actions of vit-E as a therapeutic agent against the neurotoxic influence of the heavy metal Pb.

REFERENCES

Adonaylo VN, Otieza PI. (1999). Pb^{2+} promotes lipid peroxidation and alteration in membrane physical properties. *Toxicology* **132**: 19–32.

Akitane M, Jiankang L, Xiaryan W, Motoko, K. (1994). Free Radical Scavenging by Brain Homogenate: Implication to free Radical damage and antioxidant defence in brain; *Neurochem. Int* **24**: 201–207.

Al-Attar AM. (2011). Antioxidant effect of vitamin E treatment on some heavy metals-induced renal and testicular injuries in male mice. *Saudi J Biol Sci* **18**(1): 63–72.

Armstrong JS. (2006). The role of the mitochondrial permeability transition in cell death. *Mitochondrion* **6**(5): 225–34.

ATSDR (Agency for Toxic Substances and Disease Registry), 2007. Public Health Statement, Lead, U.S. Department of Health and Human Services, Public Health Services.

Basha CD, Reddy RG. (2015). Long term changes in brain cholinergic system and behavior in rats following gestationalexposure to lead: protective effect of calcium supplement. *Interdiscip Toxicol* **8**(4): 159–68.

Basha DC, Basha SS, Reddy GR. (2012). Lead-induced cardiac and hematological alterations in aging Wistar male rats: alleviating effects of nutrient metal mixture. *Biogerontology* **13**(4): 359–68.

Battacharayya MH. (1983). Bioavailability of orally administered cadmium and lead to the mother, fetus, and neotal during pregnancy and lactation. *Sci. Total Environ* **28**: 327–42.

Beier EE, Sheu TJ, Dang D, Holz JD, Ubayawardena R, Babij P, Puzas, JE. (2015). Heavy metal ion regulation of gene expression: mechanisms by which lead inhibits osteoblastic bone forming activity through modulation of the Wnt/-catenin signaling pathway. *J. Biol. Chem* **290**: 18216–18226.

Chance B, Maehly AC. (1955). Assay of catalase and peroxidises. *Meth. Enzymol I* **11**: 764–775.

Basha DC, Reddy NS, Rani MU, Reddy GR. (2014). Age related changes in aminergic system and behavior following lead exposure: protection withessential metal supplements. *Neurosci Res* **78**: 81–9.

Dietrich KN. (1991). Human foetal lead exposure: intrauterine grow, maturation and postnatal development. *Fundam.Appl. Toxicol* **16**: 17–19.

Dobrakowski M, Pawlas N, Kasperczyk A, Kozłowska A, Olewińska E, Machoń-Grecka A, Kasperczyk S. (2017). Oxidative DNA damage and oxidative stress in lead-exposed workers. *Hum Exp Toxicol* **36**(7): 744–754.

EFSA (European Food Safety Authority). (2012). Lead dietary exposure in the European population. EFSA J. **10**: 2831.

Bruns FH, Bergmeyer HU. (1965). Fructose-1,6 di phosphatase aldolase. In: Methods of enzymatic analysis. Bergmeyer, H.U. *Academic press, New York*. 724–731.

Flora G, Gupta D, Tiwari A. (2012). Toxicity of lead: a review with recent updates. *Interdiscip. Toxicol* **5**: 47–58

Flora SJ, Pande M, Mehta A. (2003). Beneficial effect of combined administration of some naturally occurring antioxidants (vitamins) and thiol chelators in the treatment of chronic lead intoxication. *Chem. Biol. Interact* **145**: 267–280.

Gao A, Lu XT, Li QY, Tian L. (210). Effect of the delta-aminolevulinic acid dehydratase gene polymorphism on renal andneurobehavioral function in workers exposed to lead in China. *Sci Total Environ* **408**(19): 4052–5.

Gardella C. (2001). Lead exposure in pregnancy: a review of the literature and argument for routine perinatal screening. *Obstet Gyn Survey* **56**: 231–8.

Gottipolu RR, Davuljigari CB. (2014). Perinatal exposure to lead: reduction in alterations of brain mitochondrial antioxidant systemwith calcium supplement. *Biol Trace Elem Res* **162**(1–3): 270–7.

Gurer H, Ercal N. (2000). Can antioxidants be beneficial in the treatment of lead poisoning? *Free Radic. Biol. Med.* **29**: 927–945.

Gutowicz M. (2011). The influence of reactive oxygen species on the central nervous system. *Postepy Hig Med Dosw (Online)* **65**: 104–13.

Lai JC, Clark JB. (1979). Preparation of synaptic and non-synaptic mitochondria from mammalian brain. *Meth Enzymol* **55**: 51–60.

Jarrar BM, Taib NT. (2012). Histological and histochemical alterations in the liver induced by lead chronic toxicity. *Saudi J Biol Sci* **19**(2): 203–10.

Jia Q, Ha X, Yang Z, Hui L, Yang X. (2012). Oxidative stress: a possible mechanism for lead-induced apoptosis and nephrotoxicity. *Toxicol Mech Methods.* **22**(9): 705–10.

Kelman BJ, Walter BK. (1980). Transplacental movement of inorganic lead from mother to fetus. *Proc. Soc. Exp. Biol. Med* **163**: 278–282.

Kilikdar D, Mukherjee D, Mitra E, Ghosh AK, Basu A, Chandra AM, Bandyoapdhyay D. (2011). Protective effect of aqueous garlic extract against lead-induced hepatic injury in rats. *Indian J Exp Biol.* 49(7): 498–510.

Kluska K, Adamczyk J, Krężel A. (2018). Metal binding properties, stability and reactivity of zinc fingers Coordination. *Chemistry Reviews* **367**: 18–64

Kuhad, A, Chopra K. (2007). Curcumin attenuates diabetic encephalopathy in rat: Behavioral and biochemical evidence. *European Journal of Pain* **576**: 34.

Liu KS, Hao JH, Zeng Y, Dai FC, Gu PQ. (2013). Neurotoxicity and biomarkers of lead exposure: a review. *Chin Med Sci J* **28**(3): 178–88.

Lopes AC, Peixe TS, Mesas AE, Paoliello MM. (2016). Lead Exposure and Oxidative Stress: A Systematic Review. *Rev Environ Contam Toxicol* **236**: 193–238.

Lowry OH, Rosenbrough NJ, Farr AL, Randall RJ. (1951). Protein measurement with Folin-phenol reagent. *J. Biol. Chem* **193**: 265–275.

Ma L, Liu JY, Dong JX, Xiao Q, Zhao J, Jiang, FL. (2017). Toxicity of Pb2+ on rat liver mitochondria induced by oxidative stress and mitochondrial permeability transition. *Toxicol. Res* **6**: 822–830.

Machartová V, Racek J, Kohout J, Senft V, Trefil L. (2000). Effect of antioxidant therapy on indicators of free radical activity in workers at risk of leadexposure. *Vnitr Lek*. **46**(8): 444–6.

Misra HP, Fridovich I. (1972). The role of superoxide anion in the auto-oxidation of epinephrine and a simple assay for superoxide dismutase. *J. Biol. Chem* **247**: 3170–3175.

Sreenivasulu N, Kumar RM, Basha DC, Rajarami GR. (2015). Lead induced alterations in behavior and brain cholinergic system in female rats: ameliorative effect of α-tocopherol. *Indo American Journal of Pharmaceutical Research* **5**(10): 3281–3292

Nachlas MM, Marguil SI, Seligman, AM. (1960). A corlorimetric method for determination of succinate dehydrogenase activity. *J. Biol. Chem* **235**: 499–505.

Ohkawa H, Ohishi N, Yagi K. (1979). Assay for lipid peroxides in animal tissues by thiobarbituric acid reaction. *Anal. Biochem* **95**(2): 351–358.

Pande M, Flora SJ. (2002). Lead induced oxidative damage and its response to combined administration of alpha-lipoic acid and succimers in rats. *Toxicology* **15**: 177(2–3): 187–96.

Patra RC, Amiya K, Rautray, D. (2011). Oxidative Stress in Lead and Cadmium Toxicity and Its Amelioration. *Vet Med Int.* **2011**: 457327.

Patra RC, Swarup D, Dwivedi SK. (2001). Antioxidant effects of alpha tocopherol, ascorbic acid and l-methionine on lead induced oxidative stress to the liver kidney and brain in rats. *Toxicology* **162**: 81–88.

Patriarca M, Menditto, A, Rossi B, Lyon TDB, Fell GS. (2000). Enivormental exposure to metals of newborn, infants and young children. *Microchem* **1–67**: 351–361.

Patrick L. (2006). Lead toxicity. Part II. The role of free radicals damage and the use of antioxidants in the pathology and treatment of lead toxicity. *Altern. Med. Rev.* **11**: 114–128.

Prameelamma Y, Swami, KS. (1975). Glutathione dehydrogenase activity in normal and denervated gastrocnemius muscle of frog, Rana hyxadactyla. *Curr. Sci* **44**: 739–740.

Prasanthi RPJ, Devi CB, Basha DC, Reddy NS, Reddy GR. (2010). Calcium and zinc supplementation protects lead (Pb)-induced perturbations in antioxidant enzymes and lipid peroxidation in developing mouse brain. *Int. J. Devl. Neurosci* **28**: 161–167.

Pushpakiran G, Mahalakshmi K, Anuradha CV. (2004). Taurine restores ethanol-induced depletion of antioxidants and attenuates oxidative stress in rat tissues. *Amino Acids* **27**: 91–9

Ramanathan K, Shila S, Kumaran S, Paneerselvan C. (2003). Ascorbic acid and alpha-tocopherol as potent modulators on arsenic induced toxicity in mitochondria. *Journal of Nutritional Biochemistry* **14**: 416–420.

Rendón-Ramírez AL, Maldonado-Vega M, Quintanar-Escorza MA, Hernández G, Arévalo-Rivas BI, Zentella-Dehesa A, Calderón-Salinas JV. (2014). Effect of vitamin E and C supplementation on oxidative damage and total antioxidant capacity in lead-exposed workers. *Environ Toxicol Pharmacol* **37**(1): 45–54.

Rendón-Ramírez A, Cerbón-Solorzano J, Maldonado-Vega M, Quintanar-Escorza MA, Calderón-Salinas JV. (2007). Vitamin-E reduces the oxidative damage on delta-aminolevulinic dehydratase induced by lead intoxication in rat erythrocytes. *Toxicol In Vitro.* **21**: 1121–1126.

Rotruck JT, Pope AL, Ganther HE, Swanson AB, Hafeman DG, Hoekstra WG. (1973). Biochemical role as a component of glutathione peroxidase. *Science* **179**: 588–590.

Sajitha GR, Jose R, Andrews A, Ajantha KG, Augustine P, Augusti KT. (2010). Garlic Oil and Vitamin E Prevent the Adverse Effects of Lead Acetate and Ethanol Separately as well as in Combination in the Drinking Water of Rats. *Indian J Clin Biochem* **25**(3): 280–8.

Salehi I, Karamian R, Komaki A, Tahmasebi L, Taheri M, Nazari M, Shahidi S, Sarihi A. Effects of vitamin E on lead-induced impairments in hippocampal synaptic plasticity. Brain Res **10**: 629: 270–81.

Sandhir R, Julka D, Gill KD. (1994). Lipoperoxidative damage on lead treatment in rat brain and its implications on membrane bound enzymes. *Pharmacol Toxicol* **74**: 66–71

Sara EE, Hongfei G, Neal Fedarko, Amy DeZern, Linda PF, Qian-Li Xue, Sean Leng, Brock Beamer, Jeremy DW. (2008). Glutathione Peroxidase Enzyme Activity in Aging. *J Gerontol A Biol Sci Med Sci* **63**(5): 505–509.

Sousa CA, Soares EV. (2014). Mitochondria are the main source and one of the targets of Pb (lead)-induced oxidative stress in the yeast Saccharomyces Cerevisiae. *Appl Microbiol Biotechnol* **98**(11): 5153–60.

Stanton RC. (2012). Glucose-6-phosphate dehydrogenase, NADPH, and cell survival. *IUBMB Life* **64**(5): 362–9.

Stohs SJ, Bagchi D. (1995). Oxidative mechanisms in the toxicity of metal ions. *Free Radic Biol Med* **18**(2): 321–363.

Traber MG, Stevens JF. (2011). Vitamins C and E beneficial effects from a mechanistic perspective. Free Radic Biol Med **51**: 1000–1013

Viani P, Cervato G, Fiorilli A, Cestaro B. (1991). Age related differences in synaptosomal peroxidative damage and membrane Proteins. *J Neurochem* **56**: 253–258.

Villeda-Hernandez J, Barroso-Moguel R, Mendez-Armenta, M, Nava-Ruiz C, Huerta- Romero R, Rios C. (2001). Enhanced brain regional lipid peroxidation in developing rats exposed to low level lead acetate. *Brain Res Bull* **55**(2): 247–51.

Wrangler JA, Richardson JS. (1991). Oxygen Free Radicals and brain dysfunction. *Int J Neurosci* **57**: 1–17.

Lee YL, Lardy HA. (1965). Influence of thyroid hormones on L- glycerol phosphate dehydrogenase and other dehydrogenases in various organs of rat. J Biol Chem **240**: 1427–1432.

Zawia NH, Harry GJ. (1996). Developmental exposure to lead interferes with glial and neuronal differential gene expression in the rat cerebellum. *Toxicol Appl Pharmacol* **138**(1): 43–7.

ISSN: 1337-6853 *(print version)* | 1337-9569 *(electronic version)*

Interdiscip Toxicol. 2020; **Vol. 13**(1): 39–47.
doi: 10.2478/intox-2020-0005

sciendo

interdisciplinary toxicology

ORIGINAL ARTICLE

Modulatory role of quercetin against chlorpyrifos induced blood toxicity in rats

Simranjeet KAUR, Ananya SHUKLA, Neha SINGLA, D. K. DHAWAN

Department of Biophysics, Panjab University, India

ITX130120A05 • Received: 17 December 2019 • Accepted: 16 February 2020

ABSTRACT

Chlorpyrifos (CPF) is a broad-spectrum organophosphate insecticide and has been reported to cause a number of serious deleterious effects on physiological systems. The present study was designed to evaluate the role of quercetin (QC) during CPF induced toxicity in blood cells. Female Wistar rats weighing 150–200 g were divided into four different groups viz: Normal Control, CPF treated (13.5 mg/kg body weight every alternate day), QC treated (50 mg/kg body weight/day) and combined CPF + QC treated. The effects of different treatments were studied on various hematological parameters as well as on anti-oxidant defense system. CPF treated animals showed a significant decrease in total leukocyte counts (TLC), lymphocyte counts, hemoglobin (Hb) levels and aminolevulinic acid dehydratase (ALAD) activity, which however showed appreciable improvement upon simultaneous treatment with QC. Contrarily, neutrophils counts were found to be significantly increased, which, however, were decreased upon simultaneous treatment with QC. Further, CPF exposure caused a significant increase in the levels of lipid peroxidation (LPO) and protein carbonyl content (PCC) as well as increased the activities of super oxide dismutase (SOD) and catalase (CAT) in blood, which were decreased on QC co-treatment. Moreover, CPF treatment also caused inhibition of glutathione system in blood but QC co-treatment was able to up-regulate the glutathione system. Therefore, the present study, suggests that QC unveils a protective potential in containing CPF induced blood toxicity.

KEY WORDS: quercetin; oxidative stress; blood

Introduction

A large number of organophosphates are constantly used worldwide to inhibit the growth of unwanted weeds and pests. Despite the exposure from organophosphates causes a number of health hazards, its usage across the globe is still high (Hung *et al.,* 2015). CPF is an organophosphate that is widely used as an insecticide in agriculture as well as in household sectors (Fu *et al.,* 2015). It induces toxicity in various organs of reproductive (Nishi & Hundal, 2013), cardiac (Zafiropoulos *et al.,* 2014), renal and neurological systems (Nasr *et al.,* 2015).

Although there is enough information available on detrimental effects of organophosphates on brain, only limited evidences of their effects on hematological profile are available. Blood profiling has been considered as one of the vital parameters for the detection of pathophysiological alterations during stress conditions induced by various xenobiotics/chemicals (Kolesnikova *et al.,* 2014). Few studies have shown that organophosphate insecticides can induce hematological changes in experimental animals (Sunmonu & Oloyede, 2010; Enis Yonar *et al.,* 2012). Earlier findings have suggested that CPF exposure to rats can lead to microcytic hypochromic anemia by inhibiting the process of erythropoiesis and hame synthesis (Acker *et al.,* 2012; Elsharkawy *et al.,* 2013). Reports have also indicated that CPF can alter the activities of various enzymes that are associated with anti-oxidant defense system as well as apoptotic machinery (Li *et al.,* 2015; Smida *et al.,* 2017).

On the other hand, QC is a bio-flavonoid, which is abundantly found in fruits, vegetables, tea and wine (Haleagrahara *et al.,* 2013). It is one of the most widely consumed phytochemicals that exerts protective effects against various diseased conditions including cancer, diabetes and neurodegeneration (Sharma *et al.,* 2015; Yarahmadi *et al.,* 2018). Further, QC exhibits anti-carcinogenic (Maurya & Vinayak, 2015; Kashyap *et al.,* 2016) anti-inflammatory (Heeba *et al.,* 2014; Liu *et al.,* 2018), anti-apoptotic (Yang *et al.,* 2014; Roslan *et al.,* 2017) and antiviral properties (Wu *et al.,* 2015; Rojas *et al.,* 2016). Reports have revealed that QC has the ability to regulate

Correspondence address:
Prof. D. K. Dhawan & **Dr. Neha Singla**
Department of Biophysics, Panjab University
Chandigarh-160014, India
E-MAIL: dhawan@pu.ac.in; nehasbph@gmail.com

biological processes such as mitochondrial biogenesis, cell growth and cell migration (Miles *et al.,* 2014; Lan etal., 2017; Qiu *et al.,* 2018). In the light of paucity of information on hematological parameters, the present study was designed to elucidate the possible protective potential of QC during CPF induced blood toxicity in rats.

Material and methods

Chemicals

CPF was procured from Merck Ltd. (India) and was of 99.7% purity. QC was purchased from Sigma Pvt. Ltd. (USA) with 95% purity. Chemicals trichloroacetic acid, urea, thiobarbituric acid, D-aminolevulinic acid, triton X-100, cresyl violet, giemsa stain, 2,4-dinitrophenylhydrazine, Ehrlich's solution and nitro blue tetrazolium were obtained from Sigma Chemicals Company (USA). All other chemicals such as ammonia solution, 5,5'-dithiobis-(2-nitrobenzoic acid), ethanol, ethyl acetate, nitro blue tetrazolium, hydroxylamine hydrochloride methanol, tris buffer, sodium arsenite, hydrogen peroxide, 1-chloro-2,4-dinitrobenzene were procured from Merck, (India) whereas sodium chloride, nicotinamide adenine dinucleotide phosphate hydrogen, glutathione disulfide and dithioerythritol from HiMedia (India).

Experimental design

Healthy female Wistar rats in the weight range of 150–200 g were obtained from the central animal house of Panjab University, Chandigarh, India. The animals were housed in polypropylene cages with a hygienic bed of husk in a well-ventilated animal room until the end of the experimental period. The animals had free access to drinking water and standard animal feed (Ashirwad Industries, Punjab, India) throughout the treatment period. All the procedures related to animals were performed in accordance with the principles and guidelines approved by the Institutional Animal Ethics Committee.

To carry out various investigations, the animals were segregated into following four groups with 6 animals in each group. The animals in Group 1 served as normal control and were given corn oil by gavaging, which was used as a vehicle for the treatment of animals in CPF group. The animals in Group 2 were administered CPF orally every alternate day through intubation gavaging at a dose level of 13.5 mg/kg body weight in corn oil (Malhotra & Dhawan, 2014). Group 3 animals were given QC daily at a dose level of 50 mg/kg body weight in drinking water (Jahan *et al.,* 2015). The animals in group 4 were given a combined treatment of CPF and QC in a similar manner as given to Group 2 and Group 3 animals, respectively. The study was carried out for a total duration of 8 weeks.

Collection of blood samples

for the purpose of studying various hematological parameters, the blood samples were drawn after 8 weeks from all the animals belonging to different treatment groups. The samples were collected under light diethyl ether anesthesia by puncturing the ocular vein with a fine sterilized glass capillary. The blood samples were collected into the heparinized tubes and the supernatants were used as erythrocyte lysates.

Preparation of erythrocyte lysates

erythrocyte lysates were prepared by following the method of Ceballos-Picot *et al.* (1992). Lysates were obtained from the blood samples by centrifugation at 2500 rpm for 10 minutes (min) at room temperature. After centrifugation, both the plasma and buffy coats were removed. Later, the erythrocytes were washed twice with normal saline followed by removal of the supernatants. Further, water was added to the pellets (thrice its volume), which stored at –80 °C until use for future experiments. Lysed erythrocytes were prepared by freezing and thawing (two times) and cell membranes were removed by centrifugation at 3000 rpm for 20 min.

Hematological parameters

Hemoglobin estimation

Hb contents were estimated by following oxyhemoglobin method of Dacie & Lewis (1991). Fresh and non-clotted blood samples diluted in 0.004% ammonia solution (freshly prepared) and the optical densities were measured at 540 nm and Hb contents were expressed in g %.

Total Leukocytes Counts

TLC in blood samples were recorded by using the method of Dacie & Lewis (1991). Fresh blood samples were mixed with Turk's fluid to dilute the blood in the ratio 1:20 (v/v). A drop of diluted blood was immediately poured on Neubaur's chamber, which then was covered with a glass cover slip. Finally, the WBCs' were counted in the four-corner square of Neubaur's chamber.

Differential leucocytes counts (DLC)

DLC were recorded according to the method of Dacie & Lewis (1969). The blood samples were drawn from the animals of all the treatment groups by puncturing the ocular vein with a sterilized glass capillary and a drop blood was placed on a clean microscope glass slide, which was later spread by using another slide. The slides were air dried and fixed in methanol for 5–10 min. The smeared slides were stained for 30 min with giemsa stain (diluted 1:10). After staining, the excess stain was removed by running tap water followed by air-drying. Differential leucocytes were counted by using an oil immersion lens. Hundred consecutive stained white blood cells were counted starting from one direction to the other in random fashion and in all the possible planes. This process was repeated in all stained slides and percentage of neutrophils and lymphocytes were calculated.

Aminolevulinic acid dehydratase

ALAD activity was measured according to the method of Burch & Siegel (1971). In this method, incubation mixture was prepared by adding blood sample with triton X-100 reagent. Further, D-aminolevulinic acid (ALA) substrate was added to it and mixed with trichloroacetic acid (TCA). After incubation at 37 °C again, TCA reagent was added. The tubes were again centrifuged and clear supernatant

fluid was removed. Further, to aliquots, modified Ehrlich's reagent was added and absorbance was read at 555 nm.

Lipid peroxidation

LPO was determined by following the method of Wills (1966). The supernatants were added to thiobarbituric acid (TBA) and the color was developed by boiling at 100 °C for 10 min. The samples were cooled and absorbance was read at 532 nm. The amount of malondialdehyde (MDA) formed was calculated on the basis of molar extinction coefficient of MDA-TBA chromophore (1.56×10^5 $m^{-1}cm^{-1}$) and the results were expressed as nmoles of MDA/min/mg protein.

Protein carbonyl content

PCC was estimated by following the method of Levine *et al.* (1994). Blood lysates were added with 2,4-dinitrophenylhydrazine (DNPH) prior to incubation at room temperature for 1h in the dark. Further, 20% TCA was added and the solution was allowed to rest for 15 min at 4 °C. The precipitates were centrifuged at 11,000×*g* for 5 min. The bud was washed thrice with ethanol: ethyl acetate (1:1) and finally dissolved in 6 mol/l urea. Further, the reaction mixture was incubated at 37 °C for 30 min and the absorbance was read at 366 nm. The results were expressed as nmoles of reactive carbonyls formed (C=O) /mg protein, using the molar extinction coefficient of 21,000 mol/l cm^{-1}.

Superoxide dismutase

SOD activity was estimated according to the method of Kono (1978). The reaction mixture contained sodium carbonate, nitro blue tetrazolium (NBT), Triton X-100 and hydroxylamine hydrochloride. The rate of NBT reduction in the absence of the enzyme source was recorded for about 3 min with 30 seconds (sec) intervals. The reaction was followed at 560 nm against a reference containing sodium carbonate. The percentage inhibition in the rate of NBT reduction by enzyme SOD was recorded and one international unit enzyme was expressed as inverse of the amount of protein (mg) required in inhibiting the reduction rate of NBT by 50%. The activity of enzyme was expressed as international unit/ mg protein, where one unit of enzyme is defined as the amount of enzyme inhibiting the rate of reaction by 50%.

Catalase

CAT activity was determined by using the method of Luck (1971). In this method, 0.5 absorbance was measured by using H_2O_2 and phosphate buffer and later RBC lysates were added to it. The decrease in absorbance at 240 nm was read on spectrophotometer after every 15 sec for 3 min against a reference solution lacking hydrogen peroxide. The amount of hydrogen peroxide decomposed was calculated on the basis of molar extinction coefficient of H_2O_2 which is 0.0394 mol/l^{-1} cm^{-1} and the activity of enzyme was expressed as µmoles hydrogen peroxide decomposed/min/mg protein.

Glutathione-S-transferase (GST)

The activity of GST was estimated according to the method of Habig *et al.* (1974). The samples were mixed with reaction mixture consisting of sodium phosphate buffer and 1-chloro-2,4-dinitrobenzene (CDNB). The reaction was initiated by the addition of 0.05 ml of GSH to reaction mixture and absorbance was read at 340 nm after 30 sec of time interval. The enzyme activity was expressed as µmoles of GSH-CDNB conjugate formed/ min/mg protein, using molar extinction coefficient of the conjugate ($\varepsilon= 9.6\times10^6$ mol/l^{-1} cm^{-1}).

Reduced glutathione (GSH)

GSH was estimated by following the method of Moron *et al. (*1979). 25% TCA was added to the sample and the contents were thoroughly mixed. Further, the precipitated proteins were separated by centrifugation at 2000 g for about 15 min. The supernatant was diluted with 2.0 mol/l sodium phosphate buffer (pH 8.0). Finally, freshly prepared 5,5'-dithiobis-(2-nitrobenzoic acid) (DTNB) of 10 mmol/l was added to each sample and absorbance was read at 412 nm. The glutathione contents were expressed as µmoles of glutathione/g tissue.

Glutathione reductase (GR)

The assay of GR activity was performed according to the method described by Carlberg & Mannervirk (1985). To cuvette, phosphate buffer, nicotinamide adenine dinucleotide phosphate hydrogen (NADPH) and glutathione disulfide (GSSG) were added. The reaction was initiated by the addition of sample to the cuvette and the decrease in absorbance at 340 nm was followed for 2 min. A unit of GR activity is defined as the amount of enzyme that catalyses the oxidation of 1 nm of NADPH /min/mg protein using 6.22×10^3 as the molar absorption of NADPH.

Total glutathione content (TG)

The TG content was measured by following the method of Zahler & Cleland (1968). The disulfide in the sample was mixed with dithioerythritol and the reduction was allowed to proceed for 20 min. After reduction, tris buffer, sodium arsenite and water were added. DTNB prepared in sodium acetate was then added and the absorbance was recorded for 3 min. The TG contents were expressed in terms of µmoles of GSH/mg tissue.

Statistical analysis

The statistical significance of the data was determined by using one-way analysis of variance (ANOVA) and a *pos hoc* test. The results were expressed as mean ± S.D of 6 observations. The comparisons were made as follows: $^{a}p\leq0.05$, $^{b}p\leq0.01$, $^{c}p\leq0.001$ by *post hoc* analysis when values are compared with the normal control. $^{x}p\leq0.05$, $^{y}p\leq0.01$, $^{z}p\leq0.001$ by *post hoc* analysis when values are compared with CPF treated group.

Results

Hematological findings

The levels of Hb, TLC and lymphocytes were found to be decreased following CPF treatment; however, they were increased following QC co-supplementation (Figure 1 and Figure 2). On the contrary, neutrophils counts were found to be elevated in CPF treated animals when compared to the normal control animals. No significant changes were observed in differential leucocytes counts following

QC treatment to normal animals. However, neutrophils count showed an appreciable decrease following QC co-treatment. No significant changes were found in the number of monocytes and eosinophils in any of the treatment groups. On the contrary, ALAD activity was found to be significantly inhibited in the animals treated with CPF when compared to the normal controls; however, it was increased significantly following QC co-treatment (Figure 3).

Lipid peroxidation and protein carbonyl content

The MDA as well as PCC levels were found to be increased in erythrocyte lysates of CPF treated animals when compared to normal control group. No significant changes were observed in the levels of MDA and PCC of animals treated with QC alone. However, QC co-administration to CPF treated animals was able to decrease both the elevated lipid peroxidation and PCC levels (Figure 4 and Figure 5).

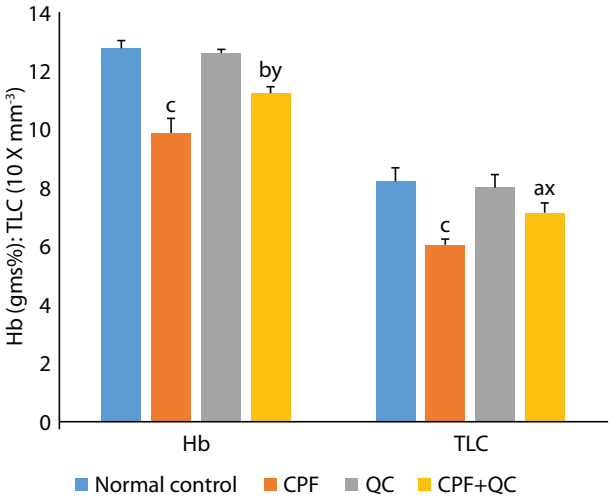

Figure 1. Effect of QC on Hb and TLC in erythrocytes of CPF intoxicated rats. All the values are represented as mean ±SD for each treatment group; n=6 for each treatment group. [a]$p \leq 0.05$ [b]$p \leq 0.01$, [c]$p \leq 0.001$ by *post-hoc* analysis when values are compared with normal control; [x]$p \leq 0.05$, [y]$p \leq 0.01$, [z]$p \leq 0.001$ by *post-hoc* analysis when values are compared with chlorpyrifos treated group.

Superoxide dismutase and catalase

The enzyme activities of SOD and CAT were found to be increased in erythrocyte lysates following CPF treatment; however, they were found to be significantly decreased upon QC supplementation (Figure 6 and Figure 7). Moreover, no significant changes were observed in the activities of SOD and CAT when QC alone was given to animals.

Glutathione system

The enzyme activities of GST and GR as well the levels of GSH and TG were observed to be decreased in erythrocyte lysates of CPF intoxicated group animals. However, simultaneous QC supplementation to CPF treated rats was able to increase the declined levels of GSH and TG as well as enzyme activities of glutathione system (Figure 8, Figure 9, Figure 10 and Figure 11).

Discussion

The present study was designed to evaluate the effects of CPF intoxication on anti-oxidant defense system in red blood cells and the protection provided by QC, if any, upon its supplementation. Here we demonstrate that CPF treatment of animals for 8 weeks resulted in significant alterations in various hematological indices; however, they were found to be modulated upon QC co-administration to CPF treated animals.

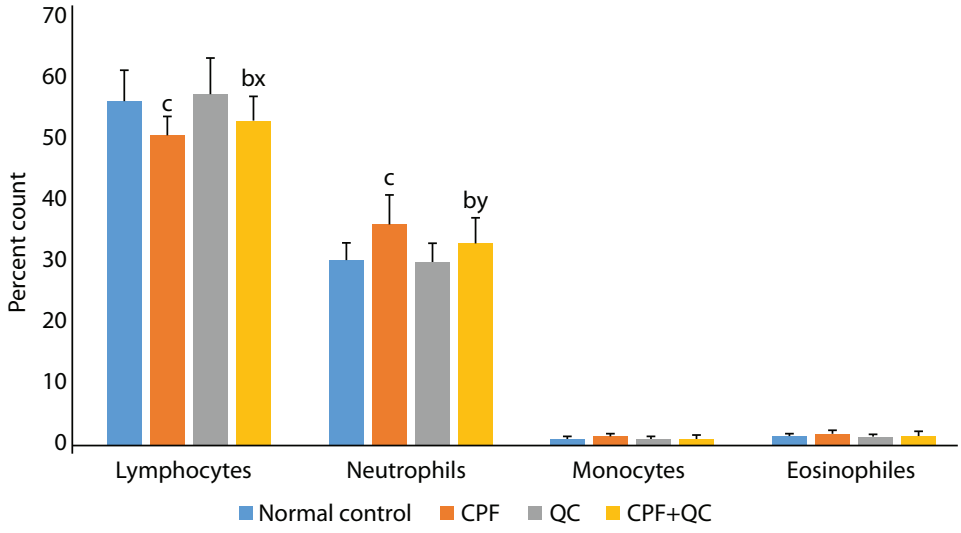

Figure 2. Effect of QC on DLC in erythrocytes of CPF intoxicated rats. All the values are represented as mean ±SD for each treatment group; n=6 for each treatment group. [a]$p \leq 0.05$, [b]$p \leq 0.01$, [c]$p \leq 0.001$ by *post-hoc* analysis when values are compared with normal control; [x]$p \leq 0.05$, [y]$p \leq 0.01$, [z]$p \leq 0.001$ by *post-hoc* analysis when values are compared with chlorpyrifos treated group.

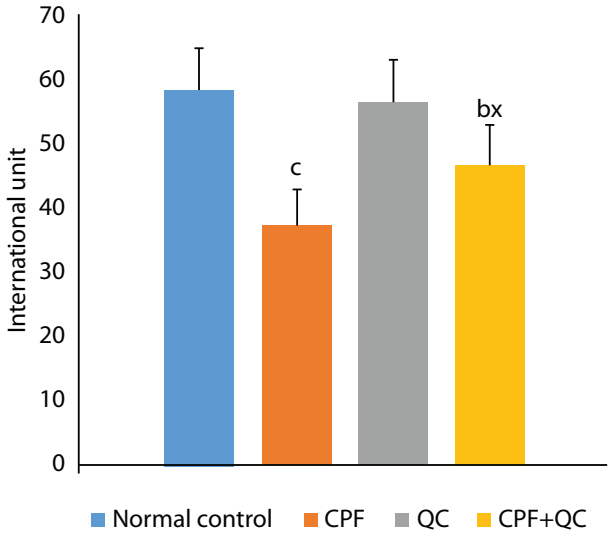

Figure 3. Effect of QC on ALAD levels in erythrocytes of CPF intoxicated rats. All the values are represented as mean ±SD for each treatment group; n=6 for each treatment group. $^{a}p\leq0.05$ $^{b}p\leq0.01$, $^{c}p\leq0.001$ by *post-hoc* analysis when values are compared with normal control; $^{x}p\leq0.05$, $^{y}p\leq0.01$, $^{z}p\leq0.001$ by *post-hoc* analysis when values are compared with chlorpyrifos treated group.

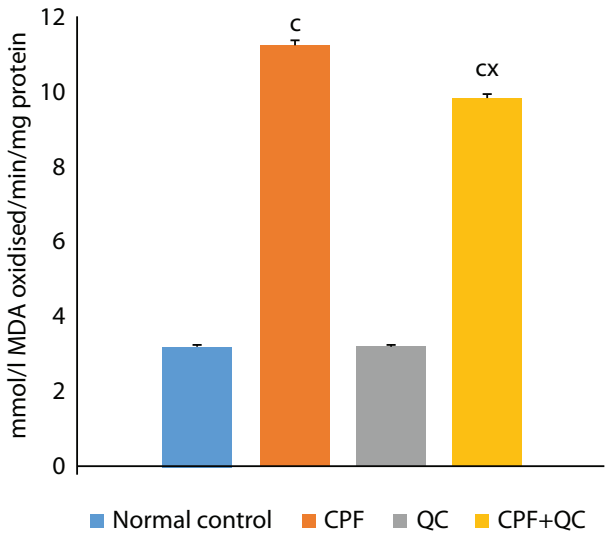

Figure 4. Effect of QC on LPO levels in erythrocytes of CPF intoxicated rats. All the values are represented as mean ±SD for each treatment group; n=6 for each treatment group. $^{a}p\leq0.05$ $^{b}p\leq0.01$, $^{c}p\leq0.001$ by *post-hoc* analysis when values are compared with normal control; $^{x}p\leq0.05$, $^{y}p\leq0.01$, $^{z}p\leq0.001$ by *post-hoc* analysis when values are compared with chlorpyrifos treated group.

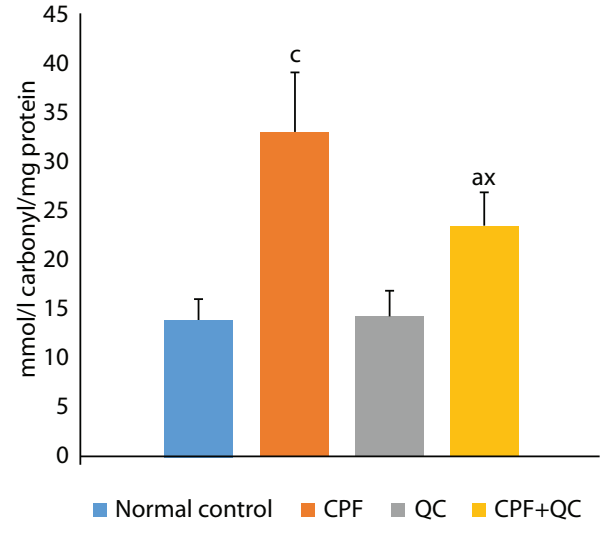

Figure 5. Effect of QC on PCC levels in erythrocytes of CPF intoxicated rats. All the values are represented as mean ±SD for each treatment group; n=6 for each treatment group. $^{a}p\leq0.05$ $^{b}p\leq0.01$, $^{c}p\leq0.001$ by *post-hoc* analysis when values are compared with normal control; $^{x}p\leq0.05$, $^{y}p\leq0.01$, $^{z}p\leq0.001$ by *post-hoc* analysis when values are compared with chlorpyrifos treated group.

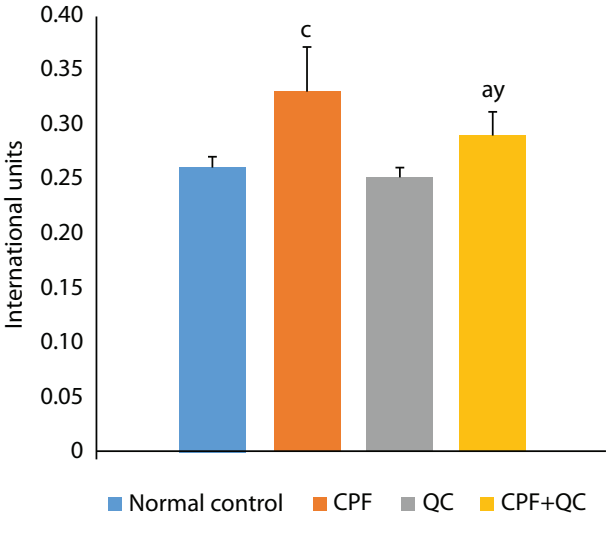

Figure 6. Effect of QC on SOD activity in erythrocytes of CPF intoxicated rats. All the values are represented as mean ±SD for each treatment group; n=6 for each treatment group. $^{a}p\leq0.05$ $^{b}p\leq0.01$, $^{c}p\leq0.001$ by *post-hoc* analysis when values are compared with normal control; $^{x}p\leq0.05$, $^{y}p\leq0.01$, $^{z}p\leq0.001$ by *post-hoc* analysis when values are compared with chlorpyrifos treated group.

In the present study, a significant decrease in Hb content was observed after 8 weeks of CPF treatment, which indicates CPF induced hematotoxicty in rats. Earlier studies have shown similar effects on Hb content in animals after CPF treatment (Akhtar *et al.,* 2009; Pala *et al.,* 2018). However, QC supplementation along with CPF treatment proved to be beneficial as it was able to increase the declined levels of Hb as compared to CPF treated group. QC has earlier been demonstrated to prevent the oxidation of hemoglobin molecule during oxidative stress and hence it has also prevented the CPF induced Hb oxidation in the current study (Krukoski *et al.,* 2009).

TLC and DLC were also found to be altered in CPF intoxicated animals that suggest severe disturbance in the immune system. TLC and DLC were found to be decreased after CPF exposure, which presumably is due to their decreased production from the germinal center of lymphoid organs or their increased lysis via chlorinated

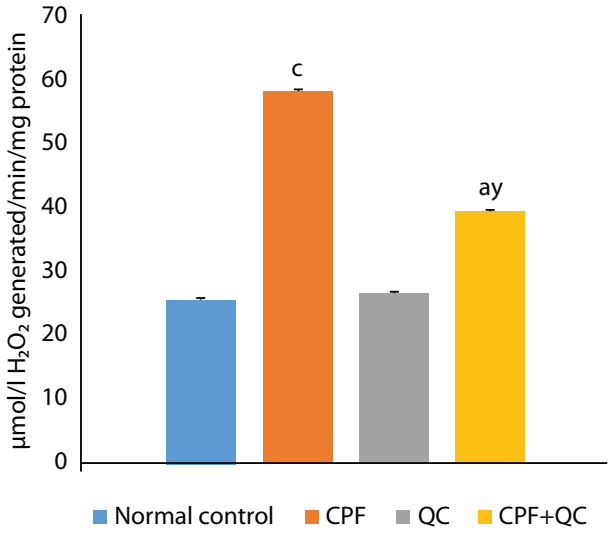

Figure 7. Effect of QC on CAT activity in erythrocytes of CPF intoxicated rats. All the values are represented as mean ±SD for each treatment group; n=6 for each treatment group. $^{a}p\leq0.05$ $^{b}p\leq0.01$, $^{c}p\leq0.001$ by *post-hoc* analysis when values are compared with normal control; $^{x}p\leq0.05$, $^{y}p\leq0.01$, $^{z}p\leq0.001$ by *post-hoc* analysis when values are compared with chlorpyrifos treated group.

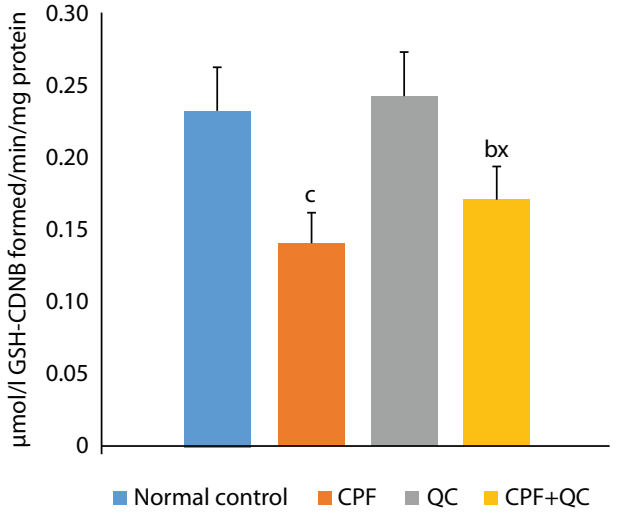

Figure 8. Effect of QC on GST activity in erythrocytes of CPF intoxicated rats. All the values are represented as mean ±SD for each treatment group; n=6 for each treatment group. $^{a}p\leq0.05$ $^{b}p\leq0.01$, $^{c}p\leq0.001$ by *post-hoc* analysis when values are compared with normal control; $^{x}p\leq0.05$, $^{y}p\leq0.01$, $^{z}p\leq0.001$ by *post-hoc* analysis when values are compared with chlorpyrifos treated group.

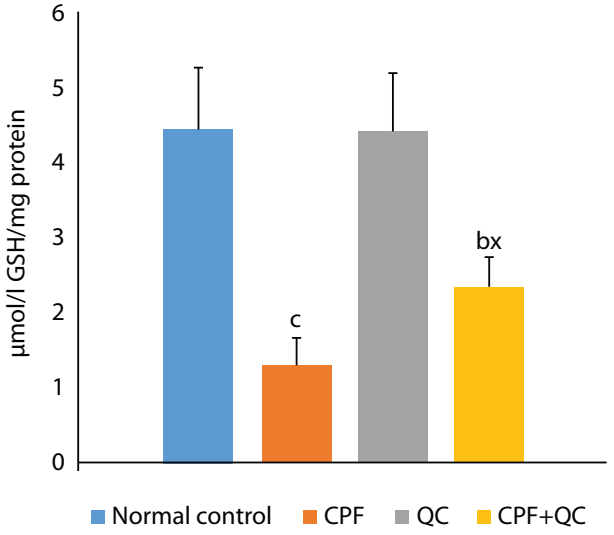

Figure 9. Effect of QC on GSH levels in erythrocytes of CPF intoxicated rats. All the values are represented as mean ±SD for each treatment group; n=6 for each treatment group. $^{a}p\leq0.05$ $^{b}p\leq0.01$, $^{c}p\leq0.001$ by *post-hoc* analysis when values are compared with normal control; $^{x}p\leq0.05$, $^{y}p\leq0.01$, $^{z}p\leq0.001$ by *post-hoc* analysis when values are compared with chlorpyrifos treated group.

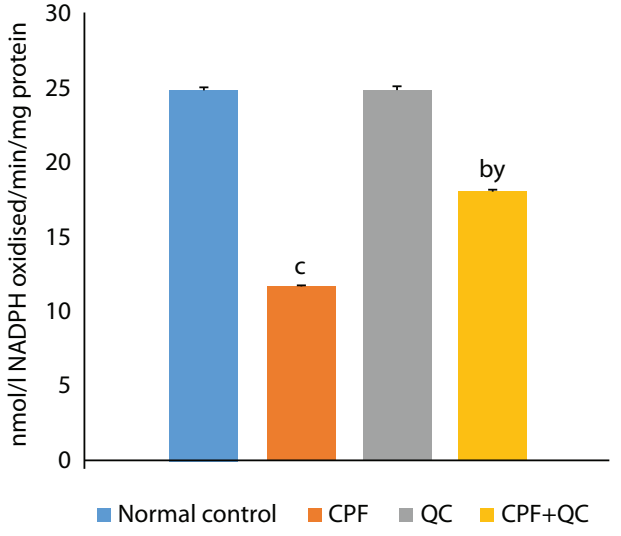

Figure 10. Effect of QC on GR levels in erythrocytes of CPF intoxicated rats. All the values are represented as mean ±SD for each treatment group; n=6 for each treatment group. $^{a}p\leq0.05$ $^{b}p\leq0.01$, $^{c}p\leq0.001$ by *post-hoc* analysis when values are compared with normal control; $^{x}p\leq0.05$, $^{y}p\leq0.01$, $^{z}p\leq0.001$ by *post-hoc* analysis when values are compared with chlorpyrifos treated group.

compounds present in the body (Goel *et al.,* 2006). On the contrary, CPF exposure caused a significant elevation in the neutrophils counts suggesting neutrophilia. The increase in neutrophils number indicates the activation of the primary defense system of the body, which caused an increased leukocyte mobilization as a consequence of CPF induced cytotoxicity and thus led to decreased leukocytes counts. QC administration to CPF treated animals significantly improved the TLC and also attenuated the disturbed DLC indices of the rats, which attributes to the immunomodulatory property of QC (Benkovic *et al.,* 2009).

During the present study, ALAD activity was also found to be significantly reduced in the CPF treated group when compared to normal control group. Earlier reports have also shown that decrease in heme synthesis and Hb content in the body can lead to altered ALAD activity (Alhawaj *et al.,* 2015; Olakkaran *et al.,* 2018). Further, QC

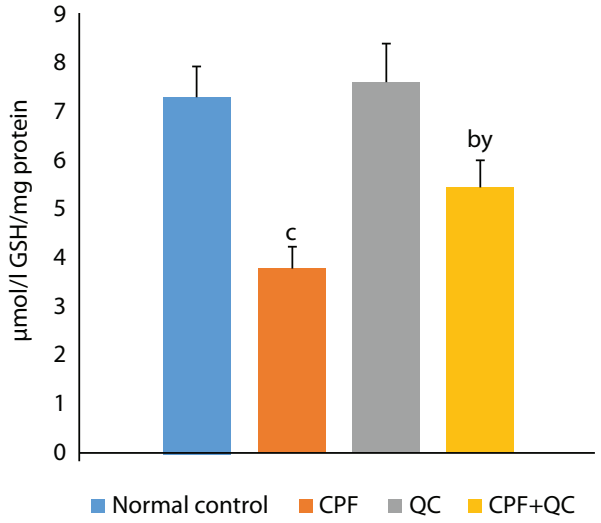

Figure 11. Effect of QC on TG levels in erythrocytes of CPF intoxicated rats. All the values are represented as mean ±SD for each treatment group; n=6 for each treatment group. $^{a}p\leq0.05$ $^{b}p\leq0.01$, $^{c}p\leq0.001$ by *post-hoc* analysis when values are compared with normal control; $^{x}p\leq0.05$, $^{y}p\leq0.01$, $^{z}p\leq0.001$ by *post-hoc* analysis when values are compared with chlorpyrifos treated group.

co-supplementation to CPF treated animals was able to elevate the declined ALAD activity, which could be a consequence of improved Hb levels and thereby upregulated the declined ALAD activity. Studies have also revealed the potential of QC in regulating various hematological parameters that get altered during chemically induced oxidative stress conditions (Mishra & Flora, 2008; Bhatt & Flora, 2009).

In the current study, CPF treatment also caused a marked increase in MDA levels in erythrocyte lysates, which indicates enhanced lipid peroxidation. CPF exposure resulted in oxidative degradation of polyunsaturated fatty acids and thereby generated a large number of free radicals, which eventually are responsible for causing alterations in the membrane structure and function. Increased LPO and erythrocyte fragility have also been observed by various researchers after CPF exposure to animals (Ambali *et al.,* 2010; Nishi & Hundal, 2013). Further, PCC content was also found to be elevated in blood of CPF treated animals, which suggests the oxidation of proteins. This elevation is due to CPF induced increase in production of free radicals in the body, which led to alteration in the activities of various cellular proteins that are important for retaining the structural and functional integrity of erythrocytes' membranes (Ambali *et al.,* 2010). These findings clearly depict that CPF treatment led to oxidation of both the lipids as well as proteins and thus is responsible for oxidative injury in RBCs via free radicals. However, QC administration to CPF treated animals decreased the previously raised levels of MDA and PCC, which attribute to the scavenging activity of QC. Thus, QC appears to have attenuated the free radical generation process and has prevented the oxidation of membrane lipids as well as proteins. Some authors have shown similar behavior of QC during chemically induced oxidative stress in different organs (Selvakumar *et al.,* 2012; Periasamy *et al.,* 2016).

Further, CPF treatment for 8 weeks resulted in increased activities of SOD and CAT that demonstrate the physiological response of the animals in mitigating the free radicals, induced oxidative stress. SOD catalyzes the conversion of superoxide radicals to hydrogen peroxide, whereas CAT converts hydrogen peroxide into water molecules. CPF exposure understandably has generated a considerable number of free radicals and in order to thwart the toxicity induced by free these radicals, the body has stimulated the activities of SOD and CAT. Previous studies have also revealed that CPF exposure is associated with the elevation of SOD and CAT activities (Kalender *et al.,* 2012; Kumar *et al.,* 2014). However, QC co-treatment to CPF treated animals was able to decrease the SOD and CAT activities. This ameliorative effect is understandably due to free radical scavenging activity of QC, which led to reduction in the load of free radicals in the cellular system and eventually has normalized the activities of antioxidants. It has been shown that QC due to its high diffusion capacity into the membranes has been considered as a strong scavenger of free radicals (Kalender *et al.,* 2012; Mohammadi *et al.,* 2014; Calabro *et al.,* 20CPF intoxication for 8 weeks suppressed the glutathione system of the body, as the activities of GSH, TG, GR and GST were found to be decreased in the erythrocyte lysates. The reduced activities are the consequence of oxidative modifications of proteins, which led to the decreased antioxidant versus oxidant ratio. These findings suggest that in order to detoxify CPF induced free radicals, a substantial amount of glutathione would have been consumed by the glutathione-related enzymes. Further, elevated LPO levels are also concomitant with our depleted GSH findings, which clearly reflect the moderating effect of GSH towards LPO induced free peroxides. Moreover, declined TG levels and GR activity also support the combating effect to contain reactive oxygen species induced by CPF exposure. Further, declined GST activity can be attributed to oxidation of SH sites or its high participation in the detoxification of CPF induced reactive species via conjugating with glutathione, which eventually decreased the GST content in the cellular system. Recently, some reports have also revealed a similar depletion of glutathione system in different organs after CPF exposure (Mosbah *et al.,* 2016; Nasr *et al.,* 2016). QC co-administration to CPF treated animals was able to ameliorate the altered glutathione system and that can be attributed to its free radical quencher capacity. The results of the present study therefore clearly demonstrate that QC treatment could up-regulate the declined glutathione system by reducing the free radical burden in the cell and thereby enhanced the antioxidant potential of the cell.

Conclusion

The present study suggests that QC mitigates CPF induced hematological alterations and therefore could be

considered as a potential candidate for alleviating CPF induced toxicity in blood.

Acknowledgements

Authors are thankful to Department of Biophysics, Panjab University, Chandigarh, India and DST-INSPIRE faculty Dr. Neha Singla for providing various facilities during this study.

We are grateful to Department of Biophysics, Panjab University, Chandigarh, India and Department of Science and Technology [DST/INSPIRE/04/2016/001368], New Delhi, India for financial support.

REFERENCES

Acker CI, Souza AC, Dos Santos MP, Mazzanti CM, Nogueira CW. (2012) Diphenyl diselenide attenuates hepatic and hematologic toxicity induced by CPF acute exposure in rats. *Environmental Science and Pollution Research* **19**: 3481–3490.

Akhtar N, Srivastava MK, Raizada RB. (2009) Assessment of CPF toxicity on certain organs in rat, Rattus norvegicus. *Journal of Environmental Biology* **30**: 1047–1053.

Alhawaj R, Patel D, Kelly MR, Sun D, Wolin MS. (2015) Heme biosynthesis modulation via δ-aminolevulinic acid administration attenuates chronic hypoxia-induced pulmonary hypertension. *American Journal of Physiology-Lung Cellular and Molecular Physiology* **308**: L719–728.

Ambali SF, Ayo JO, Ojo SA, Esievo KA. (2010) Vitamin E protects Wistar rats from chlorpyrifos-induced increase in erythrocyte osmotic fragility. *Food Chemical Toxicology* **48**: 3477–3480.

Benković V, Knezević AH, Dikić D, Lisicić D, Orsolić N, Basić I, Kopjar N. (2009) Radio-protective effects of Quercetin and ethanolic extract of propolis in gamma-irradiated mice. *Archives of Industrial Hygiene and Toxicology* **60**: 129–138.

Bhatt K, Flora SJ. (2009) Oral co-administration of α-lipoic acid, quercetin and captopril prevents gallium arsenide toxicity in rats. *Environmental Toxicology and Pharmacology* **28**: 140–146.

Burch H, Siegel AL. (1971) Improved method for measurement of delta-aminolevulinic acid dehydratase activity of human erythrocytes. *Clinical Chemistry* **17**: 1038–1040.

Calabro V, Litterio MC, Fraga CG, Galleano M, Piotrkowski B. (2018) Effects of Quercetin on heart nitric oxide metabolism in l-NAME treated rats. *Archives of Biochemistry and Biophysics* **47**: 47–53.

Carlberg I, Mannervik B. (1985) Glutathione reductase, Methods. *Enzymology* **113**: 484–490.

Ceballos-Picot I, Triever JV, Nicole A Silnet PM, Thevenin M. (1992) Age correlated modifications of copper-zinc superoxide dismutase and glutathione-related enzyme activities in human erythrocytes. *Clinical Chemistry* **38**: 66–70.

Dacie JV, Lewis SM. (1991) *Practical hematology*, 6th edn. Churchill, London

Elsharkawy EE, Yahia D, El-Nisr NA. (2013) Sub-chronic exposure to chlorpyrifos induces hematological, metabolic disorders and oxidative stress in rat: attenuation by glutathione. *Environmental Toxicology and Pharmacology* **35**: 218–227.

Enis Yonar M, Yonar SM, Ural MS, Silici S, Düşükcan M. (2012) Protective role of propolis in chlorpyrifos-induced changes in the haematological parameters and the oxidative/antioxidative status of *Cyprinus carpio carpio*. *Food Chemical Toxicology* **50**: 2703–2708.

Fu Y, Liu F, Zhao C, Zhao Y, Liu Y, Zhu G. (2015) Distribution of chlorpyrifos in rice paddy environment and its potential dietary risk. *Journal of Environmental Sciences (China)* **35**: 101–107.

Goel A, Dani V, Dhawan DK. (2006) Role of zinc in mitigating the toxic effects of chlorpyrifos on hematological alterations and electron microscopic observations in rat blood. *Biometals* **19**: 483–492.

Habig WH, Pabst MJ, Jakoby WB. (19740 Glutathione S-transferase: the first enzymatic step in mercapturic acid formation. *Journal of Biological Chemistry* **249**: 7310–7339.

Haleagrahara N, Siew CJ, Ponnusamy K. (2013) Effect of quercetin and desferri oxamine on 6-hydroxydopamine (6-OHDA) induced neurotoxicity in striatum of rats. *Journal of the Toxicological Sciences* **38**: 25–33.

Heeba GH, Mahmoud ME, El Hanafy AA. (2014) Anti-inflammatory potential of curcumin and Quercetin in rats: role of oxidative stress, heme oxygenase-1 and TNF-α. *Toxicology & Industrial Health* **30**: 551–560.

Hung DZ, Yang HJ, Li YF. (2015) The Long-Term Effects of Organophosphates Poisoning as a Risk Factor of CVDs: A Nationwide Population-Based Cohort Study. *PLoS One* **10**: e0137632.

Jahan S, Iftikhar N, Ullah H, Rukh G, Hussain I. (2015) Alleviative effect of Quercetin on rat testis against arsenic: a histological and biochemical study. *Systems Biology in Reproductive Medicine* **61**: 89–95.

Kalender Y, Kaya S, Durak D, Uzun FG, Demir F. (2012) Protective effects of catechin and Quercetin on antioxidant status, lipid peroxidation and testis-histoarchitecture induced by chlorpyrifos in male rats. *Environmental Toxicology and Pharmacology* **33**: 141–148.

Kolesnikova LI, Semyonova NV, Grebenkina LA, Darenskaya MA, Suturina LV, Gnusina SV. (2014) Integral indicator of oxidative stress in human blood. *Bulletin of Experimental Biology and Medicine* **157**: 715–717.

Kono Y (1978) Generation of superoxide radical during autooxidation of hydroxylamine and an assay for superoxide dismutase. A*rchives of Biochemistry and Biophysics* **186**: 189–195.

Krukoski DW, Comar SR, Claro LM, Leonart MS, do Nascimento AJ. (2009) Effect of vitamin C, deferoxamine, Quercetin and rutin against tert-butyl hydroperoxide oxidative damage in human erythrocytes. *Hematology* **14**: 168–172.

Kumar MS, Praveenkumar R, Jeon BH, Thajuddin N. (2014) Chlorpyrifos-induced changes in the antioxidants and fatty acid compositions of *Chroococcus turgidus* NTMS12. *Letters in Applied Microbiology* **59**: 535–541.

Lan H, Hong W, Fan P, et al. (2017) Quercetin Inhibits Cell Migration and Invasion in Human Osteosarcoma Cells. Cellular Physiology and Biochemistry 43: 553–567.

Levine RL, Williams JA, Stadtman ER, Shacter E. (1994) Carbonyl assays for determination of oxidatively modified proteins. *Methods in Enzymology* **233**: 346–357.

Li D, Huang Q, Lu M, Zhang L, Yang Z, Zong M, Tao L. (2015) The organophosphate insecticide chlorpyrifos confers its genotoxic effects by inducing DNA damage and cell apoptosis. *Chemosphere* **135**: 387–393.

Li X, Choi JS (2009) Effects of Quercetin on the pharmacokinetics of Etoposide after oral or intravenous administration of etoposide in rats. *Anticancer Research* **29**: 1411–1415.

Liu S, Tian L, Chai G, Wen B , Wang B. (2018) Targeting heme oxygenase-1 by Quercetin ameliorates alcohol-induced acute liver injury via inhibiting NLRP3 inflammasome activation. *Food and function* **9**: 4184–4193.

Luck H (1971) *Methods of enzymatic analysis*. New York: Academic Press.

Malhotra A, Dhawan DK. (2014) Current view of zinc as a hepatoprotective agent in conditions of chlorpyrifos induced toxicity. P*esticide Biochemistry and Physiology* **112**: 1–6.

Maurya AK, Vinayak M (2015) Anticarcinogenic action of Quercetin by down-regulation of phosphatidylinositol 3-kinase (PI3K) and protein kinase C (PKC) via induction of p53 in hepatocellular carcinoma (HepG2) cell line. *Molecular Biology Reports* **42**: 1419–1429.

Miles SL, McFarland M, Niles RM. (2014) Molecular and physiological actions of quercetin: need for clinical trials to assess its benefits in human disease. *Nutrition Reviews* **72**: 720–734.

Mishra D, Flora SJ. (2008) Quercetin administration during chelation therapy protects arsenic-induced oxidative stress in mice. *Biological Trace Element Research* **122**: 137–147.

Mohammadi HS, Goudarzi I, Lashkarbolouki T, Abrari K, Elahdadi Salmani M. (2014) Chronic administration of Quercetin prevents spatial learning and memory deficits provoked by chronic stress in rats. *Behavioural Brain Research* **270**: 196–205.

Moron MS, Depierre JW, Mannervik B. (1979) Levels of glutathione, glutathione reductase and glutathione S-transferase activities in rat lung and liver. *Biochimica et Biophysica Acta* **582**: 67–78

Mosbah R, Yousef MI, Maranghi F, Mantovani A. (2016) Protective role of Nigella sativa oil against reproductive toxicity, hormonal alterations, and oxidative damage induced by chlorpyrifos in male rats. *Toxicology and Industrial Health* **32**: 1266–1277.

Nasr HM, El-Demerdash FM,El-Nagar WA (2016) Neuro and renal toxicity induced by chlorpyrifos and abamectin in rats: Toxicity of insecticide mixture. *Environmental Science and Pollution Research International* **23**: 1852–1859.

Nishi K, Hundal SS. (2013) Chlorpyrifos induced toxicity in reproductive organs of female Wistar rats. *Food Chemical Toxicology* **62**: 732–738.

Olakkaran S, Antony A, Kizhakke Purayil A, Tilagul Kumbar S, Hunasanahally Puttaswamygowda G. (2018) Lead modulated Heme synthesis inducing oxidative stress mediated Genotoxicity in Drosophila melanogaster. *The Science of the Total Environment* **634**: 628–639.

Pala A, Şeker E, Yonar ME. (2018) Effect of Tunceli garlic on some immunological parameters in Cyprinus carpio exposed to chlorpyrifos. *Cell Mol Biol (Noisy-le-grand)* **64**: 108–112.

Periasamy R, Kalal IG, Krishnaswamy R, Viswanadha V. (2016) Quercetin protects human peripheral blood mononuclear cells from OTA-induced oxidative stress, genotoxicity, and inflammation. *Environmental Toxicology* **31**: 855–865.

Qiu L, Luo Y, Chen X. (2018) Quercetin attenuates mitochondrial dysfunction and biogenesis via upregulated AMPK/SIRT1 signaling pathway in OA rats. *Biomedicine & Pharmacotherapy* **103**: 1585–1591.

Rojas Á, Del Campo JA, Clement S, Lemasson M, García-Valdecasas M, Gil-Gómez A, Ranchal I, Bartosch B, Bautista JD, Rosenberg AR, Negro F, Romero-Gómez M.(2016) Effect of Quercetin on Hepatitis C Virus Life Cycle: From Viral to Host Targets. *Science Report* **6**: 31777.

Roslan J, Giribabu N, Karim K, Salleh N. (2017) Quercetin ameliorates oxidative stress, inflammation and apoptosis in the heart of streptozotocin-nicotinamide-induced adult male diabetic rats. B*iomedicine & Pharmacotherapy* **86**: 570–582.

Selvakumar K, Bavithra S, Krishnamoorthy G, Venkataraman P, Arunakaran J. (2012) Polychlorinated biphenyls-induced oxidative stress on rat hippocampus: a neuroprotective role of quercetin. *Scientific World Journal* **2012**: 980314.

Sharma DR, Sunkaria A, Wani WY, Sharma RK, Verma D, Priyanka K, Bal A, Gill KD. (2015) Quercetin protects against aluminium induced oxidative stress and promotes mitochond- rial biogenesis via activation of the PGC-1α signaling pathway. *Neurotoxicology* **51**: 116–137.

Smida A, Ncibi S, Taleb J, Ben Saad A, Ncib S, Zourgui L. (2017) Immunoprotective activity and antioxidant properties of cactus (*Opuntia ficus indica*) extract against chlorpyrifos toxicity in rats. *Biomedicine & Pharmacotherapy* **88**: 844–851.

Sunmonu TO, Oloyede OB. (2010) Performance and haematological indices in rats exposed to monocrotophos contamination. *Human and Experimental Toxicology* **29**: 845–850.

Wills ED. (1966) Mechanism of lipid peroxide formation in animal tissue. *The Biochemical Journal* **99**: 667–676.

Wu W, Li R, Li X, He J, Jiang S, Liu S, Yang J. (2015) Quercetin as an Antiviral Agent Inhibits Influenza A Virus (IAV) Entry. *Viruses* **8**: 6

Yang T, Kong B, Gu JW, Kuang YQ, Cheng L, Yang WT, Xia X, Shu HF. (2014) Anti-apoptotic and anti-oxidative roles of Quercetin after traumatic brain injury. *Cellular and Molecular Neurobiology* **34**: 797–804.

Yarahmadi A, Khademi F, Mostafavi-Pour Z, Zal F. (2018) In-Vitro Analysis of Glucose and Quercetin Effects on m-TOR and Nrf-2 Expression in HepG2 Cell Line (Diabetes and Cancer Connection). *Nutrition and Cancer* **70**: 770–775.

Zafiropoulos A, Tsarouhas K, Tsitsimpikou C, Fragkiadaki P, Germanakis I, Tsardi M, Maravgakis G, Goutzourelas N, Vasilaki F, Kouretas D, Hayes A, Tsatsakis A. (2014) Cardiotoxicity in rabbits after a low-level exposure to diazinon, propoxur, and chlorpyrifos. *Human & Experimental Toxicology* **33**: 1241–1252.

Zahler WL, Cleland WW. (1968) A specific and sensitive assay for disulfides. *The Journal of Biological Chemistry* **243**: 716–719.